

RICE UNIVERSITY

**Interrogating brain and behavioral state transitions with a spontaneous
C. elegans sleep behavior**

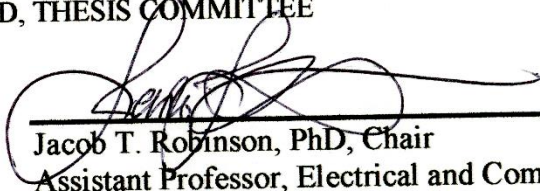
by

Daniel Luis Gonzales

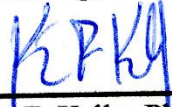
A THESIS SUBMITTED
IN PARTIAL FULFILLMENT OF THE
REQUIREMENTS FOR THE DEGREE

Doctor of Philosophy


APPROVED, THESIS COMMITTEE



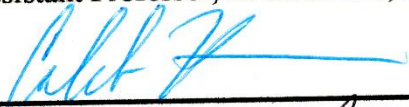
Jacob T. Robinson, PhD, Chair
Assistant Professor, Electrical and Computer
Engineering, Rice University



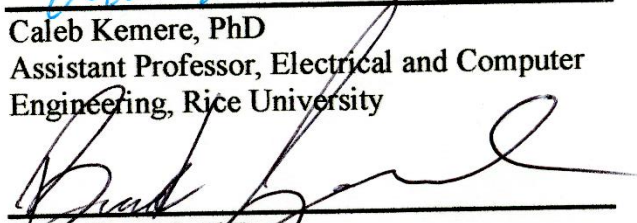
Kevin F. Kelly, PhD
Associate Professor, Electrical and Computer
Engineering, Rice University



Julia Saltz, PhD
Assistant Professor, BioSciences, Rice University



Caleb Kemere, PhD
Assistant Professor, Electrical and Computer
Engineering, Rice University



Buck Samuel, PhD
Assistant Professor, Molecular Virology and
Microbiology, Baylor College of Medicine

HOUSTON, TEXAS
April 2019

ABSTRACT

Interrogating brain and behavioral state transitions with a spontaneous *C. elegans* sleep behavior

by

Daniel Luis Gonzales

One remarkable feature of the nervous system is its ability to rapidly and spontaneously switch between activity states. In the extreme example of sleep, animals arrest locomotion, reduce their sensitivity to sensory stimuli, and dramatically alter their neural activity. Small organisms are useful models to better understand these sudden changes in neural states because we can simultaneously observe whole-brain activity, monitor behavior and precisely regulate the external environment. Here, we show a spontaneous sleep-like behavior in *C. elegans*, termed “ μ Sleep,” that is associated with a distinct global-brain state and regulated by both the animal’s internal physiological state and input from multiple sensory circuits. Specifically, we found that when confined in microfluidic chambers, adult worms spontaneously transition between periods of normal activity and short quiescent bouts, with behavioral state transitions occurring every few minutes. This quiescent state, which we call μ Sleep, meets the behavioral requirements of *C. elegans* sleep, is dependent on known sleep-promoting neurons ALA and RIS, and is associated with a global down-regulation of neural activity. Consistent with prior studies of *C. elegans* sleep, we found that μ Sleep is regulated by satiety and temperature. In addition, we show for the first time that quiescence can be either driven or

suppressed by thermosensory input, and that animal restraint induces quiescence through mechanosensory pathways. Together, these results establish a rich model system for studying how neural and behavioral state transitions are influenced by multiple physiological and environmental conditions. Furthermore, the combination of this spontaneous sleep state with the microfluidic platform serves as a powerful method to uncover the fundamental function of invertebrate sleep using whole-brain imaging, high-throughput behavioral recordings, and longitudinal monitoring across animal lifespan. (abstract adapted from Gonzales, Zhou, & Robinson, 2019).

Acknowledgments

To my wife: you are the single biggest supporter in my life. I can't say enough about the ways in which you have helped me through this process. You encourage me. You strengthen me. You occasionally tear apart my writing and brainstorm about what could be going wrong with my experiments. *You convince me we can take on anything.* We've been figuring out life, parenting, and marriage together—and there are so many more adventures ahead of us.

To my boys: the entire world is at your feet—take hold of it. You are capable of achieving anything you could possibly want. Be ambitious. Do hard things. Succeed. But always know that you are not defined by your accomplishments, nor your failures. You have an identity rooted in love, and this is what defines you.

To my parents: we have never had much, but you gave me everything I could have possibly needed to succeed. Regardless of what I chose to do in life, I knew two things: 1) you loved me, 2) you supported me.

To Jacob: I could not have asked for a better PhD advisor. Looking back, I started this PhD feeling like an out-of-place West Texas kid, and you helped mold and empower me into a young professional and scientist (with a strong dash of Texan, of course). I look up to who you are as a scientist, mentor, and person. I have known since day-one that you had my back, and I know that will continue to be the case for many years to come.

I would also like to thank specific members from the lab, notably Jasmine Zhou, who was an excellent undergraduate researcher and did great work in the whole-brain imaging section of this thesis. Bo Fan designed the high-throughput behavioral devices, which significantly improved the latest experiments in this project. I would also like to thank my committee. This group consists of a huge range of disciplines—genetics, microbiomes, neuroengineering, and physics—all with unique input and insight that I find extremely valuable. In addition, this work was strengthened by an incredible *C. elegans* community and external funding. We thank the Fang-Yen lab for providing the WorMotel device. Henrik Bringmann provided the HRB1361 strain for RIS imaging. Anne Hart, David Raizen and Henrik Bringmann all gave fantastic input on our work. Several strains were provided by the CGC, which is funded by NIH Office of Research Infrastructure Programs (P40 OD010440). Much of my graduate work has been funded by the National Science Foundation (NSF) Graduate Research Fellowship Program 1842494 and a training fellowship from the Keck Center of the Gulf Coast Consortia on the NSF IGERT: Neuroengineering from Cells to Systems 1250104. In addition, the Smalley-Curl Institute's Student Training for Advising Research program provided funds for both materials and Jasmine Zhou's undergraduate research. We also thank the Rice Shared Equipment Authority where devices were fabricated and Tim Gilheart for consistent help in our fabrication needs.

Contents

Acknowledgments	iv
Contents	vi
List of Figures	ix
List of Tables	xi
Nomenclature	xii
Review of Relevant Literature	13
1.1. Microfluidic approaches to study <i>C. elegans</i> neurobiology.....	17
1.1.1. Chemosensation	17
1.1.2. Mechanosensation	21
1.1.3. Sleep	23
1.1.4. Long-term imaging.....	25
1.1.5. Electrophysiology.....	28
1.1.6. High-throughput screenings	30
1.1.7. Conclusions on <i>C. elegans</i> microfluidics	33
1.2. Review of <i>C. elegans</i> sleep and quiescence	34
1.2.1. Developmental Sleep.....	35
1.2.2. Environmentally-induced sleep and quiescence	43
1.2.2.1. Stress-induced sleep	44
1.2.2.2. Swimming-induced quiescence and neural circuits underlying <i>C. elegans</i> behavioral states	49
1.2.2.3. Satiety quiescence	55
1.2.3. Conclusions and open questions in <i>C. elegans</i> sleep	57
1.3. Methods for whole-brain imaging in <i>C. elegans</i>	60
1.3.1. Whole-brain imaging in freely-moving animals	62
1.3.2. Whole-brain imaging in chemically paralyzed animals	65
1.3.3. Conclusions and future directions of whole-brain imaging for <i>C. elegans</i> neuroscience.....	70
<i>C. elegans</i> μSleep Behavior	75

2.1. Comparison of μ Sleep with stress-induced sleep and swimming-induced quiescence.....	76
2.2. μ Sleep meets behavioral requirements for sleep.....	79
2.3. μ Sleep is dependent on <i>C. elegans</i> sleep-promoting neurons	84
A Global Brain-State Transition Underlies μSleep Behavior.....	86
3.1. The advantages of μ Sleep for capturing brain-state transitions	87
3.2. μ Sleep is associated with a global-brain state transition	88
3.3. The RIS neuron is more active during μ Sleep	90
μSleep is Regulated by Satiety, Thermosensation, and Mechanosensation	93
4.1. Defining baseline environmental conditions	94
4.2. High satiety abolishes μ Sleep.....	96
4.3. Bi-directional thermosensory input can increase or decrease total sleep	97
4.4. Confinement and restraint increase total sleep through mechanosensory circuits	98
4.5. μ Sleep phenotypes partially correlate with animal stress.....	99
4.6. Constantly replenishing fluidic buffer does not reduce μ Sleep.....	101
4.7. Summary of factors that regulate μ Sleep	102
Experimental Methods and Data Analysis.....	105
5.1. <i>C. elegans</i> strains and maintenance.....	105
5.2. Microfluidic device fabrication.....	106
5.3. Behavioral quantification and sleep detection	107
5.4. Standard microfluidic behavioral assays.....	109
5.5. WorMotel assays.....	110
5.6. Heat-shock.....	110
5.7. Reversibility and decreased response to stimuli	111
5.8. Whole-brain imaging.....	112
5.9. RIS imaging	114
5.10. Environmental control.....	115
5.11. DAF-16::GFP imaging.....	116
Summary of μSleep, Future Directions, and Outlook on <i>C. elegans</i> Sleep.....	118
6.1. Summary of results	118

6.2. Future directions with μ Sleep behavior	120
6.2.1. Capturing the activity of more neurons during sleep-wake transitions.....	120
6.2.2. High-throughput behavior	124
6.2.3. Longitudinal imaging for understanding the need for invertebrate sleep....	126
6.3. Metabolic tradeoffs as a potential unifying mechanism for <i>C. elegans</i> sleep.....	128
References.....	131

List of Figures

Figure 1.1 – Microfluidics for chemosensory stimulation.	19
Figure 1.2 – Controlled mechanosensory stimulation with microfluidic valves.	22
Figure 1.3 – Microfluidics for behavioral monitoring of sleep and quiescence.	24
Figure 1.4 – On-chip microfluidic-assisted electrophysiology.	29
Figure 1.5 – High-throughput microfluidic drug screening.	32
Figure 1.6 – Developmentally-timed sleep during <i>C. elegans</i> lethargus.	36
Figure 1.7 – Model for <i>C. elegans</i> sleep driven by the RIS neuron.	41
Figure 1.8 – A global-brain state underlies <i>C. elegans</i> sleep.	43
Figure 1.9 – <i>C. elegans</i> stress-induced sleep.....	45
Figure 1.10 – Model for <i>C. elegans</i> stress-induced sleep.	49
Figure 1.11 – Extended swimming induces spontaneous quiescence.	51
Figure 1.12 – <i>C. elegans</i> spontaneously transition to quiescence in both solid and liquid environments.	53
Figure 1.13 – Whole brain imaging in freely moving animals.	64
Figure 1.14 – Whole brain imaging in paralyzed worms reveals low- dimensional neural manifolds.....	67
Figure 1.15 – PCA captures brain-wide changes in neural dynamics during <i>C.</i> <i>elegans</i> sleep.....	70
Figure 2.1 – Microfluidic-induced quiescence is phenotypically distinct from SIS and SIQ.....	78
Figure 2.2 – Microfluidic-induced quiescence is reversible and animals shown a decreased response to weak external stimuli.....	81

Figure 2.3 – μSleep shows micro-homeostatic rebound.....	83
Figure 2.4 – ALA and RIS defective mutants show less sleep compared to WT.	85
Figure 3.1 – μSleep is a global-brain state.....	89
Figure 3.2 – RIS neuron is more active during sleep and low-behavioral activity.	91
Figure 4.1 – Satiety, thermosensation, and mechanosensation regulate μSleep.	95
Figure 4.2 – DAF-16::GFP imaging shows that μSleep partially correlates with <i>C. elegans</i> stress.....	100
Figure 4.3 – Constantly replenishing fluidic buffer does not reduce sleep.....	102
Figure 4.4 – Raster plots of detected sleep for all animals during temperature and mechanical regulation.....	103
Figure 6.1 – Summary of μSleep results.....	119
Figure 6.2 – Whole-brain imaging during μSleep in paralyzed animals.	121
Figure 6.3 – Setup for two-color whole-brain volumetric imaging.....	123
Figure 6.4 – High-throughput behavioral measurements in microfluidics. ...	125

List of Tables

Table 1.1 - Genetic and molecular conservation of *C. elegans* sleep..... 39

Nomenclature

ACh	Acetylcholine
cAMP	Cyclic adenosine monophosphate
cGMP	Cyclic guanosine monophosphate
DTS	Developmentally-timed sleep
EGF	Epidermal growth factor
EPG	Electropharyangeogram
FOV	Field-of-view
lf	Loss-of-function
nano-SPEARs	Nanoscale suspended electrode arrays
NGM	Nematode growth media
PCA	Principle component analysis
PC	Principle component
PDF	Pigment dispersing factor
PDMS	Polydimethylsiloxane
PKG	Protein kinase G
SIS	Stress-induced sleep
SIQ	Swimming-induced quiescence
WT	Wild-type

Chapter 1

Review of Relevant Literature

Understanding how animals select behaviors based on sensory information is a fundamental goal of neuroscience (Clark, Freifeld, & Clandinin, 2013; Fetsch, Deangelis, & Angelaki, 2013; Van Atteveldt, Murray, Thut, & Schroeder, 2014); however, sensorimotor transformations can vary dramatically depending on the state of the animal's nervous system (Anderson, 2016; C. I. Bargmann & Marder, 2013; Marder, 2012; Tye, 2018). Wakefulness and arousal (McGinley et al., 2015), locomotor activity states (C. Bennett, Arroyo, & Hestrin, 2013), satiety (Lim, Eyjólfsdóttir, Shin, Perona, & Anderson, 2014), attention (Talsma, Senkowski, Soto-Faraco, & Woldorff, 2010), and emotions (Anderson, 2016; Tye, 2018) represent a spectrum of physiological and neural states that can dramatically affect how animals respond to a given stimuli. Small animals like the nematode *C. elegans* are tractable model organisms for understanding how physiological and neural states combine

with information from multiple sensory pathways and give rise to specific behavior (Anderson, 2016; C. I. Bargmann & Marder, 2013; Calhoun & Murthy, 2017; Clark et al., 2013; D. D. Ghosh, Nitabach, Zhang, & Harris, 2017; Kaplan, Nichols, & Zimmer, 2018; Watanabe et al., 2017). (paragraph adapted from Gonzales, Zhou, & Robinson, 2019, which is currently under review as of April 2019).

Sleep is one example of a neural state that dramatically alters an animal's sensorimotor transformations (Brown, Basheer, McKenna, Strecker, & McCarley, 2012; Saper, Fuller, Pedersen, Lu, & Scammell, 2010). Studies of sleep across the phylogenetic tree have shown that sensory systems transition to a reduced activity state that leads to a decreased animal response to external stimuli (Campbell & Tobler, 1984; J. Y. Cho & Sternberg, 2014; J. C. Hendricks et al., 2000; Nath et al., 2017; Raizen et al., 2008). Additionally, sleep and wakefulness have been shown to correspond with distinct patterns of neural activity in humans (Brown et al., 2012; Saper et al., 2010), cats (Steriade, McCormick, & Sejnowski, 1993), rodents (Brown et al., 2012), and fruit flies (Nitz, Van Swinderen, Tononi, & Greenspan, 2002). Likewise, whole-brain recordings from *C. elegans* suggest that the majority of worm brain activity can be represented on a low-dimensional manifold, and that the activity on this manifold shifts from phasic to fixed-point attractor dynamics during developmental sleep (see Section 1.3.2) (Kato et al., 2015; Nichols, Eichler, Latham, & Zimmer, 2017). Additionally, studies with *C. elegans* have revealed molecular pathways (Monsalve, Van Buskirk, & Frand, 2011; Raizen et al., 2008; Singh et al., 2011; C. Van Buskirk & Sternberg, 2010; Cheryl Van Buskirk & Sternberg, 2007),

neural circuits (Choi, Chatzigeorgiou, Taylor, Schafer, & Kaplan, 2013; Hill, Mansfield, Lopez, Raizen, & Buskirk, 2014; M. D. Nelson et al., 2013; Turek, Besseling, Spies, König, & Bringmann, 2016; Turek, Lewandrowski, & Bringmann, 2013; Cheryl Van Buskirk & Sternberg, 2007; Wu, Masurat, Preis, & Bringmann, 2018), and neuropeptides (Nath, Chow, Wang, Schwarz, & Sternberg, 2016; M. D. Nelson et al., 2013; Matthew D. Nelson et al., 2014; Turek et al., 2016) that drive nematode sleep and arousal, and some of these mechanisms are conserved in other animals (see Section 1.2) (Kayser & Biron, 2016; Nicholas F. Trojanowski & Raizen, 2016). **These reports have paved the way for using *C. elegans* sleep as a model system to understand spontaneous brain-state transitions between sleep and wakefulness. Given the number of unique regulators of *C. elegans* sleep, there is a need to identify a behavior that facilitates our understanding of how brain-wide neural circuits transduce multiple external and internal factors to drive sleep-wake transitions.** (paragraph adapted from Gonzales, Zhou, & Robinson, 2019, which is currently under review as of April 2019).

This thesis establishes μ Sleep: spontaneous, brief *C. elegans* sleep bouts in microfluidic environments. We will show that the microfluidic environment drives nematode sleep, that μ Sleep is accompanied by a brain-wide transition in neural activity, and that distinct neural circuits monitor the surrounding environment to regulate behavioral states. This behavior enables a wide-range of future experiments into the genetic and molecular mechanisms of sleep, nematode multi-sensory integration, and how brain-wide neural circuits control sleep-wake

behavioral transitions. Furthermore, the microfluidic platform provides distinct advantages to perform these experiments with precise environmental control, high-throughput assays, and cellular-resolution whole-brain imaging in behaving animals.

Of course, the findings in this thesis are rooted in *C. elegans* research that spans many of the previous decades. This chapter contains three sections that describe this rich scientific history. In the first section, I will review microfluidics as a tool to study *C. elegans* neurobiology. In the second section, I will review *C. elegans* sleep studies. In the final section, I will review *C. elegans* studies that use whole-brain imaging to understand the neural basis of behavior. Overall, this literature review will summarize key points and lay the foundation for the μ Sleep platform:

1. Microfluidics was and continues to be a powerful method for studying *C. elegans* neurobiology,
2. *C. elegans* sleep is a powerful behavior to not only understand the molecular and genetic mechanisms of sleep, but also how neural circuits drive behavioral transitions,
3. *C. elegans* whole-brain imaging will uncover fundamental principles of how ensemble neural activity regulates animal behavior.

Together, this discussion will place μ Sleep in the appropriate context, demonstrating the scientific value of a microfluidic-based sleep behavior for studying the neural circuit basis of brain and behavioral state transitions.

1.1. Microfluidic approaches to study *C. elegans* neurobiology

Since the first reports of microfluidic devices tailored to accommodate *C. elegans* more than a decade ago (Chronis, Zimmer, & Bargmann, 2007), a vast number of studies have adopted microfluidic approaches to study nematode neurobiology. Though *C. elegans* are most typically raised and tested on “Nematode Growth Media” (NGM, an agar-based environment), many behaviors and senses are conserved and reliably studied in microfluidics. These devices enable dynamic environmental control, high-throughput assays, and facilitate high-resolution imaging. Many reviews are widely available that discuss methods for microfluidic device fabrication, including soft-lithography with polydimethylsiloxane (PDMS, a silicone material) and design considerations (Ferry, Razinkov, & Hasty, 2011; San-Miguel & Lu, 2013; Tang & Whitesides, 2010). Rather than discuss these well-established elements, this section will focus on a wide range of *C. elegans* subdisciplines, from chemosensation to screenings for disease treatments, that have benefited from microfluidic technologies.

1.1.1. Chemosensation

The field of *C. elegans* chemosensation has seen one of the largest surges of microfluidic technologies. In fact, the first reported microfluidic device tailored for worms—the “olfactory chip”—is also one of the most widely adopted (Figure 1.1A-B) (Chronis et al., 2007). With this device, animals are placed in an immobilization chamber, but their noses are exposed to a separate channel with a controllable flow

(Figure 1.1A-B). In this geometry, researchers gently flow a non-stimulating control buffer over the animal nose, but can rapidly switch to a stimulating odorant (Figure 1.1A-B). The stimulant flow can be precisely monitored in real-time with a colored dye and multiple alternations between the control buffer and stimulant can be generated for a single animals (Chronis et al., 2007). Combining this stimulation with calcium-imaging has provided a powerful platform to understand the neural circuits underlying *C. elegans* olfaction in the ASH sensory neuron, olfactory nociception, pheromone detection and compartmental encoding of motor transformations (C. Bargmann, 2006; Chalasani et al., 2007; C. E. Cho, Brueggemann, L'Etoile, & Bargmann, 2016; Chokshi, Bazopoulou, & Chronis, 2010; Gordus, Pokala, Levy, Flavell, & Bargmann, 2015; M. Hendricks, Ha, Maffey, & Zhang, 2012; Kato, Xu, Cho, Abbott, & Bargmann, 2014; MacOsko et al., 2009; Yoshida et al., 2012; Zaslaver et al., 2015). Furthermore, this device is also useful for studying gustation by replacing the odorant flow with water-soluble salts or pheromones (C. Bargmann, 2006; Kunitomo et al., 2013; Leinwand & Chalasani, 2013; Luo et al., 2014; Oda, Tomioka, & Iino, 2011; Ohno, Sakai, Adachi, & Iino, 2017; Tomida, Oda, Takekawa, Iino, & Saito, 2012). In addition to this already powerful method, second-generation olfactory chips have been fully automated, recording from hundreds of animals per hour and allowing for screens of the genetic basis of olfaction (Chokshi et al., 2010). Indeed, the olfactory chip is the ideal case-study demonstrating the powerful of microfluidics for studying *C. elegans* neurobiology in a dynamically-controlled, high-throughput platform.

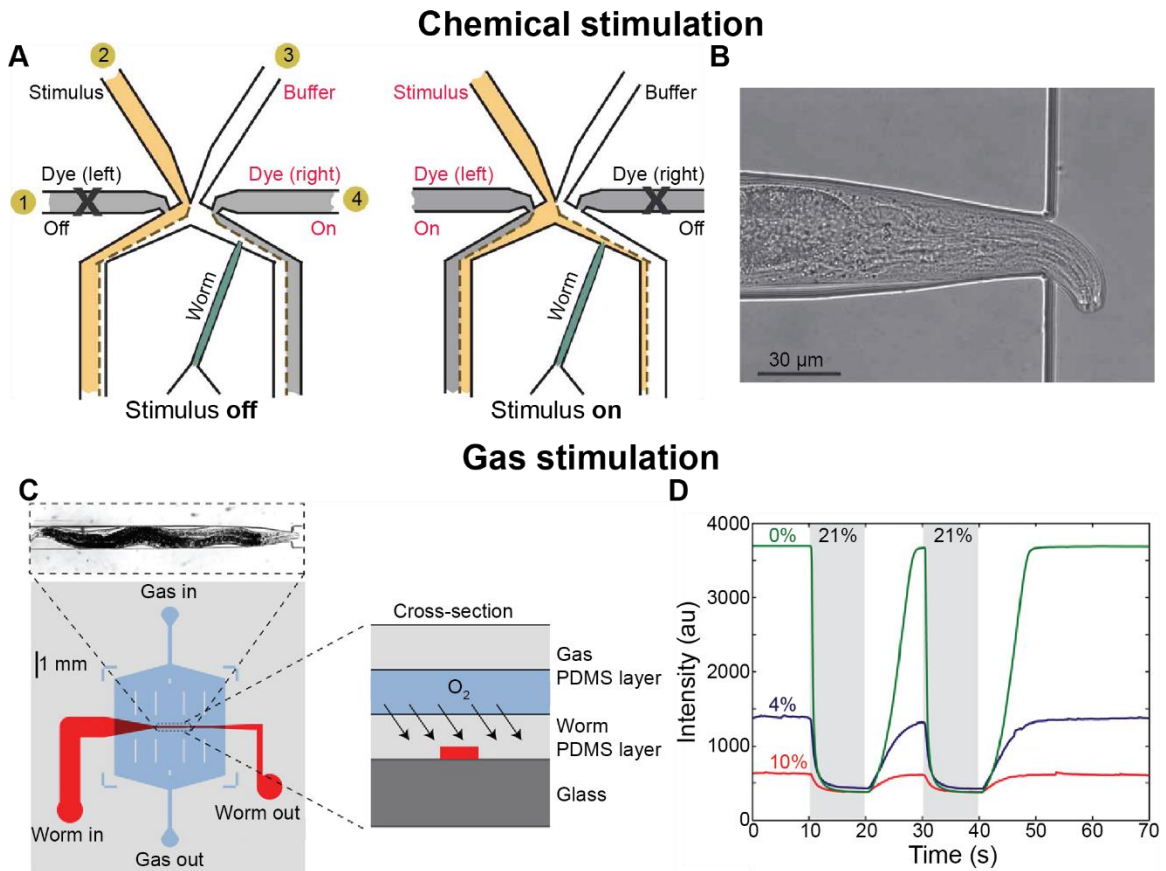


Figure 1.1 – Microfluidics for chemosensory stimulation.

(A) Olfactory chip layout and operation with chemosensory stimulation off and on. The indicated flow channels are (1) A dye channel, (2) the odorant stimulus channel, (3) a buffer channel with no odorant, and (4) a second dye channel. Animals are confined to a tailored “worm” channel. During chip operation, the stimulant channel is always flowing. However, the stimulant is directed away from (left, “stimulus off”) or towards (right, “stimulus on”) the animal nose by switching the left and right dye channels on and off. **(B)** Optical micrograph of the animal nose protruding into the stimulus channel. **(C)** Two-layer PDMS layout for controlling the gas environment. A gas-stimulation layer (blue) sits above a worm layer (red) with a thin layer of PDMS between each. Gas from the stimulation layer quickly permeates the PDMS barrier. Thus, the O_2 concentration of the gas layer equals the O_2 concentration of the worm layer at equilibrium. **(D)** Recordings with O_2 -sensitive dye from the worm layer shows that the O_2 concentration surrounding animals can rapidly be controlled on the order of seconds. Panels (A-B) adapted from (Chronis et al., 2007) and (C-D) from (Zimmer et al., 2009).

In addition to using microfluidics to facilitate calcium-imaging during chemical stimulation, devices have been developed to animal behaviors in chemical gradients (chemotaxis) (Albrecht & Bargmann, 2011; McCormick, Gaertner, Sottile, Phillips, & Lockery, 2011). Rather than immobilizing animals as in the olfactory chip (Figure 1.1A-B), these geometries can either partially restrain animals (McCormick et al., 2011), or allow animals to fully roam in large arenas of micropillars termed “artificial dirt” (Albrecht & Bargmann, 2011; S R Lockery et al., 2008). In the partially-restrained scheme, the head is exposed to buffer flow from two different channels and animals can choose to move their heads into one stream of flow or the other. Adding food and other stimulants to these channels allows researchers to evaluate decision making (Cohen et al., 2018; Faumont, Lindsay, & Lockery, 2012; McCormick et al., 2011) and study sensorimotor integration (Ouellette, Desrochers, Ghetta, Ramos, & Hendricks, 2018). Similarly, microfluidic chemotaxis experiments have also been performed in freely-moving animals (Albrecht & Bargmann, 2011; Larsch et al., 2015). Precise chemical gradients can be constructed across a large (1-5 cm²) microfluidic arenas, allowing researchers to monitor chemotaxis behavior in a population of animals (Albrecht & Bargmann, 2011; Larsch et al., 2015). This method can also be combined with wide-field calcium-imaging to study how chemosensory neurons encode chemical gradients in freely-moving animals (Larsch, Ventimiglia, Bargmann, & Albrecht, 2013).

Similar to the olfactory chip, which delivers chemical stimuli to study chemosensation, devices have been developed to rapidly change gas concentrations

to study O₂ and CO₂ sensing with calcium imaging (Figure 1.1C-D) (Persson et al., 2009; Zimmer et al., 2009). The most commonly used method to control the gaseous environment takes advantage of the fact that PDMS is highly permeable to gas (Figure 1.1C-D) (Zimmer et al., 2009). Thus, with two microfluidic layers separated by a thin PDMS membrane—one layer for holding worms in fluid and a second gaseous layer—the gasses in the second layer can rapidly diffuse across the membrane and dissolve into the fluidic worm layer (Figure 1.1C-D). Devices combining gas-control and calcium-imaging have revealed fundamental mechanisms underlying *C. elegans* O₂ and CO₂ sensation (Bretscher et al., 2011; Fenk & de Bono, 2015; McGrath et al., 2009; Zimmer et al., 2009) and how gas sensation can regulate the global animal activity state (Busch et al., 2012; Laurent et al., 2015). Furthermore, like microfluidic devices with chemical gradients, PDMS-based microdevices have been developed for constructing CO₂ gradients to monitor *C. elegans* aerotaxis (Jesse M Gray et al., 2004).

1.1.2. Mechanosensation

In the same way that microfluidics enables controllable chemical and gaseous stimulation (see Section 1.1.1), technologies have been developed for precise spatiotemporal control of mechanical stimulation (Figure 1.2). Classical methods for studying *C. elegans* mechanosensation include dragging eyebrow hair picks over animal bodies for assaying gentle touch, tapping a petri dish to mechanically stimulate an entire plate of animals, or prodding animals with a

platinum wire to test harsh touch (Chalfie, 2014). These assays have led to a rich understanding of *C. elegans* mechanosensation (Krieg, Dunn, & Goodman, 2015); however, these experiments are largely performed by hand, leading to highly variable mechanical stimuli (Nekimken, Mazzochette, Goodman, & Pruitt, 2017). Therefore, researchers have recently developed several systems to overcome the issue of stimuli variability. These devices take advantage of microfluidic valves—thin PDMS membranes that can be pressurized and inflated to deliver mechanical touch (Figure 1.2A) (Unger, 2000).

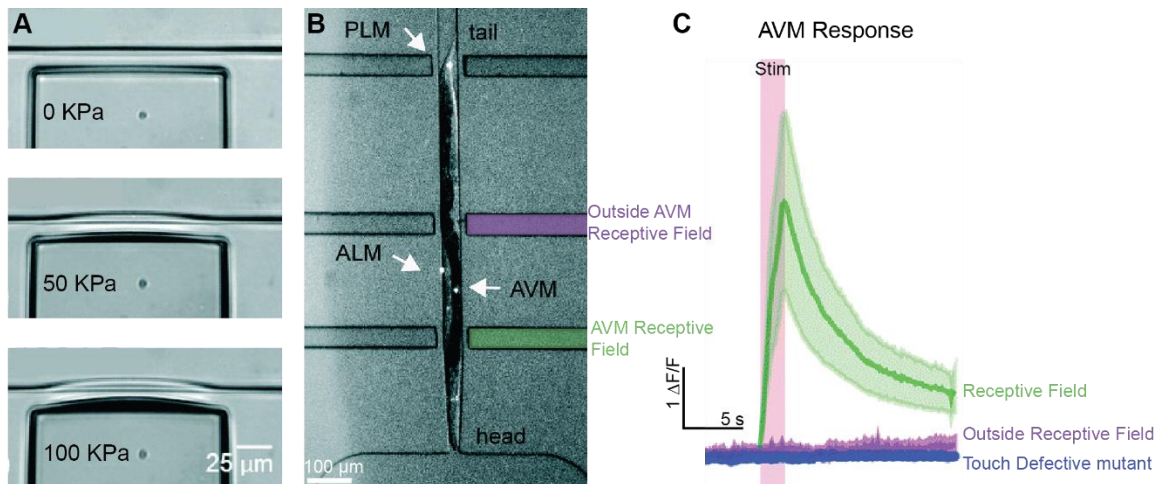


Figure 1.2 – Controlled mechanosensory stimulation with microfluidic valves.

(A) Optical micrographs of a pressurized valve. Increasing the pressure leads to more deflection of the PDMS membrane, which can be used as a controllable mechanical stimulus. **(B)** Combined fluorescent and bright-field imaging of a worm in a trap channel lined with stimulation valves. The valves allow for spatiotemporal control of body touch. Touch-receptive neurons ALM, AVM and PLM express GCaMP6s. **(C)** Example calcium activity of the AVM neuron during mechanical stimulation. Green trace indicates pressurization of the green valve in (B), which is within AVM’s receptive field. Purple trace indicates stimulation with a valve outside of AVM’s receptive field. Blue trace indicates receptive-field stimulation, but in a touch-defective mutant animal. Figure adapted from (Nekimken, Fehlauer, et al., 2017).

Coupled with calcium-imaging in immobilized animals, valve-stimulation can be precisely delivered to points along the worm body and the response of mechanosensory neurons recorded (Figure 1.2B-C) (Y. Cho et al., 2017; Y. Cho, Oakland, Lee, Schafer, & Lu, 2018; Nekimken, Fehlaue, et al., 2017). Because the pressure of the valve can be easily tuned across animals, the stimuli variability is significantly better-controlled than classical methods (Nekimken, Fehlaue, et al., 2017). These devices can be tailored to accommodate small larva (Y. Cho et al., 2018) and automated for high-throughput screenings of drugs that affect mechanosensation (Y. Cho et al., 2017). Likewise, in addition to calcium-imaging, micro-technologies have been developed to deliver mechanical stimulation in moving animals to monitor animal behavioral responses to gentle and harsh touch (McClanahan, Xu, & Fang-Yen, 2017). In this case, not only are stimulations highly controllable, but measurements of behavioral responses are significantly more scalable, providing a path to screening for genes that are involved in mechanosensation.

1.1.3. Sleep

As with many nematode behaviors, *C. elegans* developmental sleep (sometimes referred to as “lethargus”) was initially discovered and characterized on NGM plates (Raizen et al., 2008) (see Section 1.2.1 for a full discussion on developmental sleep). However, recent years have seen a transition to microfluidic platforms (H. Huang, Singh, & Hart, 2017; Nagy, Raizen, & Biron, 2014), to scale

measurements across several animals, confine animals to separated modules, and mitigate the effects of random external stimuli (Figure 1.3). These devices are typically quite simple, mostly using “artificial dirt” micropillars with food added to the chamber for imaging animals over the course of several hours (Figure 1.3). By timing the imaging period to fall during larval transitions, clear periods of behavioral quiescence can be distinguished between larval stages (Nagy, Raizen, et al., 2014). These methods have been applied to studying the mechanisms underlying homeostatic rebound (H. L. Bennett et al., 2018; Nagy, Tramm, et al., 2014), the effects of sleep deprivation on survival (H. L. Bennett et al., 2018), and the critical role of gap junction signaling during sleep (H. Huang et al., 2018).

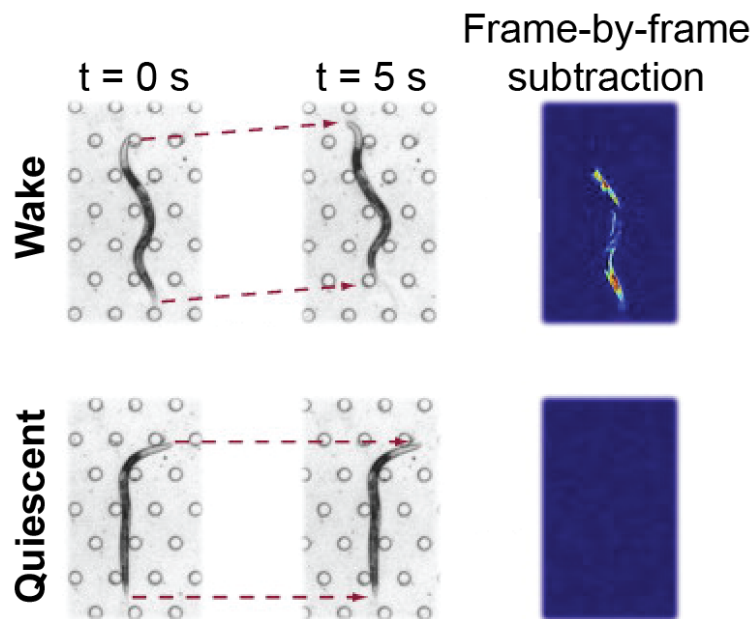


Figure 1.3 – Microfluidics for behavioral monitoring of sleep and quiescence.

Animals are confined to “artificial dirt” behavioral modules (S R Lockery et al., 2008), where microfluidic pillars facilitate crawling in a fluidic environment. Top and bottom image pairs

show a wake and quiescent animals, respectively. Subtracting the consecutive frames allows for easy detection of behavioral quiescent. Figure adapted from (Nagy, Raizen, et al., 2014).

In addition to studying sleep behavior, microfluidic devices have been used to understand the underlying neural mechanisms of sleep using calcium-imaging (J. Y. Cho & Sternberg, 2014; Nichols et al., 2017). Using the olfactory chip design (see Figure 1.1), Cho and Sternberg delivered precise odorant stimuli to animals before, during and after lethargus and showed that the ASH sensory neuron responds with reduced activity during lethargus (J. Y. Cho & Sternberg, 2014). Furthermore, Nichols, *et al.* also used a microfluidic platform to facilitate whole-brain imaging with cellular-resolution during lethargus and observed a large-scale downregulation of neural activity during sleep (Nichols et al., 2017) (discussed in more detail in Section 1.2.1). These reports combined show that microfluidic devices have assisted the study of *C. elegans* sleep by facilitating both behavioral and neural measurements.

1.1.4. Long-term imaging

A significant number of microfluidic technologies have been developed for the sole purpose of long-term monitoring animals (Cornaglia et al., 2016; Cornaglia, Lehnert, & Gijs, 2017; Gupta & Rezai, 2016; San-Miguel & Lu, 2013). Each of the devices discussed here enables imaging at least over 24 hr, providing powerful platforms to monitor aging and development while simultaneously facilitating worm maintenance and allowing for precise control of the external environment.

Due to their short lifespan (3-4 weeks), *C. elegans* are a powerful model for studying aging and development, particularly for understanding the wide range of genetic, metabolic and sensory factors that affect lifespan and longitudinal behavior (Apfeld & Kenyon, 1999; Churgin, Jung, et al., 2017; Herndon et al., 2002; C. Huang, Xiong, & Kornfeld, 2004; S. S. Lee, Kennedy, Tolonen, & Ruvkun, 2003; Murphy et al., 2003; Uno & Nishida, 2016). Classically, as we have seen in previous sections, lifespan experiments are agar-based (Apfeld & Kenyon, 1999; Hsu, Murphy, & Kenyon, 2003; Kenyon, Chang, Gensch, Rudner, & Tabtiang, 1993). Thus, an entire population of animals (30-70 animals) must be confined to a plate with a limited food supply. Therefore, animals must be transferred to fresh plates every few days. In addition, this approach has the disadvantage of requiring chemical treatment with 5-fluoro-2'-deoxyuridine (FUDR) to kill progeny as embryos and avoid the growth of a second-generation animals. Finally, monitoring an intermixed population of animals over the course of days and weeks makes it impossible to track individual animals and study variability.

To overcome these challenges, a wide range of microfluidic and PDMS-based technologies have been developed to enclose and image animals. These devices vary in scalability, depending on the needs of the researcher. Some devices confined only a handful of animals (<20 worms) (Berger et al., 2018; Hulme et al., 2010; Krajniak & Lu, 2010), while others an entire population (50-100 worms) (Chung et al., 2011; Kopito & Levine, 2014; H. Lee et al., 2014; Xian et al., 2013; Zhuo, Lu, & McGrath, 2017). These environments take advantage of the fact that PDMS is permeable to

gas (Tang & Whitesides, 2010), allowing worm modules to maintain a healthy O₂ concentration while dissipating animal byproducts such as CO₂. To further maintain healthy environments, these devices also typically flow a gentle stream of buffer containing an *E. coli* food source, constantly replenishing the food supply (Berger et al., 2018; Hulme et al., 2010; Kopito & Levine, 2014; Krajniak & Lu, 2010; H. Lee et al., 2014; Xian et al., 2013; Zhuo et al., 2017). The ability to flow buffer on-demand also offers a wide-range of advantages over agar-based assays. Geometries have been constructed that automatically wash away embryos and larvae (Berger et al., 2018; Hulme et al., 2010; Kopito & Levine, 2014) and deliver chemical stimuli (Chung et al., 2011; Rohde, Zeng, Gonzalez-Rubio, Angel, & Yanik, 2007) .

Furthermore, some chips have also been tailored for high-resolution imaging of *in vivo* development by incorporating clever methods for animal immobilization (Berger et al., 2018; Kopito & Levine, 2014; Krajniak & Lu, 2010; H. Lee et al., 2014), while others monitor other age and development-related phenotypes such as behavior and developmental arrest (Hulme et al., 2010; Xian et al., 2013; Zhuo et al., 2017). Finally, these technologies also offer the ability to longitudinally monitor individual animals, allowing for powerful studies of individual variability (Berger et al., 2018; Chung et al., 2011; Hulme et al., 2010; Kopito & Levine, 2014; Krajniak & Lu, 2010; H. Lee et al., 2014; Rohde et al., 2007).

1.1.5. Electrophysiology

Previous sections have discussed several microfluidic geometries that facilitate calcium-imaging (Y. Cho et al., 2018; Chronis et al., 2007; Larsch et al., 2013; Zimmer et al., 2009). Calcium-imaging is a powerful, genetically-targeted and non-invasive technique to record neural activity, particularly in transparent *C. elegans* (T.-W. Chen et al., 2013; Kerr, 2006; Tian et al., 2009), but it lacks the temporal resolution of direct electrical recordings such as patch-clamp measurements (Goodman, Lindsay, Lockery, & Richmond, 2012; Molleman, 2002). Patch-clamping from muscle cells (Richmond & Jorgensen, 1999) and neurons (Goodman, Hall, Avery, & Lockery, 1998) has revealed a wealth of information about *C. elegans* neurobiology with unprecedented detail, yet these methods are not scalable and require highly invasive dissections (Goodman et al., 2012). While direct electrical readouts continue to remain one of the most challenging assays in *C. elegans* neurobiology, recent years have seen strong strides towards scalable, non-invasive platforms for electrophysiology using microfluidics (Gonzales et al., 2017; Hu et al., 2013; Shawn R Lockery et al., 2012).

Lockery, *et al.* made the first significant advance in this field with a microfluidic device for recording “electropharyngeograms” (EPGs) — electrocardiogram-like signals from the *C. elegans* pharynx (Shawn R Lockery et al., 2012) (Figure 1.4A). The pharynx is jaw-like organ located near the mouth that almost constantly suctions and grinds food. For more than a decade, the

conventional method for studying the neuromuscular circuits underlying pharyngeal pumping included tightly suctioning the entire worm nose into a micropipette, forming a tight seal for EPGs recordings when paired with a differential amplifier (Raizen & Avery, 1994). Lockery, *et al.* were essentially able to recapitulate this micropipette geometry in microfluidic form (Figure 1.4A). This finding unlocked an entirely new set of experimental capabilities, such as multi-worm EPG recordings and drug screenings (Hu et al., 2013; Shawn R Lockery et al., 2012; Weeks et al., 2016).

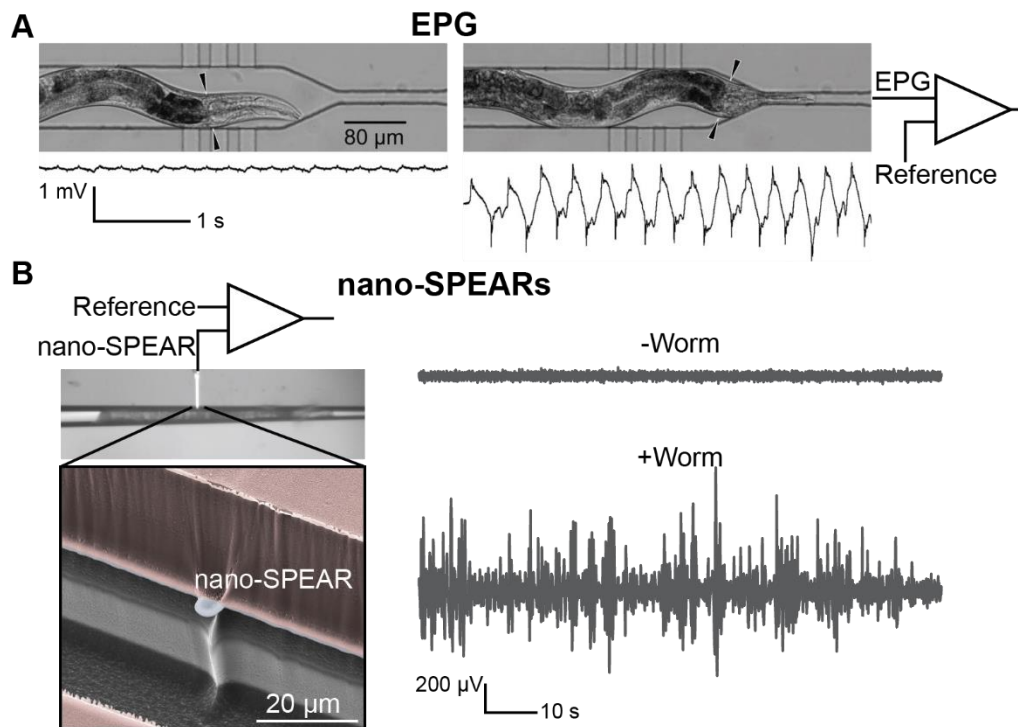


Figure 1.4 – On-chip microfluidic-assisted electrophysiology.

(A) EPG recordings from the *C. elegans* pharynx. By forming a tight seal between the worm pharynx (arrows) and the worm body, a differential amplifier can be used to detect stereotyped neuromuscular electrical activity during pharyngeal pumping. **(B)** Nano-SPEARs for body-wall muscle electrophysiology. Worms are immobilized in a microfluidic channel.

From the wall of the channel, a platinum nanoelectrode—the nano-SPEAR—horizontally protrudes and tightly presses against the worm body wall. This tight seal enables recordings of worm body-wall muscle electrophysiology. Figure adapted from (Gonzales et al., 2017; Shawn R Lockery et al., 2012).

The microfluidic-based EPG was a powerful demonstration for microfluidic-enabled electrical recordings at the pharynx. Similarly, devices have been developed for recording body-wall muscle activity (Gonzales et al., 2017) (Figure 1.4B), from which direct electrical outputs were only possible with patch-clamping (Richmond & Jorgensen, 1999). These hybrid nanoelectronic/microfluidic devices incorporated nanoscale suspended electrode arrays (nano-SPEARs) into a worm immobilization chamber (Figure 1.4B). When animals were restrained in the chamber, the platinum electrode pressed against the body-wall, forming a tight seal and recording body-wall muscle activity (Gonzales et al., 2017) (Figure 1.4B). Like EPG recordings, this technology dramatically improved experimental throughput by recording from multiple animals in parallel (Gonzales et al., 2017), and was also adapted to record from the cnidarian *Hydra* (Badhiwala, Gonzales, Vercosa, Avants, & Robinson, 2018).

1.1.6. High-throughput screenings

Many of the discussed technologies thus far improve experimental throughput compared to classical assays, often allowing for measuring from tens of animals simultaneously (Gupta & Rezai, 2016; San-Miguel & Lu, 2013; Yanik, Rohde, & Pardo-Martin, 2011). While many of these experiments can indeed qualify as “high-throughput,” particularly when compared to studies with mammalian models,

this section will cover several high-throughput screening and sorting technologies that have an experimental throughput greater than 100 animals per day.

Geometrically simple devices using arrays of clamp-like traps have been developed for immobilizing more than a hundred animals simultaneously for high-resolution imaging (Hulme, Shevkoplyas, Apfeld, Fontana, & Whitesides, 2007; H. Lee et al., 2014). By simply flushing in a population of animals, the traps can be filled and animals held for minutes or hours of imaging cellular and sub-cellular structures (Figure 1.5). An ideal case-study for the power of this simple technique comes in the form of a multiplexed clamp array for an ultra-high-throughput platform for drug discovery (Mondal et al., 2016) (Figure 1.5). Rather than using a single microfluidic chip that immobilizes dozens of animals with clamp traps, multiple microchips capable of immobilizing 40 animals each can be incorporated onto a 96-well plate for immobilizing nearly 4000 animals simultaneously (Figure 1.5). After loading, a camera on an automated stage approaches each microarray and captures high-resolution images of each subset of animals, a process that takes only 16 min for the entire 4000-animal device (Figure 1.5). This technique allows for a throughput that dwarfs any other current microfluidic screening technologies, reaching screening rates of nearly 14,000 animals/hr. Researchers have specifically used this technology to study *C. elegans* poly-glutamine (PolyQ) aggregation, which is relevant to Huntington's disease in humans. By quantifying PolyQ aggregation with fluorescence microscopy, they screened 1000 FDA-approved drugs to search

for those that significantly reduced aggregation and may be potential treatments for humans (Mondal et al., 2016) (Figure 1.5).

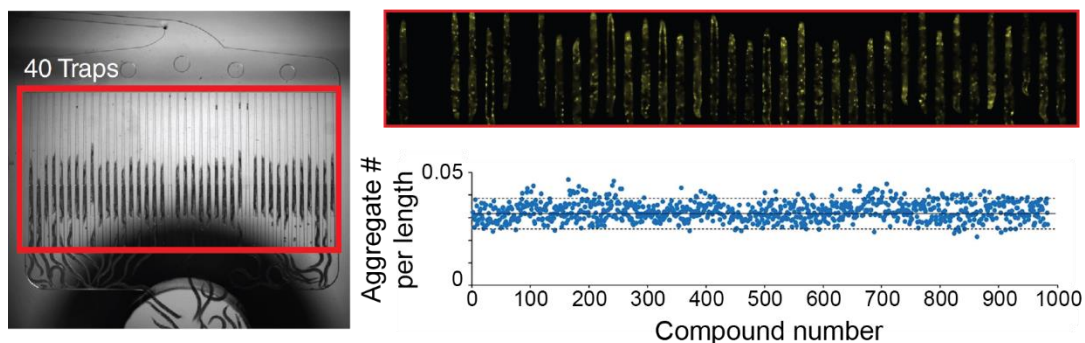


Figure 1.5 – High-throughput microfluidic drug screening.

Left micrograph shows a microfluidic device capable of immobilizing up to 40 animals simultaneously. Many of these trap devices are integrated onto a 96-well plate. Thus nearly 4000 animals are immobilized simultaneously. In this case, researchers used a *C. elegans* Huntington's disease model in which PolyQ aggregation serves as a proxy for disease progression. An automated stage and fluorescence microscopy are used to count the number of PolyQ aggregates (see fluorescence micrograph) in all 4000 animals within 16 min. Researchers used this high-throughput device to screen 1000 FDA-approved drugs to search for compounds that reduce PolyQ aggregation (bottom right). Figure adapted from (Mondal et al., 2016).

Similar to screening for potential drug treatments, high-throughput high-resolution imaging has also revealed the genetic basis of synaptogenesis (Crane et al., 2012). This technology images only single animals, but can do so rapidly, automatically, and with subcellular imaging resolution; importantly, this device also has the advantage of sorting animals based on the imaging results (Chung, Crane, & Lu, 2008). A fully-autonomous version of this technology not only allowed for imaging individual GFP-tagged synapses at a rate of 220 animals/hr, but machine-

vision algorithms could detect distinguish phenotypes based on synaptic morphology not visible by-eye (Crane et al., 2012). With a large-scale forward screen, these researchers detected morphological outliers, screened ~20,000 haploid genomes, and identified 60 mutant strains with altered synaptic phenotypes (Crane et al., 2012).

1.1.7. Conclusions on *C. elegans* microfluidics

This review section only scratches the surface of the vast number of microfluidic technologies available for *C. elegans* (Cornaglia et al., 2017; Gupta & Rezai, 2016; San-Miguel & Lu, 2013; Yanik et al., 2011). Even in this brief review, it is clear that microfluidics has provided many experimental advantages across a wide range of subfields. Microchips allow for precise spatiotemporal control of the environment; chemicals, odorants, gas concentrations and food availability can all be dynamically modulated. The geometry of the chambers can also be tailored to allow for swimming, crawling, or immobilization in single and multi-animal modules. Regardless of the geometric configuration, behavioral measurements from dozens of animals per day are often achievable. Finally, these microchips also commonly facilitate calcium-imaging for understanding the neural circuits underlying sensory perception and behavior. Indeed, though microfluidic technologies were developed for *C. elegans* more than a decade ago (Chronis et al., 2007), these devices continue to be relevant and provide powerful advantages for behavior and neurobiology.

In Chapter 2, we will see many of these elements combined when revealing the mechanisms underlying a microfluidic-induced behavioral transition we call μ Sleep. The microfluidic platform will allow for precise control of the environment and mechanical geometry, facilitate behavioral and neural recordings, and enable high-throughput measurements. All of these aspects strengthen our findings and make for a promising future using *C. elegans* μ Sleep to study the neural circuits underlying *C. elegans* sleep behavior.

1.2. Review of *C. elegans* sleep and quiescence

Sleep is one of the most widely conserved behaviors across animal phyla (Campbell & Tobler, 1984); however, only relatively recently has sleep in genetically-tractable, small model organisms been discovered (Kayser & Biron, 2016; Miyazaki, Liu, & Hayashi, 2017; Zimmerman, Naidoo, Raizen, & Pack, 2008). Periods of quiescence in fruit flies (J. C. Hendricks et al., 2000), zebrafish (Zhdanova, Wang, Leclair, & Danilova, 2001), *Aplysia* (Vorster, Krishnan, Cirelli, & Lyons, 2014), nematodes (Raizen et al., 2008), and jellyfish (Nath et al., 2017) have all been established as sleep or sleep-like states (“sleep-like” is an often-used term used to describe invertebrate sleep states, though these behaviors often meet all the classical requirements of sleep). These discoveries have opened new paradigms of research into the molecular, genetic and neural control of sleep and wakefulness, and many of the mechanisms discovered in small animals are conserved in mammals (Kayser & Biron, 2016; Miyazaki et al., 2017; Zimmerman et al., 2008).

In Chapter 2, we will demonstrate that *C. elegans* μ Sleep—brief periods of quiescence in microfluidic devices—is a spontaneous sleep state. Many of the experiments we performed at the behavioral, neural, and environmental level to establish μ Sleep were informed by a decade of research in invertebrate sleep by the *C. elegans* community. It is well-established that *C. elegans* exhibits many quiescent behaviors, some of which are classified as sleep (Kayser & Biron, 2016; Nicholas F. Trojanowski & Raizen, 2016; Zimmerman et al., 2008). This section will review these sleep and quiescent behaviors. Overall, we will find that research with *C. elegans* has contributed a rich amount of knowledge describing the mechanisms that drive worm sleep and wakefulness, yet there are still many questions left to be answered regarding the neural circuits underlying these behavioral states and the evolutionary purpose of these sleep states.

1.2.1. Developmental Sleep

C. elegans exhibit developmentally-time sleep (DTS) between larval transitions (Raizen et al., 2008). There are four larval stages each lasting 12-16 hr before the transition to adulthood (Figure 1.6A) (Cassada & Russell, 1975; Corsi, Wightman, & Chalfie, 2015). Between each larval stage is a 1-2 hr period of lethargus (Figure 1.6A), where animals form a new outer cuticle.

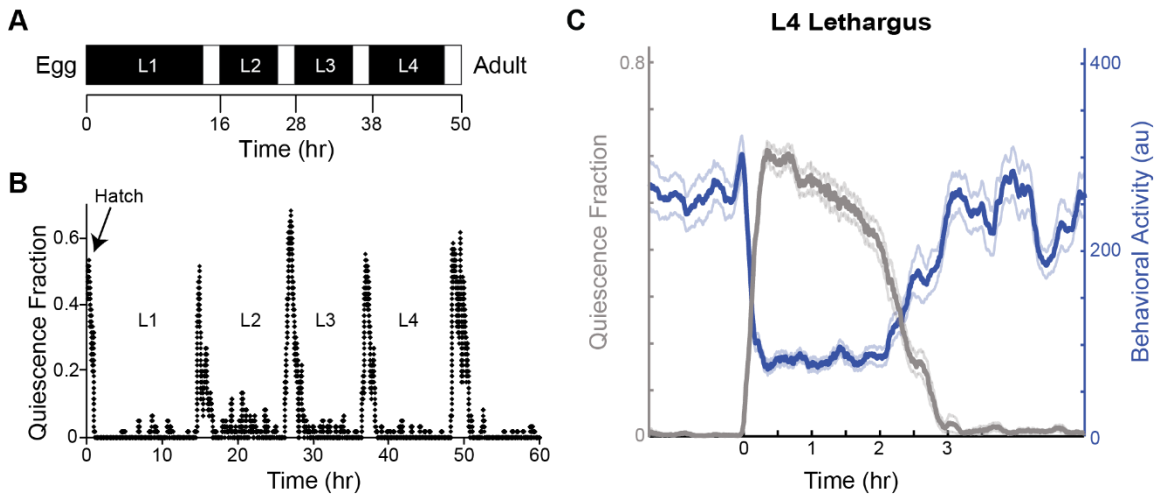


Figure 1.6 – Developmentally-timed sleep during *C. elegans* lethargus.

(A) *C. elegans* stages of development between hatching and adulthood. Larval stages are labeled in black and white portions between stages indicate lethargus. (B) Synchronized with lethargus, are periods where animals begin to exhibit quiescent bouts, leading to a high fraction of animals displaying quiescence across the population. (C) Data from only L4 lethargus. Animal behavioral activity (i.e. movement) falls as the quiescence fraction dramatically increases. Figure adapted from (Iwanir et al., 2013; Raizen et al., 2008).

During lethargus, *C. elegans* exhibit distinctly different behaviors compared to baseline activity (Cassada & Russell, 1975; Raizen et al., 2008) (Figure 1.6B-C). Pharyngeal pumping drops dramatically from 150-250 pumps/min to only ~ 1 pump/min (Cassada & Russell, 1975). In addition, animals display brief bouts of quiescence compared to their normal behavior of near-constant locomotion (Figure 1.6C). For example, Raizen *et al.* observed that L4 lethargus lasted an average of 2.6 ± 0.1 hr, during which animals exhibited a total of 46.6 ± 3.1 min of quiescence with quiescent bouts lasting an average of 24.0 ± 0.7 s (Raizen et al., 2008). At the time, Raizen, *et al.* hypothesized that, similar to the discovery that *Drosophila* rest

periods were sleep (J. C. Hendricks et al., 2000), *C. elegans* quiescence during lethargus was also a sleep state. Indeed, they found that quiescent animals:

- Resumed normal locomotion following tail stimulation
- Showed a decrease in sustained behavioral responses to mechanosensory stimulation (dish taps)
- Showed an increased response latency to chemical stimulation (1-octanol and ethanol)
- Displayed longer quiescent bouts after an extended period of quiescence deprivation.

Thus, they showed that *C. elegans* quiescence is a sleep state, termed “developmentally time sleep” (DTS), that meets some of the basic behavioral criteria for sleep, namely reversibility, a decreased response to stimuli and homeostasis (Campbell & Tobler, 1984).

This pivotal work led to a number of studies that further characterized DTS behavior. Quiescent *C. elegans* exhibit a characteristic “hockey-stick” posture with less body curvature and decreased muscle activity, showing that DTS meets another standard behavioral requirement of sleep—stereotypical posture (Campbell & Tobler, 1984; Iwanir et al., 2013; Schwarz, Spies, & Bringmann, 2012; Tramm, Oppenheimer, Nagy, Efrati, & Biron, 2014). In addition, it was also found that the quiescent bout length increased as the previous motion bout length increased

(Iwanir et al., 2013). This observation differs from sleep deprivation assays with external stimuli and suggests a micro-homeostatic mechanism regulates DTS at short timescales. Furthermore, forced sleep deprivation through mechanical stimulation can be lethal following lethargus (Driver, Lamb, Wyner, & Raizen, 2013). However, similar to recent results in fruit flies (Geissmann, Beckwith, & Gilestro, 2019), *C. elegans* sleep deprivation via genetic manipulations surprisingly does not lead to death following lethargus, suggesting that normal DTS bouts are not essential for survival (H. L. Bennett et al., 2018; Wu et al., 2018). Therefore, DTS behaviorally shares much in common with mammalian sleep (reversibility, stereotypical posture, and homeostasis), but some aspects appear to be unique to *C. elegans* and other invertebrates (essential for survival).

In addition to meeting many conserved behavioral criteria for sleep, *C. elegans* DTS also shares many common genetic and molecular pathways with mammalian and *Drosophila* sleep (Table 1.1) (Kayser & Biron, 2016; Nicholas F. Trojanowski & Raizen, 2016; Zimmerman et al., 2008). Notably, the *Drosophila* PERIOD gene regulates circadian rhythms and cycles in expression with light/dark cycles (Hardin, Hall, & Rosbash, 1990). Likewise, LIN-42, the *C. elegans* homologue of PERIOD, cycles in expression with lethargus and is essential for rhythmically timed DTS (Monsalve et al., 2011; Nicholas F. Trojanowski & Raizen, 2016). In addition, Protein-Kinase G (PKG) signaling promotes sleep across multiple species, as well as many *C. elegans* sleep-like behaviors (Raizen et al., 2008; Nicholas F. Trojanowski & Raizen, 2016). Gain-of-function mutants in the *C. elegans* cyclic

guanosine monophosphate (cGMP)-dependent PKG homologue, EGL-4, causes increased quiescence and arousal threshold, even outside of DTS (Raizen et al., 2008; Nicholas F. Trojanowski & Raizen, 2016). These pathways, in addition to others such as epidermal growth factor (EGF) and dopamine signaling (Table 1.1) (Singh, Ju, Walsh, DiIorio, & Hart, 2014; C. Van Buskirk & Sternberg, 2010; Cheryl Van Buskirk & Sternberg, 2007), demonstrate that *C. elegans* DTS not only displays evolutionarily-conserved behavioral criteria, but also genetic and signaling pathways consistent with sleep in other species.

Table 1.1 – Genetic and molecular conservation of *C. elegans* sleep.

Many genetic and signaling pathways are conserved in mammals and invertebrates such as *Drosophila* and *C. elegans*. Table adapted from (Nicholas F. Trojanowski & Raizen, 2016).

	MAMMALS	DROSOPHILA	C. ELEGANS
PERIOD REGULATES TIMING	Yes	Yes	Yes
PDF PROMOTES WAKE	Unknown	Yes	Yes
EGF PROMOTES SLEEP	Yes	Yes	Yes
CAMP PROMOTES WAKE	Yes	Yes	Yes
DOPAMINE PROMOTES WAKE	Yes	Yes	Yes
PKG REGULATES SLEEP	Yes	Yes	Yes

Calcium-imaging has proven to be a powerful method for understanding the neural mechanisms of DTS. Imaging during mechanical and chemical stimulation

revealed that the sensory neurons ALM and ASH, respectively, showed a decreased calcium response to stimuli during lethargus (J. Y. Cho & Sternberg, 2014; Schwarz, Lewandrowski, & Bringmann, 2011). Furthermore, ASH chemosensory neurons also showed decoupled and asynchronous activity with downstream interneurons (J. Y. Cho & Sternberg, 2014). These results provided an elegant neural mechanism describing why *C. elegans* showed latent and reduced responses to external stimuli during DTS (Raizen et al., 2008). Other studies present strong evidence that a single interneuron, RIS, drives behavioral quiescence (Figure 1.8) (Spies & Bringmann, 2018; Turek et al., 2016, 2013; Wu et al., 2018). RIS not only depolarizes and becomes more active at the onset of behavioral quiescence, but optogenetic activation of RIS induces behavioral quiescence, a process mediated by FLP-11 neuropeptides (Figure 1.8) (Turek et al., 2016, 2013).

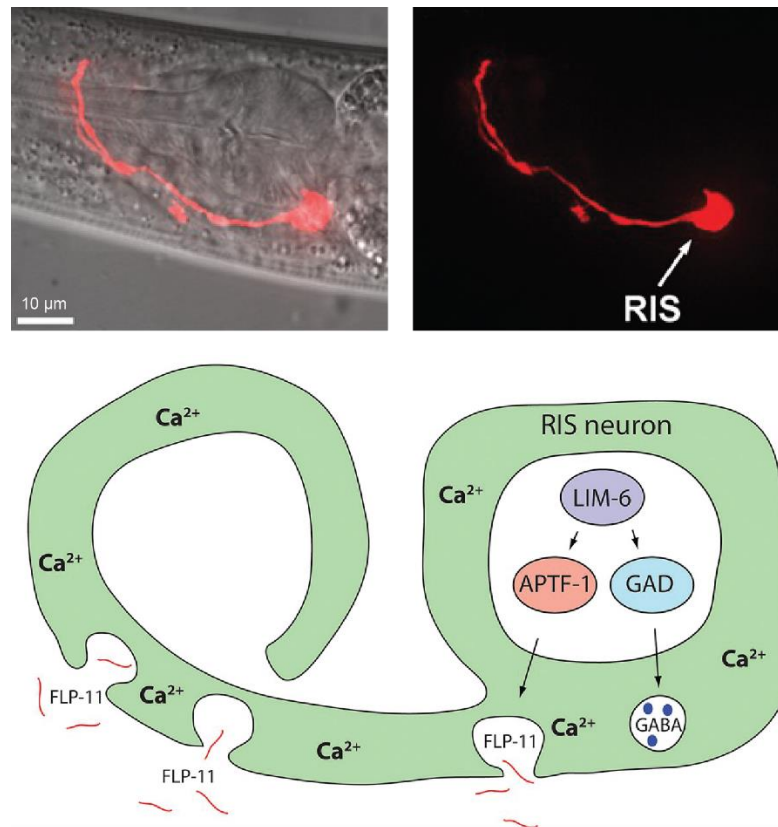


Figure 1.7 – Model for *C. elegans* sleep driven by the RIS neuron.

Proposed neural mechanism for sleep via the RIS neuron. (Top) Fluorescent micrographs of the RIS neurons expressing mKate. (Bottom) Proposed mechanism for sleep. At the onset of sleep, RIS increases in calcium activity, depolarizes, and releases the FLP-11 neuropeptide that induces whole-animal behavioral quiescence. Figure adapted from (Turek et al., 2016).

Finally, whole-brain calcium imaging has revealed that a distinct brain state governs DTS (Figure 1.8) (Nichols et al., 2017). These experiments were enabled by the discovery that quiescent bouts in the *npr-1* mutants strain were essentially controllable via a large, rapid change in environmental oxygen levels during lethargus (Figure 1.8A) (Nichols et al., 2017). During lethargus and at 21% O₂, *npr-1* animals were largely active and roamed an agar plate (Figure 1.8A). However,

shifting the O₂ level to 10% lead to a rapid behavioral state change to quiescence (Figure 1.8A), essentially activating developmental sleep on-demand (Nichols et al., 2017). Nichols *et al.* took advantage of their on-demand sleep-wake switch to image whole-brain calcium activity during each behavioral state (Figure 1.8B). Similar to distinct global-brain activity states revealed by EEG in mammals (Brown et al., 2012; Saper et al., 2010), *C. elegans* exhibit a large-scale downregulation of neural activity during DTS (Figure 1.8B) (Nichols et al., 2017). However, not every neuron displayed less activity. Consistent with our previous discussion (Turek et al., 2016, 2013; Wu et al., 2018), the RIS neuron actually increased in activity suggesting that a unique brain state governs *C. elegans* sleep in a manner synonymous to mammalian sleep (Brown et al., 2012; Saper et al., 2010). Furthermore, this same brain state was later observed in adult animals spontaneously transitioning between sleep and wakefulness after an extended 16 hr period of starvation, demonstrating that downregulated neural activity is a general hallmark of *C. elegans* sleep (Skora, Mende, & Zimmer, 2018). The methods used for these whole-brain recordings are discussed in more detail in Section 1.3.2.

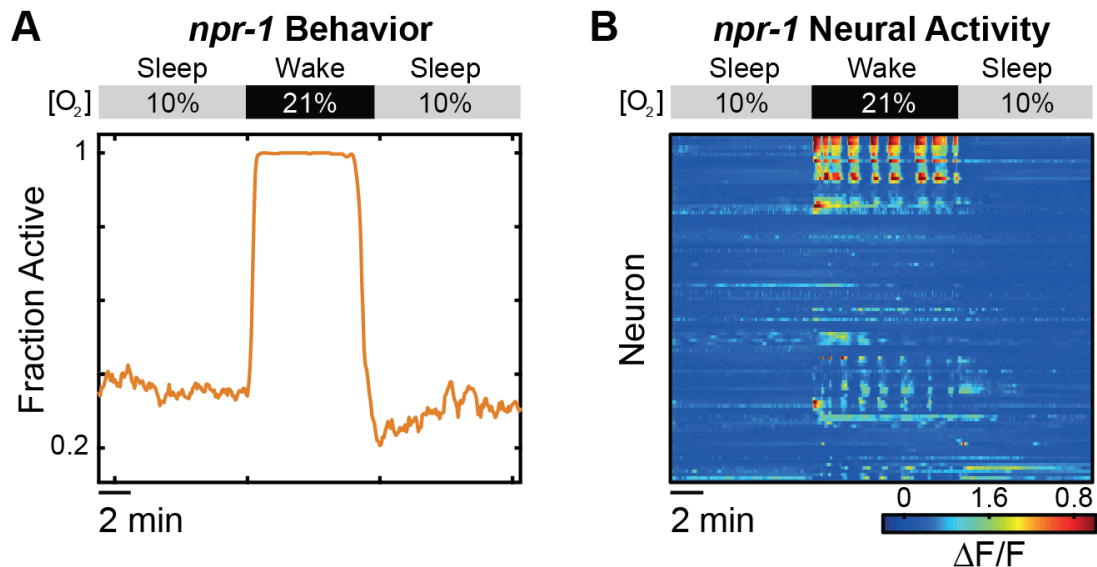


Figure 1.8 – A global-brain state underlies *C. elegans* sleep.

(A) During L4 lethargus wake and sleep behavior can be controlled in *npr-1* animals. 10% oxygen levels artificially induce a DTS and quiescence, while 21% oxygen drive wake behavior. (B) Whole-brain recordings during sleep-wake switching with oxygen control (>100 neurons). The wake state is characterized by large-scale coordinated activity. The sleep state exhibits a global downregulation of activity, demonstrating that distinct brain states govern *C. elegans* sleep and wakefulness. Methods for whole-brain imaging discussed in more detail in Section 1.3.2. Figure adapted from (Nichols et al., 2017).

1.2.2. Environmentally-induced sleep and quiescence

Outside of DTS, *C. elegans* quiescence has only been observed under specific environmental and genetic manipulations. Surprisingly, after sleeping during lethargus during their first ~3 days as larvae, *C. elegans* adults maintained in favorable conditions appear to no longer need sleep throughout their final 3-4 weeks of life (Kayser & Biron, 2016). However, in environments such as extreme heat or extended periods of swimming, animals exhibit distinct periods of quiescence. In this section, we will review these reported quiescent behaviors and

see many similarities with μ Sleep (presented in Chapter 2) as well as the genetic and molecular mechanisms of DTS (reviewed in Section 1.2.1). These quiescent and sleep behaviors are interesting in their own respect, particularly from the perspective of how the *C. elegans* nervous system controls these behavioral states.

1.2.2.1. Stress-induced sleep

When under environmental stress, *C. elegans* enter a protective sleep state, termed “stress-induced sleep” (SIS) (Figure 1.9) (Hill et al., 2014). SIS can occur at any stage of development but is most often studied in adult animals. The types of stressors that have been shown to drive SIS are:

- Heat shock (30-40 °C, 30-60 min)
- Cold shock (-15 °C, 15 min)
- Osmotic shock (500 mM NaCl, 15 min)
- Toxin exposure (Cry5B toxin, 15 min)
- UVC irradiation (500-2500 J/m², 30 min)

(DeBardeleben, Lopes, Nessel, & Raizen, 2017; Hill et al., 2014). Like DTS, SIS is hallmarked by a cessation of both feeding and locomotion (Figure 1.9) (Hill et al., 2014); however, these quiescent behaviors are driven by at least partially distinct mechanisms (N. F. Trojanowski, Nelson, Flavell, Fang-Yen, & Raizen, 2015). In

addition, the severity of the stressor determines the length of time animals spend quiescent (DeBardeleben et al., 2017; Jones & Candido, 1999).

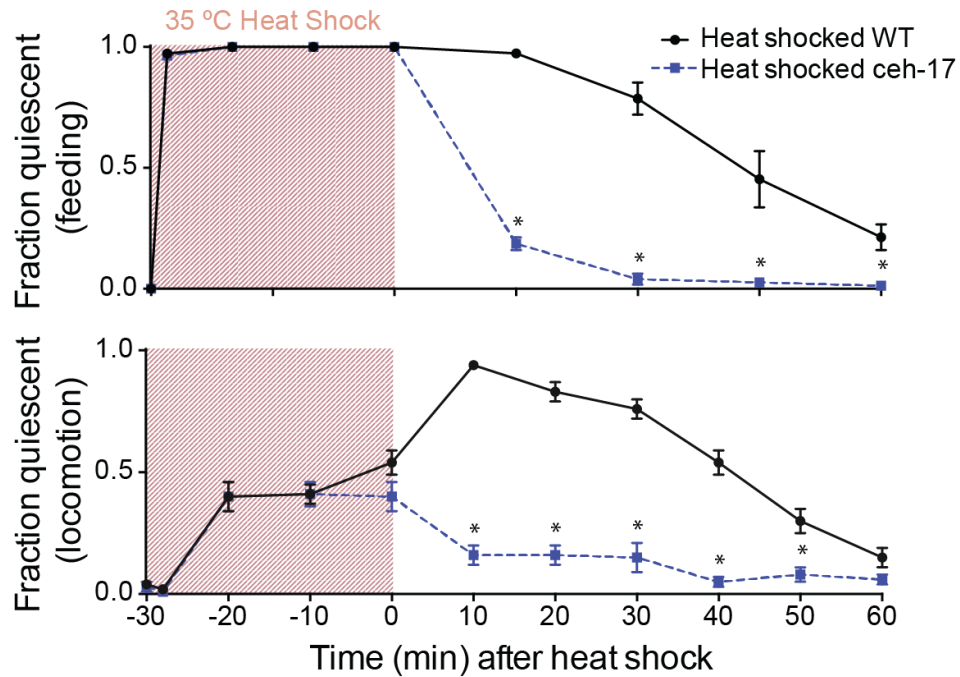


Figure 1.9 – *C. elegans* stress-induced sleep.

Stress-induced sleep via heat shock. A 35 °C heat shock for 30 min rapidly induces feeding quiescence (top, animal cease pharyngeal pumping) and locomotion quiescence (bottom, animals cease to move). This quiescence persists for up to an hour in WT animals (black trace), depending on the stimulus strength. ALA defective mutants, *ceh-17(lf)*, show less quiescence during the recovery period following the stimuli. Figure adapted from (Hill et al., 2014).

Similar to DTS, SIS meets some of the basic behavioral criteria for sleep (Hill et al., 2014). Namely, quiescence is reversible when animals receive a harsh mechanical stimuli and animals showed a decreased response to brief exposures of blue light and 1-octanol (Hill et al., 2014). However, unlike DTS, SIS has yet to be associated with a homeostatic response to sleep deprivation (Nicholas F.

Trojanowski & Raizen, 2016). This is likely because the sleep pressure associated with SIS is driven by environmental changes and not circadian factors or developmental timing. In fact, while light and temperature cycling can lead to circadian-like behavioral patterns and genetic expression in *C. elegans* (Goya, Romanowski, Caldart, Bénard, & Golombek, 2016; Saigusa et al., 2002; Simonetta, Migliori, Romanowski, & Golombek, 2009), it remains untested whether circadian factors strongly regulate sleep. Furthermore, testing for homeostasis requires sleep deprivation with external stimuli, which has been shown to induce stress responses in *C. elegans* (Driver et al., 2013), making homeostatic rebound and stress-induced sleep difficult to differentiate. Recent advances using optogenetic suppression of sleep-promoting neurons to sleep deprive animals is a clever experimental tool that will certainly be useful for testing for homeostatic rebound in many types of *C. elegans* sleep (Wu et al., 2018).

At the neuronal level, SIS is heavily regulated by a single interneuron, ALA (DeBardleben et al., 2017; Hill et al., 2014; Iannacone et al., 2017; Nath et al., 2016; Matthew D. Nelson et al., 2014, 2015; Cheryl Van Buskirk & Sternberg, 2007). ALA-defective mutants, *ceh-17(lf)* (loss-of-function (lf) in CEH-17, which controls ALA axonal growth), show dramatically reduced quiescence compared to WT following extreme environmental conditions (Figure 1.9) (Hill et al., 2014; Pujol, Torregrossa, Ewbank, & Brunet, 2000). However, while the stimulus is being applied, *ceh-17(lf)* animals exhibit identical amounts of quiescence as WT, indicating that ALA-dependent SIS serves as a means for recovery following cellular stress (Hill et al.,

2014). In fact, following an intense 40 °C heat shock, *ceh-17(lf)* mutants not only display less recovery quiescence, but also a decreased survival compared to WT, providing further evidence that SIS is a protective mechanism (although it should be noted that survival rate remained unchanged at 35 and 37°C heat shocks) (Hill et al., 2014).

There exists very limited knowledge on the neural activity occurring upstream of ALA during SIS, such as how sensory circuits that monitor the external temperature during heat shock drive ALA activity (Pralhad, Cornelius, & Morimoto, 2008). Yet it is well-established that cellular stress from the environment induces the release of the epidermal growth factor (EGF) homologue LIN-3, which triggers ALA activity through the EGF-receptor homologue LET-23 (Figure 1.10) (Hill et al., 2014; Cheryl Van Buskirk & Sternberg, 2007). EGF signaling is also involved in sleep in other species, such as drosophila and mice (Table 1.1) (Foltenyi, Greenspan, & Newport, 2007; Kramer et al., 2001), again demonstrating that *C. elegans* sleep relies on conserved molecular pathways (Kayser & Biron, 2016; Nicholas F. Trojanowski & Raizen, 2016; Zimmerman et al., 2008). EGF leads to ALA depolarization, which is necessary for SIS (Matthew D. Nelson et al., 2014). In fact, optogenetic activation of ALA via channelrhodopsin promotes quiescence-like behavior (Matthew D. Nelson et al., 2014); however, the relationship between ALA neuronal activity and sleep behavior is mediated by a complex interaction between many neuropeptides (Figure 1.10) (Nath et al., 2016; Matthew D. Nelson et al., 2014). Four primary neuropeptides, *flp-24*, *flp-7*, *flp-13* and *nlp-8*, each strongly expressed in ALA, have

been identified as behavioral regulators of SIS (Figure 1.10) (Nath et al., 2016). Each neuropeptide plays a unique role, for example, *flp-13* release strongly inhibits pumping, thus driving feeding quiescence. Furthermore, while *flp-13*, *flp-24* and *nlp-8* individually have an insignificant effect on locomotion, the combined release of these peptides together drives the characteristic cessation of locomotion associated with SIS (Nath et al., 2016). While it remains to be tested what neurons these neuropeptides act on, these results from Nath *et al.* (2016) give insightful clues into how a single neuron like ALA can drive whole-animal quiescence and sensory deprivation (Figure 1.10). These results also demonstrate the power and flexibility of using neuromodulators to control behavior.

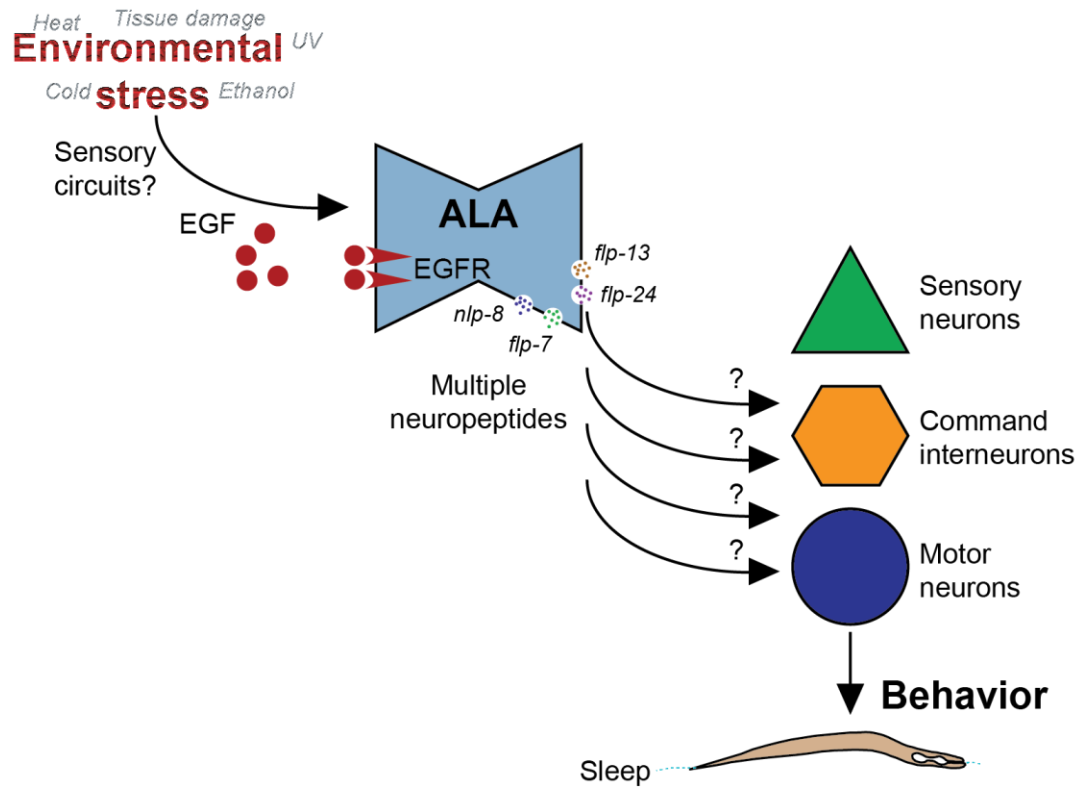


Figure 1.10 – Model for *C. elegans* stress-induced sleep.

Environmental triggers lead to cellular stress and EGF release. The role of sensory circuits is unclear. EGF-receptors lead to ALA depolarization and the release of many neuropeptides. Each neuropeptide plays a role in driving whole-animal quiescence (e.g. feeding quiescence and locomotion quiescence), but it is unclear on what circuits these peptides act. This neural activity downstream of ALA leads to sleep behavior. Figure adapted from (Hill et al., 2014; Nath et al., 2016).

1.2.2.2. Swimming-induced quiescence and neural circuits underlying *C.*

elegans behavioral states

After prolonged swimming (>1 hr) in large volumes of liquid (8-200 μ L), *C. elegans* spontaneously begin to alternate between periods of high activity and quiescence, which we will term “swimming-induced quiescence” (SIQ) (Churgin,

McCloskey, Peters, & Fang-Yen, 2017; R. Ghosh & Emmons, 2008, 2010; McCloskey, Fouad, Churgin, & Fang-Yen, 2017). Ghosh and Emmons (2008) initially discovered and characterized this behavior in multi-well plates (Figure 1.11). When individual animals were placed in 200 μ L of buffer in the absence of food, animals immediately swam with fast undulations continuously for a period averaging 92.6 ± 2.5 min (mean \pm sem) (Figure 1.11B). After this prolonged swimming, animals initiate a different sequence of behaviors and rapidly transition in and out of quiescence for several hours (Figure 1.11B). Excluding the first, long swimming bout, animals displayed motion bouts lasting 14.0 ± 0.5 min and quiescent periods lasting 4.8 ± 0.1 min, with transitions between each behavioral state lasting only 6.9 ± 1.3 s. It was found that acetylcholine (ACh, acting on many parts of the neuromuscular system) and PKG signaling (homologue EGL-4, acting in sensory neurons) promoted quiescence, while the protein phosphatase calcineurin homolog, TAX-6, (also acting in sensory neurons) promoted swimming (R. Ghosh & Emmons, 2008, 2010).

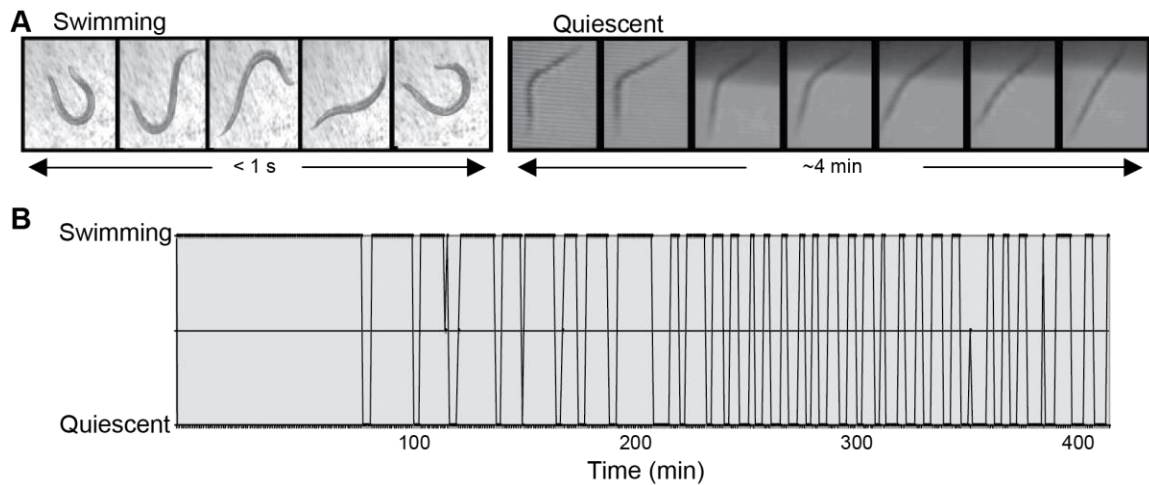


Figure 1.11 – Extended swimming induces spontaneous quiescence.

(A) Comparison of *C. elegans* swimming (left, rapid undulations that occur at 2-4 Hz) and quiescence (right, near motionless for several minutes). **(B)** Representative data from an animal during swimming-quiescence switching. The animal swims continuously for ~90 min, then begins to spontaneously transition between swimming and quiescence throughout the duration of the 6 hr recording. Figure adapted from (R. Ghosh & Emmons, 2008).

Sleep criteria, such as a decreased response to stimuli, have not been observed for SIQ. However, it was indeed found that the quiescent state is rapidly reversed when animals were mechanically prodded after 1 min of entering quiescence (R. Ghosh & Emmons, 2008). In fact, after prodding, animals resumed a swimming bout of normal length (16 ± 1.5 min), rather than transiently responding to stimuli before quickly returning to the quiescent bout as seen in DTS and SIS (Hill et al., 2014; Raizen et al., 2008). Yet, if animals were prodded within 1 min of quiescence, the response was significantly reduced from 100% to 40%. This interesting effect was found to be due to ACh signaling, which remained high during the first minute of quiescence and prevented animal swimming (R. Ghosh &

Emmons, 2008). Thus, it is unclear if sensory circuits are in a reduced activity state and respond differently to external stimuli during SIQ.

While the initial observation and characterization of SIQ occurred in multi-well plates with 200 μ L of buffer and no food (R. Ghosh & Emmons, 2008, 2010), more recent studies have used WorMotel devices to further understand the environmental and neural factors that regulate motion and quiescence bouts (Churgin, McCloskey, et al., 2017; McCloskey et al., 2017). WorMotel is a multi-well, PDMS-based device that essentially miniaturizes a standard multi-well plate in order to confine and image large numbers of individual animals longitudinally (Churgin, Jung, et al., 2017). WorMotel studies can be conducted in either small volumes of buffer (8-12 μ L) or on agar pads (Figure 1.12).

In WorMotel, it was discovered for the first time that SIQ is in fact not limited to fluidic environments, as initially observed (Figure 1.12) (R. Ghosh & Emmons, 2008). When swimming in the absence of food, like multi-well plates, approximately 5 min-long quiescent bouts began to emerge after approximately 1 hr (Figure 1.12) (McCloskey et al., 2017). When animals were instead placed on agar pads with no food source, SIQ continued to be observed but on a dramatically different timescale, with the first quiescent bout occurring after approximately 3 hours of continuous crawling and averaging 15 min in length (Figure 1.12) (McCloskey et al., 2017). It was also found that quiescent bouts after 16 hr in WorMotel are approximately 300% longer than quiescent bouts within the first 2 hr of imaging, suggesting that

quiescence is related to the time away from food (McCloskey et al., 2017). These results strongly suggest that “swimming induced quiescence” likely falls under a broader umbrella of starvation-induced quiescence, regulated by the metabolic state and food availability.

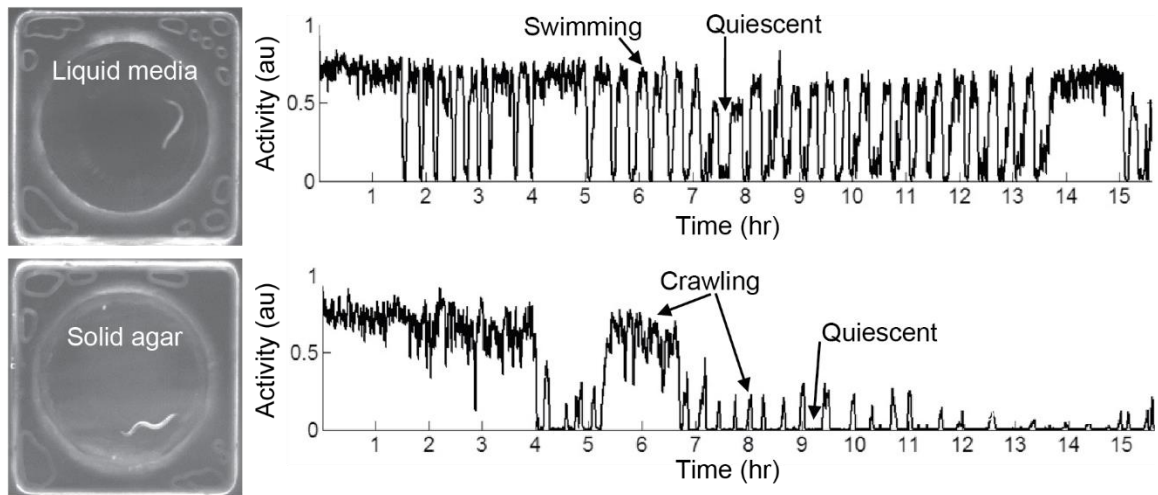


Figure 1.12 – *C. elegans* spontaneously transition to quiescence in both solid and liquid environments.

Representative data demonstrating that both swimming (top) and crawling (bottom) *C. elegans* eventually exhibit quiescence behavior in the absence of food. Notably, quiescence onset is significantly delayed in crawling animals. Figure adapted from (McCloskey et al., 2017).

Indeed, it was observed that the amount of time animals spend active and quiescent can change dramatically in different food concentrations; however, food also promoted a third behavioral state, termed “dwelling” (McCloskey et al., 2017). During dwelling, animals are generally sedentary, exhibit very little body movement, and remain in one place to feed, as opposed to the high-activity

displayed during swimming or crawling (Ben Arous, Laffont, & Chatenay, 2009; Flavell et al., 2013). As with SIS and DTS (Hill et al., 2014; Raizen et al., 2008), EGL-4, promoted the low-activity behaviors (i.e. quiescence and dwelling) (McCloskey et al., 2017). Likewise, insulin-like signaling, which is known to play a powerful role in food sensation and satiety (Avery, 2010), also regulated transitions between roaming, dwelling and quiescence during fasting and in the presence of food (McCloskey et al., 2017).

Further work in WorMotel interrogated the specific neural circuits underlying these behavioral states and demonstrated the complex nature of behavioral regulation in different environments (Churgin, McCloskey, et al., 2017). Serotonin was found to be highly important for regulating food-based behaviors, promoting roaming when released by the ADF neurons but suppressing roaming when released by the NSM neurons (Churgin, McCloskey, et al., 2017). Conversely, octopamine regulated behavior in fasting environments, promoting roaming via the RIC neurons (Churgin, McCloskey, et al., 2017). Thus, not only does chemical signaling promote or suppress behavioral states in *C. elegans*, but the precise neural origin of the signaling pathway strongly influences the behavioral output. This intricate interaction leads to highly flexible behavioral adaptation in varying mechanical, chemical and satiety conditions, regulating transitions between the behaviors we came across in this section: roaming, dwelling and quiescence (Churgin, McCloskey, et al., 2017; R. Ghosh & Emmons, 2008; McCloskey et al., 2017).

This section is a case study for how an intriguing behavioral observation (R. Ghosh & Emmons, 2008) can lead to a cascade of work that furthers our understanding of the neural architecture underlying *C. elegans* behavioral states (Churgin, McCloskey, et al., 2017; R. Ghosh & Emmons, 2010; McCloskey et al., 2017). Furthermore, we only touched the surface of how SIQ fits into a broader scheme of *C. elegans* behavior. A significant amount of literature exists studying the genetic, neuromodulatory signaling, and neural activity underlying nematode behavioral state regulation in varying environmental conditions (Avery & You, 2012; Ben Arous et al., 2009; Flavell et al., 2013; Thomas Gallagher, Bjorness, Greene, You, & Avery, 2013; J M Gray, Hill, & Bargmann, 2005; Juozaityte et al., 2017; Sawin, Ranganathan, & Horvitz, 2000; Waggoner, Zhou, Schafer, & Schafer, 1998)

1.2.2.3. Satiety quiescence

In addition to SIQ, *C. elegans* cessation of locomotion and feeding has also been observed in response to high satiety states, termed “satiety quiescence” (Avery & You, 2012; Davis, Choi, Kim, & You, 2018; T. Gallagher, Kim, Oldenbroek, Kerr, & You, 2013; Thomas Gallagher & You, 2014; You, Kim, Raizen, & Avery, 2008). When placed on high- and low-quality food (HB101 and DA837 bacteria, respectively), animals on high-quality food were significantly more likely to exhibit quiescence (You et al., 2008). In addition, animals that were starved for 12 hr, then refed, exhibited dramatically more quiescence on both low- and high-quality food compared to non-starved animals (You et al., 2008). Essentially, conditions of high-

satiety—high food intake, high-quality food, rapid increases in food availability—induced quiescence.

As with many quiescent behaviors we have reviewed, satiety quiescence was found to be strongly regulated by PKG signaling (via the EGL-4 homolog). *egl-4(lf)* mutants exhibited essentially no quiescence, even after fasting, while gain-of-function mutants displayed more satiety quiescence. Furthermore insulin, cGMP, and TGF- β signaling are also necessary for satiety quiescence (You et al., 2008). At the neuronal level, it was found that the ASI neuron responds strongly to high-quality food, suggesting that ASI monitors the nutrition value of the external environment (T. Gallagher et al., 2013). TGF- β signaling via ASI then acts on downstream neurons RIM and RIC through *daf-1* receptors to regulate food intake by controlling feeding behavior and quiescence (T. Gallagher et al., 2013; You et al., 2008). In addition, the ASI neuron works together with other sensory neurons, such as the ASH chemosensory neurons, to monitor the environment and regulate behavior (Davis et al., 2018). When the ASH neurons are active, ASI responses to appetitive stimuli are reduced. Furthermore, when comparing well-fed and starved animals, it was observed that ASH is highly responsive to noxious stimuli in well-fed conditions, but decreases in responsiveness as animals become starved. Conversely, ASI is less sensitive to appetitive stimuli when animals are well-fed, but it more sensitive to food when animals are starved (Davis et al., 2018). Thus, these data provide elegant insight into how sensory neurons that monitor the environment

drive downstream pathways that control feeding, monitor satiety and drive satiety quiescence.

1.2.3. Conclusions and open questions in *C. elegans* sleep

Here, we reviewed prominent *C. elegans* quiescent behaviors.

Developmentally-timed sleep (DTS) occurs on a rhythmic developmental timescale and meets all classical criteria as sleep (Nicholas F. Trojanowski & Raizen, 2016).

Outside of DTS, quiescence has only been observed under specific conditions: stress-induced sleep (SIS), swimming-induced quiescence (SIQ), and satiety quiescence

(Nicholas F. Trojanowski & Raizen, 2016). We also discussed how SIQ likely falls

under a broader behavioral umbrella of starvation-induced quiescence to promote longevity and survival (Wu et al., 2018). Many studies have worked to establish the

genetic and molecular mechanisms underlying sleep (Table 1.1). These have

revealed conserved signaling such as PERIOD regulation of timing, PDF promotion of wake, and EGF promotion of sleep (D. Chen, Taylor, Hall, & Kaplan, 2016;

Monsalve et al., 2011; Raizen et al., 2008; Nicholas F. Trojanowski & Raizen, 2016;

Cheryl Van Buskirk & Sternberg, 2007), demonstrating that these nematodes hold

incredible value for understanding the signaling pathways that control sleep and

wakefulness. Furthermore, researchers have used the powerful genetic toolbox of *C. elegans* to isolate individual neurons that promote sleep, such as ALA and RIS (Hill

et al., 2014; Nath et al., 2016; Turek et al., 2016, 2013). These discoveries have

enabled studies that demonstrate the complex interaction between the external

environment, satiety states, neural activity, chemical signaling, and neuromodulators to drive whole-organism behaviors.

Despite more than a decade of research and insightful studies, there is still much work left to do to fully understand nematode sleep. In the case of developmental sleep, where animals appear to no longer need sleep after the transition to adulthood, there is over-arching question: *Why do nematodes sleep as larvae?* Strong evidence suggests that mammalian sleep is an essential mechanism for waste clearance, memory consolidation, and is critically important for survival (Björn Rasch and Jan Born, 2013; Brown et al., 2012; Stickgold & Walker, 2005; Xie et al., 2013). Yet nematodes appear to only need sleep during development, and thus far there is no evidence to suggest that nematode sleep consolidates their basic memories (e.g. the culture temperature). In addition, DTS is not required for survival into adulthood or a normal lifespan (H. L. Bennett et al., 2018; Wu et al., 2018). If developmentally-timed sleep is non-essential, what is its purpose?

With respect to *C. elegans* sleep states outside of development, how does sleep promote survival in harmful environments? One hypothesis is that *C. elegans* use sleep as a method for energy conservation. “Shutting down” the brain during sleep may allow for physiological resources to be allocated elsewhere for cellular repair. Can this hypothesis also be applied to developmental sleep? Answering these questions in the humble nematode may provide fundamental insight into sleep across phyla.

At the circuit level, there is still much left to reveal about the neural control of *C. elegans* sleep. For example, many studies focus on how ALA and RIS regulate SIS and DTS, respectively, yet there is likely more overlap in these neural mechanisms than the literature suggests (N. F. Trojanowski et al., 2015). RIS was recently found to be involved in a wide range of physiological sleep states outside of lethargus, including starvation-induced sleep (Wu et al., 2018), suggesting that RIS plays a powerful role in SIS as well. Furthermore, few studies probe upstream neural circuits that drive ALA and RIS activity. For example, the heat-shock response is strongly mediated by AFD thermosensory neurons (Prahlad et al., 2008) and genetic manipulations to sensory neurons are known to alter quiescence behavior (Singh et al., 2011); however the direct causal link between sensory circuits and downstream sleep-promoting neurons is like ALA and RIS remains unestablished. Furthermore, although many neuropeptides are released by ALA and RIS to regulate behavior, it remains unclear what circuits and neurons these peptides directly modulate (see Figure 1.10). In addition, the large number of neuromodulators at play—and our inability to record neuropeptide release—dramatically complicate our ability to understand the signaling mechanisms underlying *C. elegans* sleep.

Work that continues to unravel the genetic and micro-circuit mechanisms of *C. elegans* sleep will play an incredibly valuable role in driving forward our understanding of invertebrate sleep. Yet, these nematodes also offer a powerful advantage over other model organism—whole brain imaging—to reveal how sleep behavior emerges from the collective action of brain-wide circuits (Nichols et al.,

2017). As discussed in Section 1.2.1, Nichols *et al.* (2017) discovered for the first time that, as in mammalian sleep, the *C. elegans* nervous systems exhibits a dramatically different brain state during lethargus. Approaches to whole-brain imaging during sleep will not only allow researchers to interrogate the neurons and circuits that govern the sleep brain state, but also reveal how brain-wide activity spontaneously transitions between dramatic brain states.

1.3. Methods for whole-brain imaging in *C. elegans*

In the idealistic neuroscience experiment, animals perform a task, recall a memory, or exhibit specific behaviors while researchers record the activity of every neuron in the nervous system with high temporal resolution. For example, consider a rodent that has the goal of efficiently navigating a maze in order to receive a reward: a prime cut of cheese. The animal must continuously recall unique maze-specific features, follow odors, make decisions based on these cues, then locomote towards to goal. Presumably, all of this information is “encoded” within sensory circuits and acted upon with motor circuits. Thus, by recording whole-brain activity, researchers may be able to disentangle how the brain senses the external environment, compares this data to memory, computes a decision, then performs the chosen locomotive behavior. While there may be many caveats to this hypothesis—such as neuromodulatory signaling not observable by solely recording neural activity—an entire field of neuroengineering is dedicated to capturing the activity of as many neurons in brain as possible.

Their compact nervous system, transparent bodies, simple behaviors, and suite of genetic tools make *C. elegans* one of the few model organisms primed for using combining whole-brain calcium imaging to understand how behaviors emerge from global brain activity. While methods have been developed to record calcium activity in large populations of neurons in rodents (Allen et al., 2017; Ghanbari et al., 2018; T. H. Kim et al., 2016), even the most advanced techniques capture only a small fraction of mammalian brain activity and often lack cellular-resolution. Thus, whole-brain imaging techniques have been developed for small animals such as fruit flies (Aimon et al., 2018; Chhetri et al., 2015; Lemon et al., 2015), zebrafish (Ahrens et al., 2012; Cong et al., 2017; Dunn et al., 2016; Haesemeyer, Robson, Li, Schier, & Engert, 2018; Keller, Ahrens, & Freeman, 2014; D. H. Kim et al., 2017; Prevedel et al., 2014; Wolf et al., 2015), *Hydra* (Badhiwala et al., 2018; Dupre & Yuste, 2017) and *C. elegans* (Kato et al., 2015; Nguyen et al., 2015; Nguyen, Linder, Plummer, Shaevitz, & Leifer, 2017; Nichols et al., 2017; Scholz et al., 2018; Schrödel, Prevedel, Aumayr, Zimmer, & Vaziri, 2013; Venkatachalam et al., 2015). These methods capture large fractions of animal brain activity (>50%), allowing researchers to begin to understand how global brain activity drives simple behaviors and sensory perception.

For *C. elegans*, methods for whole-brain imaging largely exists in two experimental schemes: freely-moving and chemically-paralyzed. This section will review these techniques and their pros and cons and discuss the insights they have given the field of nematode neurobiology. This discussion will demonstrate the

power of whole-brain imaging for revealing fundamental aspects of the global brain states underlying simple behaviors such as locomotion and sleep. Overall, this section will set the stage for whole-brain imaging during μ Sleep state transitions, which we performed in restrained but behaving animals (see Chapter 2).

1.3.1. Whole-brain imaging in freely-moving animals

Whole-brain calcium imaging is ideally performed in freely-moving animals in order to simultaneously quantify neural activity and behavior. For rodents and mammals, engineers envision a small, head-mounted microscope, like Miniscope (K. Ghosh et al., 2011), such that the field-of-view (FOV) remains relatively constant during animal movement. Clearly, for microscopic animals like *C. elegans*, this experimental approach is inadequate. Instead, cellular-resolution calcium imaging (40-60X magnification) in moving animals often requires automated stages that rapidly and precisely track animal movement in real-time to keep the brain within the FOV (Cong et al., 2017; D. H. Kim et al., 2017; Nguyen et al., 2015; Venkatachalam et al., 2015). In addition, imaging the entire brain requires a form of volumetric imaging, such as light-field microscopy (Aimon et al., 2018; Cong et al., 2017; Prevedel et al., 2014; Schrödel et al., 2013), scanning light-sheet microscopy (Ahrens, Orger, Robson, Li, & Keller, 2013; Bouchard et al., 2015; Keller et al., 2014; Wolf et al., 2015), or rapid z-scanning with an objective mounted onto a piezo driver (D. H. Kim et al., 2017; Nguyen et al., 2015; Venkatachalam et al., 2015). Furthermore, once these experimental challenges are overcome, extracting single-

neuron data requires rigorous post-processing, neuron identification, and tracking individual neurons in a moving (often deformable) brain throughout the duration of the recording (Nguyen et al., 2017).

To date, only two research groups have reported accomplishing this incredibly challenging task in *C. elegans* (Nguyen et al., 2015, 2017; Scholz et al., 2018; Venkatachalam et al., 2015). The microscopy systems are quite similar (Nguyen et al., 2015; Venkatachalam et al., 2015). Low magnification imaging and near-infrared illumination captured animal behavior and head position, which was fed into a closed-loop tracking system that controls an automated stage to keep the head position near the center of the FOV (Figure 1.13A). For high-resolution volumetric imaging, researchers implemented a spinning-disk confocal microscope and high-NA objective mounted to a scanning piezo driver, allowing for an imaging rate of 6 vol/s. Notably, these systems also utilized the benefits of two-color ratiometric imaging (Figure 1.13A). Transgenic animals not only expressed the calcium-sensitive indicator GCaMP6s pan-neuronally (T.-W. Chen et al., 2013), but also RFP in the nuclei of all neurons. Therefore, with dual-color excitation and emission, the microscopy system rapidly captured both RFP and GCaMP6s fluorescence simultaneously. The RFP channel can then be used to not only yield neuron locations during post-processing, but also to correct for motion artifacts. Standard calcium-imaging experiments report the normalized fluorescence, $\Delta F/F_0$. However, in a behaving and crawling animal, the GCaMP signal can exhibit pervasive noise. Therefore, calcium-imaging experiments in moving animals often report the

ratio of the GCaMP signal to the RFP control channel, $\Delta R/R_0$, reducing motion artifacts.

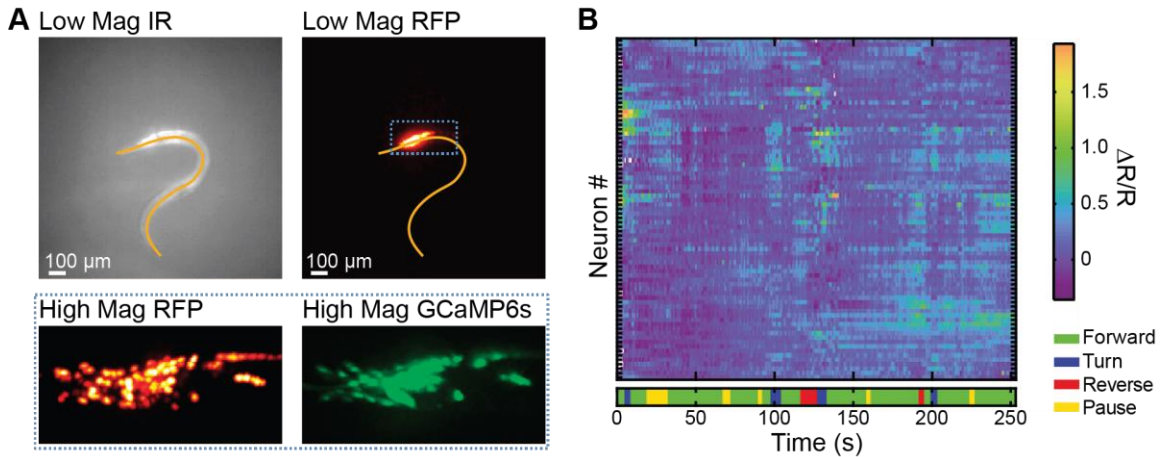


Figure 1.13 – Whole brain imaging in freely moving animals.

(A) Simultaneous image acquisitions necessary for whole-brain imaging. Low magnification with infrared illumination allows for imaging the entire animal and monitoring animal behavior (animal centerline is shown). Low magnification with RFP imaging allows for real-time identification of the worm brain and drives an automated stage to keep the brain in the center of the FOV. Two-color high magnification then allows for simultaneously imaging RFP to acquire neuron location and GCaMP to monitor neural activity. **(B)** Heatmap of example whole-brain recording (~80 neurons) and simultaneous locomotive behavior. Figure adapted from (Nguyen et al., 2015).

These advanced systems have the powerful advantage monitoring whole-brain activity (50-100 neurons) with cellular resolution while simultaneously recording animal behavior (Figure 1.13B). Therefore, the activity of individual neurons can be correlated with locomotor motifs, such as forward and backward locomotion and turning (Nguyen et al., 2015; Venkatachalam et al., 2015).

Venkatachalam *et al.* also performed their recordings while cycling the

environmental temperature between 14.5 °C and 17.5 °C and were able to identify a subset of neurons that responded to these temperature fluctuations (Venkatachalam et al., 2015). These results corroborate previous reports that specific neurons drive behaviors and sensations (Luo, Clark, Biron, Mahadevan, & Samuel, 2006; Piggott, Liu, Feng, Wescott, & Xu, 2011; Zhen & Samuel, 2015); however, a specific goal of these experiments is to understand how ensemble neural activity causally drives animal behavior. The Leifer lab has recently made strides in this aspect, demonstrating that a sparse linear model can accurately decode animal locomotion, providing insight into how this simple brain encodes and controls behaviors (Scholz et al., 2018).

1.3.2. Whole-brain imaging in chemically paralyzed animals

As discussed in the previous section, tracking a moving nematode brain in real-time during experiments and tracking the location of individual neurons during post-processing is a challenging problem (Nguyen et al., 2015, 2017; Scholz et al., 2018; Venkatachalam et al., 2015). To circumvent these challenges during whole-brain imaging, many *C. elegans* researchers immobilize animals with chemical paralytics (1-5 mM tetramisole) (Kato et al., 2015; Nichols et al., 2017; Prevedel et al., 2014; Schrödel et al., 2013; Skora et al., 2018). When coupled with microfluidic chambers that restrain animals, this powerful method, pioneered by Manuel Zimmer's laboratory, essentially eliminates all animal motion while maintaining stable brain activity. Thus, there is no need to track the animal head during

experiments, nor track neuron positions during post-processing, dramatically simplifying experiments and image processing.

Using a spinning-disk confocal microscope, researchers image at 2.5-4 vol/s when monitoring GCaMP activity and consistently capture more than 100 individual neurons in the worm head (Figure 1.14A) (Kato et al., 2015; Nichols et al., 2017; Skora et al., 2018). The unchanging position of the neuron cell body also yields a high-quality 3D reconstruction of the volume, allowing for comparison with known *C. elegans* anatomy and the identification of neuron identities (Figure 1.14A) (Kato et al., 2015; Nichols et al., 2017; Skora et al., 2018). Therefore, not only can whole-brain activity be quantified, but researchers can study how individual sensory-, locomotor-, and inter-neurons drive brain-wide dynamics.

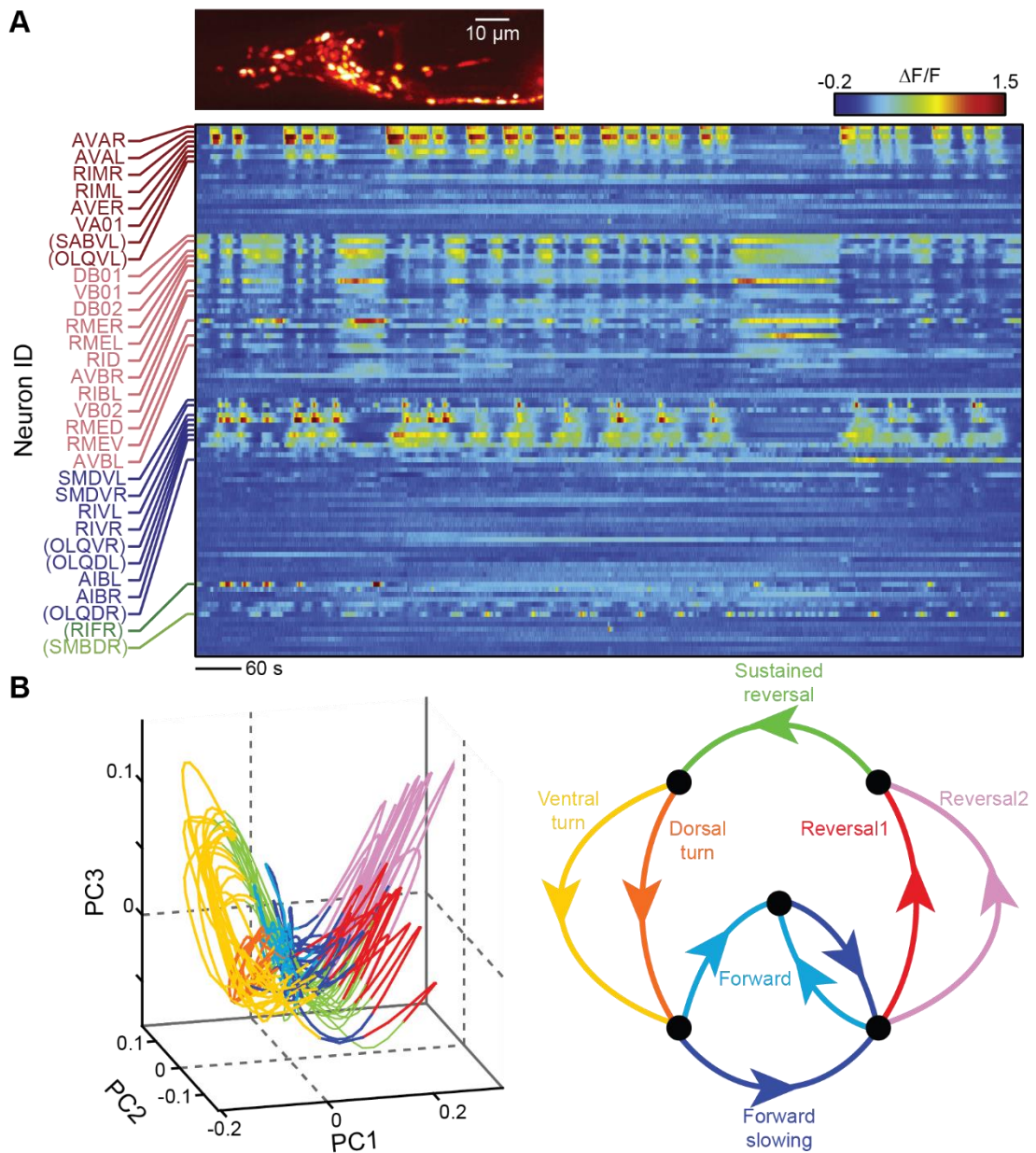


Figure 1.14 – Whole brain imaging in paralyzed worms reveals low-dimensional neural manifolds.

(A) Whole-brain calcium activity in a paralyzed animal. Paralyzation enables imaging > 100 neurons simultaneously, and neuron identification (left axis). In this experimental scheme, many neurons across the brain exhibit highly coordinated activity. (B) PCA reveals low-dimensional neural manifolds. A majority of the variance in neural activity can be captured with the first three PCs. (Left) Using neuron identification and results from single-neuron imaging, Kato et al. mapped the motor command sequence and what portions of the neural

manifold correspond to specific locomotive behaviors. Figure adapted from (Kato et al., 2015).

These recordings typically reveal large-scale, coordinated activity across the worm brain; yet a clear question that arises when recording from paralyzed animals is: *How does this neural activity relate to behavior?* Initial studies approached this question by comparing whole-brain recordings in paralyzed animals to a subset of single-neuron recordings in freely-moving animals (Kato et al., 2015). For example, they found that rising activity in interneurons such as RIM, AVA, and AVE strongly correlated with animal reversals, and falling activity with forward locomotion (Kato et al., 2015). Therefore, by identifying these neurons in whole-brain recordings from paralyzed animals, researchers were able to assume the likely *intended* animal behavior and correlated brain-wide neural dynamics with locomotion (Figure 1.14B) (Kato et al., 2015).

Using principal component analysis (PCA) to reduce the dimensionality of whole-brain calcium imaging recordings (1 neuron = 1 dimension), researchers discovered that a majority (65%) of the variance in *C. elegans* neural activity can be captured with only the first three principle components (PCs) (Figure 1.14B) (Kato et al., 2015). These PCs form a low-dimensional space, and the neural activity in this space forms a smooth manifold with cyclical dynamics (Figure 1.14B). The activity on this manifold largely represent animal locomotive motifs—forward locomotion, backward locomotion, and turning (Figure 1.14B)—consistent with single-unit

recordings from mammalian motor cortex demonstrating that the neural activity driving animal locomotion can largely be captured with only a few dimensions (Cunningham & Yu, 2014; Gallego, Perich, Miller, & Solla, 2017; Pandarinath et al., 2018; Sadtler et al., 2014). Furthermore, *C. elegans* interneuron activity dominates this low-dimensional space, suggesting that this subset of neurons drive nematode global-brain activity states (Kato et al., 2015).

Follow-up studies with whole-brain recordings from paralyzed animals sought to understand the brain-wide neural activity governing *C. elegans* developmentally-timed sleep (DTS) (reviewed in Section 1.2.1) (Nichols et al., 2017). As expected (Kato et al., 2015), during wakefulness (21% O₂) the worm brain exhibited coordinated activity (see Figure 1.8), large groups of neurons were active in unison, and the activity on the manifold displayed cyclical dynamics (Figure 1.15). However, the neural activity during sleep (10% O₂) displayed strikingly different characteristics—a large-scale downregulation of activity across nearly every neuron in the brain (see Figure 1.8) and a transition to fixed-point attractor dynamics in PCA space (Figure 1.15) (Nichols et al., 2017).

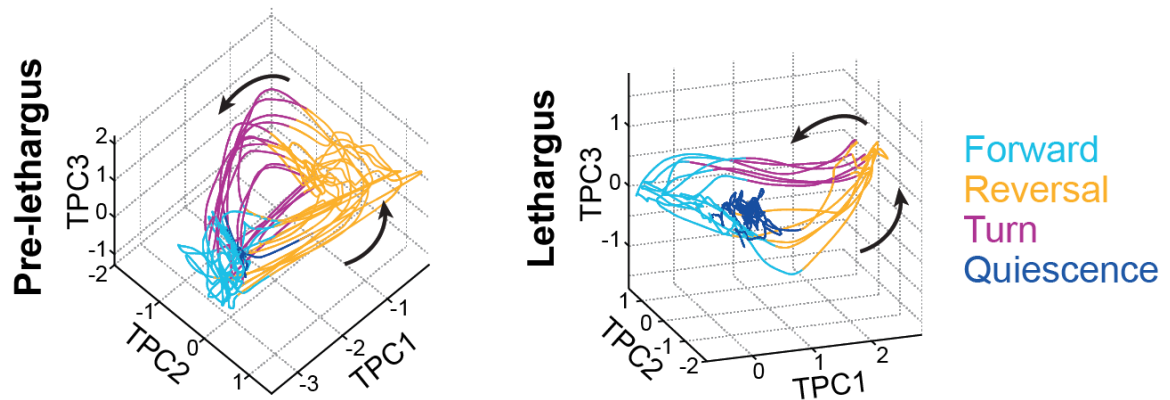


Figure 1.15 – PCA captures brain-wide changes in neural dynamics during *C. elegans* sleep.

(Left) During pre-lethargus (when there is no sleep), the activity on the neural manifold strongly resembles the cyclic activity previously observed by Kato et al. (2015). (Right) During lethargus, the oxygen switch induces sleep. During sleep, brain-wide dynamics in PCA space shift from cyclical dynamics to fixed-point attractor dynamics. The fixed-point is non-zero, suggesting that some neural activity—a “sleep circuit”—remains active. Figure adapted from (Nichols et al., 2017).

1.3.3. Conclusions and future directions of whole-brain imaging for *C.*

elegans neuroscience

C. elegans whole-brain imaging has already revolutionized our understanding of the neural computations underlying this tiny animal’s behavior, yet this field is still in its infancy and has much to offer not only nematode neurobiology, but neuroscience as a whole. Indeed, we can use these microscopic animals and imaging techniques to interrogate fundamental questions into how the brain encodes sensory information and drives behaviors with ensemble neural activity.

Recordings from paralyzed animals (Section 1.3.2) will continue to be an invaluable tool. These high-quality, low-noise recordings capture the activity of nearly all neurons in the worm head, allow for single-neuron identification, and the microfluidic device is advantageous for the controlled delivery of stimuli (Kato et al., 2015; Nichols et al., 2017; Schrödel et al., 2013; Skora et al., 2018). In addition, this experimental approach provides a path towards whole-nervous system recordings for high-resolution imaging systems with large FOVs (Prevedel et al., 2014).

Reports that have used chemical paralytics for *C. elegans* whole-brain imaging have laid a high bar for all future studies utilizing whole-brain recordings; however, the lack of a ground-truth behavioral output is a significant disadvantage and limits the outlook of these experiments. Furthermore, recent results have suggested that chemical paralysis itself leads to low-dimensional manifolds and that the PCs of neural activity do not accurately predict behavior (Scholz et al., 2018). The future of *C. elegans* whole-brain imaging lies in recordings from freely-behaving animals, but technological advances are needed to improve data quality, reduce the complexity of neuron tracking, and analyze these complicated and high-dimensional data sets:

- **Hardware and microscopy:** The fastest reported imaging rate of 6 vol/s in freely-moving animals leads to large amounts of motion—a single neuron can move up to the length of the worm head between volumes (Nguyen et al., 2017). This large amount of movement also significantly complicates tracking

individual cell locations across an entire recording, which requires extensive and robust machine-learning approaches for automated tracking (Nguyen et al., 2017). Rapid volumetric imaging methods, such as Swept, Confocally-Aligned Planar Excitation microscopy (SCAPE, a hybrid light-sheet/confocal imaging technique (Bouchard et al., 2015)), that can capture volumetric data at rates > 20 vol/s will not only increase the temporal resolution for recording neural dynamics, but also make automated cell tracking more accessible.

1. **Protein-engineering:** Advances in protein engineering will lead to brighter genetically-encoded calcium indicators with better kinetics that improve upon the current signal-to-noise ratios and make the acquired data more reliable (Broussard, Liang, & Tian, 2014a; T.-W. Chen et al., 2013; Muto et al., 2011; Storace et al., 2016). In addition, the field will likely move towards red-shifted calcium indicators in the near future (Dana et al., 2016) to reduce the reliance on blue-light excitation, which can dramatically affect animal behavior (Edwards et al., 2008; Gong et al., 2016; Ward, Liu, Feng, & Xu, 2008). Eventually, the field will move away from calcium imaging entirely and instead use genetically-encoded voltage indicators for direct optical readouts of neural membrane potentials with high temporal resolution throughout the entire worm brain (Broussard, Liang, & Tian, 2014b; Flytzanis et al., 2014; Storace et al., 2016).

2. **Computational modeling:** The field of whole-brain imaging will also need new computational techniques for determining how ensemble neural activity causally drives animal behavior. Researchers envision capturing brain-wide activity and quantifying global-brain states, but also identifying specific neural circuits and patterns of activity that control behavior and sensory perception (Feierstein, Portugues, & Orger, 2015; Kaplan et al., 2018; Kutz, 2019). Furthermore, researchers also want to accurately decode behavior using neural activity alone, and predict future behaviors in real-time. Such advances are beginning to be made in behaving and “fictive-behaving” (immobilized animals in virtual reality) zebrafish during whole-brain imaging (X. Chen et al., 2018; Dunn et al., 2016; Haesemeyer et al., 2018; Portugues, Feierstein, Engert, & Orger, 2014; Severi et al., 2014; Vladimirov et al., 2018). For example, Vladimirov *et al.* (2018) developed a system that records whole-brain activity, performs rapid online processing that quantifies brain states, identifies single neurons as central hubs of computation, optically ablates these neurons, then records the subsequent brain-wide changes in activity. Such experiments will continued to be paired with advanced computational modeling that reveal the how individual circuits across the small-organism brain compute and drive global-brain states.

The field of whole-brain imaging in small animals like *C. elegans* is highly interdisciplinary with a bright future for answering fundamental questions in neuroscience. In the next chapter will detail our findings with μ Sleep: a behavioral

state transition accompanied by a global-brain state transition. As technological advances continued to be made in whole-brain imaging, μ Sleep can serve as an ideal fundamental behavior to understand the neural control of sleep and dramatic brain state transitions.

***C. elegans* μ Sleep Behavior**

In Chapter 1, I reviewed *C. elegans* microfluidics, sleep and whole-brain imaging. We saw how microfluidics enabled and strengthened a wide-range of *C. elegans* subfields in neurobiology, how worm sleep provides a model for understanding the neural circuit control of state transitions, and how whole-brain imaging allows for elucidating how brain-wide activity generates specific behaviors. In the following chapters, I combine all of these aspects into one platform—describing a previously unreported *C. elegans* sleep behavior using behavioral measurements, tailored microfluidic environments, and whole-brain calcium imaging. In this chapter, I will describe and quantify μ Sleep behavior and show behavioral evidence that this is a *C. elegans* sleep behavior. This chapter is largely adapted from Gonzales, Zhou, & Robinson, 2019, which is currently under review as of April 2019. A non-peer reviewed preprint can be found at <https://doi.org/10.1101/547075>.

2.1. Comparison of μ Sleep with stress-induced sleep and swimming-induced quiescence

When confined to microfluidic chambers we found that adult *C. elegans* rapidly and spontaneously switch between normal activity and brief quiescent bouts without any additional stimuli (Figure 2.1A). We initially observed this behavior when immobilizing worms for recording body-wall muscle electrophysiology (Gonzales et al., 2017). In these electrical recordings we observed minutes-long periods of muscle inactivity that corresponded to whole-animal quiescence (Gonzales et al., 2017). We have since found that this quiescence occurs in a wide range of microfluidic geometries, such as large chambers and artificial dirt micropillars.

We found that the onset, frequency, and duration of quiescent bouts in microfluidic chambers are unique compared to previously-reported sleep behaviors in adult *C. elegans* (Figure 2.1B-F). While larval *C. elegans* display quiescence during lethargus (reviewed in Section 1.2.1) (Raizen et al., 2008), quiescence in adult worms occurs in only a few situations (reviewed in Section 1.2.2), such as after several hours of swimming (Churgin, McCloskey, et al., 2017; R. Ghosh & Emmons, 2008; McCloskey et al., 2017) or after exposure to extreme environmental conditions (DeBardeleben et al., 2017; Hill et al., 2014; Iannacone et al., 2017; Nath et al., 2016; Matthew D. Nelson et al., 2014). To determine how microfluidic-induced quiescence compares to the well-established “swimming-induced quiescence” (SIQ)

that occurs in swimming animals and “stress-induced sleep” (SIS) that occurs from a 30 min heat shock, we quantified these behaviors using the same methods to analyze μ Sleep (Figure 2.1B-F). During a 4 hr imaging period, we found that animals partially immobilized in microfluidic channels (50 μ m width, \sim 0.004 μ L per chamber) displayed short (1.3 ± 0.1 min, mean \pm sem, Figure 2.1E) bouts that, on average, began within the first hour of imaging (51 ± 4 min, mean \pm sem, Figure 2.1D). Likewise, we also observed frequent, but longer (2.4 ± 0.3 min, mean \pm sem, Figure 2.1E) quiescent bouts when the microfluidic chambers were large enough to allow animals to swim (500 μ m width, \sim 0.1 μ L per chamber). We compared these data to SIQ, where animals alternate between swimming and quiescence in a large multi-well device or “WorMotel” (Figure 2.1B, 8 μ L of buffer per well) (Churgin, Jung, et al., 2017). In WorMotel, we recorded 5-7 times less sleep over the imaging period compared to microfluidic chambers (Figure 2.1C) and longer quiescent bouts compared to either microfluidic geometry (3.6 ± 0.3 min, mean \pm sem, Figure 2.1E). Additionally, the average quiescence onset time was more than double what we observed for μ Sleep (175 ± 6 min, mean \pm sem, Figure 2.1D). For our final comparison point, we heat-shocked animals in the large microfluidic device for 30 min at 30 °C to record SIS (Hill et al., 2014) (Figure 2.1B). As expected, during the noxious heat stimulus animals displayed their first quiescent bout more than 4-6 times faster than in microfluidic chambers with no external heat applied (13 ± 0.7 min, mean \pm sem, Figure 2.1D).

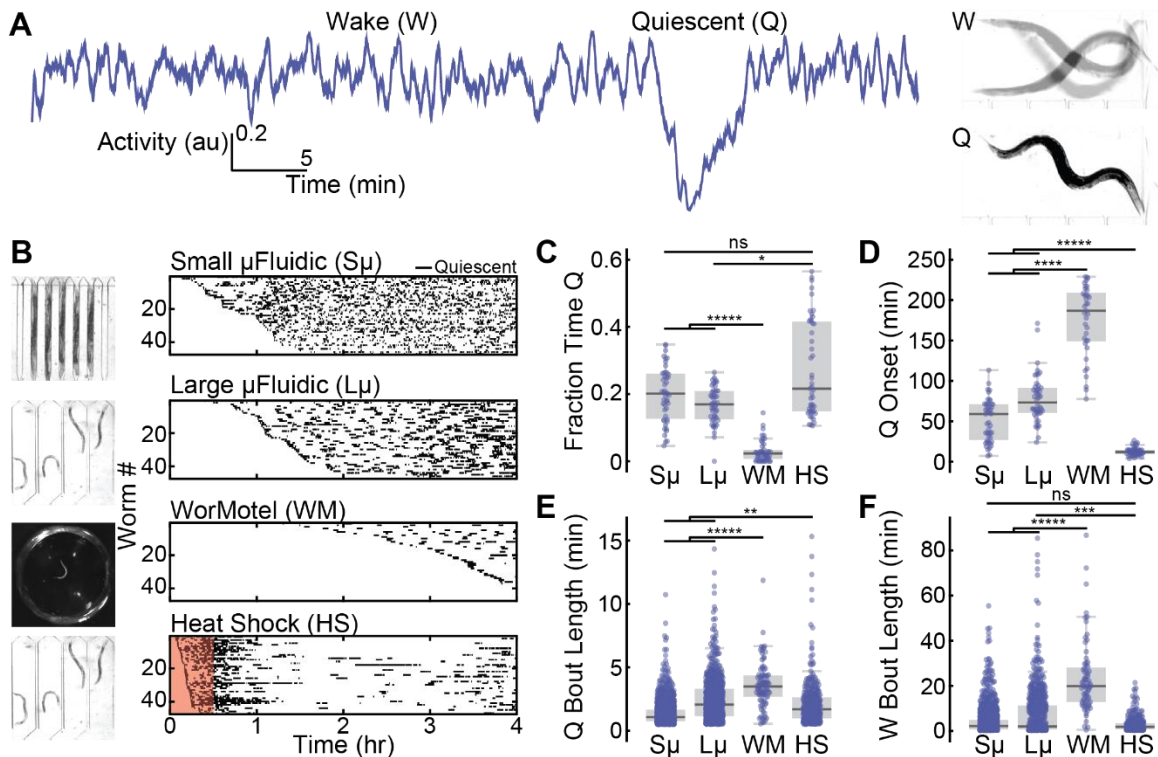


Figure 2.1 – Microfluidic-induced quiescence is phenotypically distinct from SIS and SIQ.

(A) Characteristic worm quiescence in a microfluidic chamber. (Left) 1 hr activity trace from a worm swimming in a microfluidic chamber, calculated by subtracting consecutive frames to quantify movement (see Chapter 5). Quiescence is hallmarked by a clear drop in animal activity to near zero. (Right) 1 s overlap of frames shows the animal swimming during the wake period (W) and immobile during quiescence (Q). (B) All quiescent bouts recorded from animals in a small microfluidic chamber (50 μm width), large microfluidic chamber (500 μm width), WorMotel multi-well PDMS device, and large microfluidic device during a 30 min heat shock at 30 $^{\circ}\text{C}$ (see inset images). Raster plots show the bouts recorded from each animal during a 4 hr imaging period ($n = 47$ animals for each condition). Experiments represented in the raster plots are sorted by the onset of the first detected sleep bout. (C-F) Quantitative sleep metrics. S_{μ} = small microfluidic chambers, L_{μ} = large microfluidic chambers, WM = WorMotel, HS = first hour of heat shock. (C) The total fraction of time each animal spent in the quiescent state. (D) Onset time of the first quiescent bout. (E) Length of individual quiescent bouts. (F) Length of individual wake bouts, excluding the first period of wake after animals are loaded into the chamber. ($n = 47$ animals for each condition; * $p < 0.05$, ** $p < 0.01$, *** $p < 0.001$, **** $p < 0.0001$, ***** $p < 0.00001$; Kruskal-Wallis with a post-hoc Dunn-Sidak test). (Figure adapted from Gonzales et al., 2019, under review as of April 2019).

It is important to note that while the μ Sleep phenotype shows a number of quantitative differences when compared to SIQ and SIS (Figure 2.1), it is not clear if microfluidic-induced quiescence can be classified as a new *C. elegans* behavior. It is possible that the microfluidic environment accelerates episodic swimming or introduces mild stressors that more slowly lead to stress-induced quiescence. Thus, we consider μ Sleep behavior to be phenotypically distinct from other reported quiescent behaviors in *C. elegans* adults, and not necessarily a new behavioral state.

2.2. μ Sleep meets behavioral requirements for sleep

Our observation of spontaneous *C. elegans* quiescence in microfluidic chambers led us to determine whether this behavioral state transition meets the evolutionarily-conserved criteria for classification as sleep: reversibility, a decreased response to stimuli, homeostasis, and a stereotypical posture (Campbell & Tobler, 1984). *C. elegans* developmentally-timed sleep as larvae meets all requirements (reviewed in Section 1.2.1) (J. Y. Cho & Sternberg, 2014; Driver et al., 2013; Iwanir et al., 2013; Nagy, Tramm, et al., 2014; Raizen et al., 2008; Schwarz et al., 2011; Tramm et al., 2014; Nicholas F. Trojanowski & Raizen, 2016). However, sleep in adult worms—which occurs in only specific environmental conditions—is typically defined based on reversibility and a decreased response to stimuli (reviewed in Section 1.2.2.1) (Hill et al., 2014; Nicholas F. Trojanowski & Raizen, 2016). Here, we tested for reversibility, decreased response to stimuli and a micro-homeostatic rebound.

To test for reversibility, we used blue light (5 s pulse, 5 mW/cm²) as a strong stimulus and found that this rapidly and reliably reversed the quiescent state (Figure 2.2A). To test for a decreased response to stimuli, we fabricated microfluidic push-down valves designed to deliver tunable mechanical stimuli, similar to previously developed technology for worms (McClanahan et al., 2017). We found that when we applied a strong stimulus (high pressure, 30 psi), both wake and quiescent animals robustly responded with a significant increase in behavioral activity, which provides additional confirmation that the quiescent state is reversible (Figure 2.2B). When we applied a weak stimulus to wake animals (low pressure, 15 psi), we again reliably recorded a significant increase in activity (Figure 2.2B). However, when we delivered a weak stimulus to quiescent animals, they responded weakly, exhibiting an average behavioral activity less than half that of all other conditions (Figure 2.2B-C). These data suggest that during quiescence, sensory systems are less responsive and in a reduced activity state, consistent with previous reports during *C. elegans* sleep (J. Y. Cho & Sternberg, 2014; Hill et al., 2014; Raizen et al., 2008; Schwarz et al., 2011).

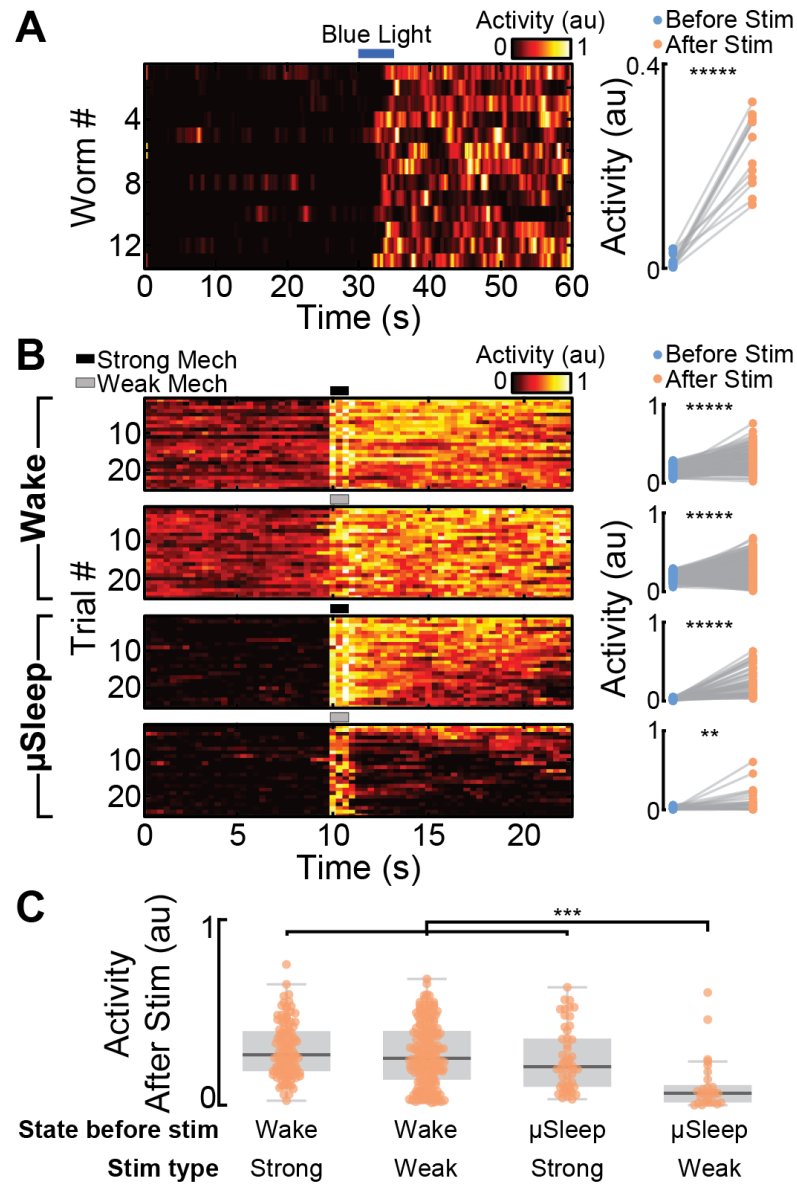


Figure 2.2 – Microfluidic-induced quiescence is reversible and animals shown a decreased response to weak external stimuli.

(A) The quiescent state is reversible. (Left) Heatmap of animal activity. Measurements begin with all animals in the quiescent state. The 5 s light pulse at $t = 30$ s results in a rapid increase in animal activity. (Right) Mean activity of each animal during the first and second 30 s of imaging shows a clear transition from quiescent to wake states ($n = 13$ worms, **** $p < 0.00001$, paired t-test). (B) Quiescent animals have a decreased response to weak sensory stimuli. Heatmaps of activity from wake and quiescent animals that received strong or weak mechanical stimuli from microfluidic valves. For each condition, only the 25 trials with the highest mean activity post-stimulation are shown. “Wake” indicates trials in which animals

were awake but have a below-average activity before stimulation (see Chapter 5). “ μ Sleep” indicates trials in which animals were quiescent before stimulation. All conditions show an increase in activity upon stimulation, but fewer animals are responsive when receiving weak stimuli. (C) Mean activity after mechanical stimulation from the trials in (B). Behavioral activity is identical in all cases other than when quiescent animals received weak mechanical stimuli (Wake-Strong $n = 108$, Wake-Weak $n = 176$, μ Sleep-Strong $n = 51$, μ Sleep-Weak $n = 29$; *** $p < 0.001$, Kruskal-Wallis with a post-hoc Dunn-Sidak test). (Figure adapted from Gonzales et al., 2019, under review as of April 2019).

In addition, we also tested for homeostatic rebound, which is found in worm developmental sleep (Iwanir et al., 2013; Raizen et al., 2008; Wu et al., 2018). Because sleep deprivation produced with external stimuli (e.g. mechanical pulses) can produce a stress response (Driver et al., 2013), we tested whether sleep bout length depends on the length of the previous wake bout (Figure 2.3). We hypothesized that longer wake bouts would lead to longer sleep bouts due to micro-homeostatic mechanisms, as previously observed for developmental sleep (Iwanir et al., 2013). Indeed, we found that sleep bouts increased from 1.5 ± 0.1 min to 2.5 ± 0.1 min (mean \pm sem) as the preceding wake bout increased in length from < 1 min to 20 min (Figure 2.3). However, even when wake bout lengths increased to longer than an hour, the sleep bouts lengths plateaued to an average of only 2.3 ± 0.1 min (Figure 2.3), contradicting the hypothesis that extended wake periods lead to sleep deprivation and homeostatic rebound. These results suggest that micro-homeostasis may be present in μ Sleep; however, future work is needed to test for homeostatic rebound based on non-stress-inducing sleep deprivation, such as optogenetic inhibition of sleep-promoting neurons (Wu et al., 2018). Together our

results indicate that microfluidic-induced quiescence indeed meets the behavioral precedents to be called a *C. elegans* sleep state: reversibility and a decreased response to stimuli.

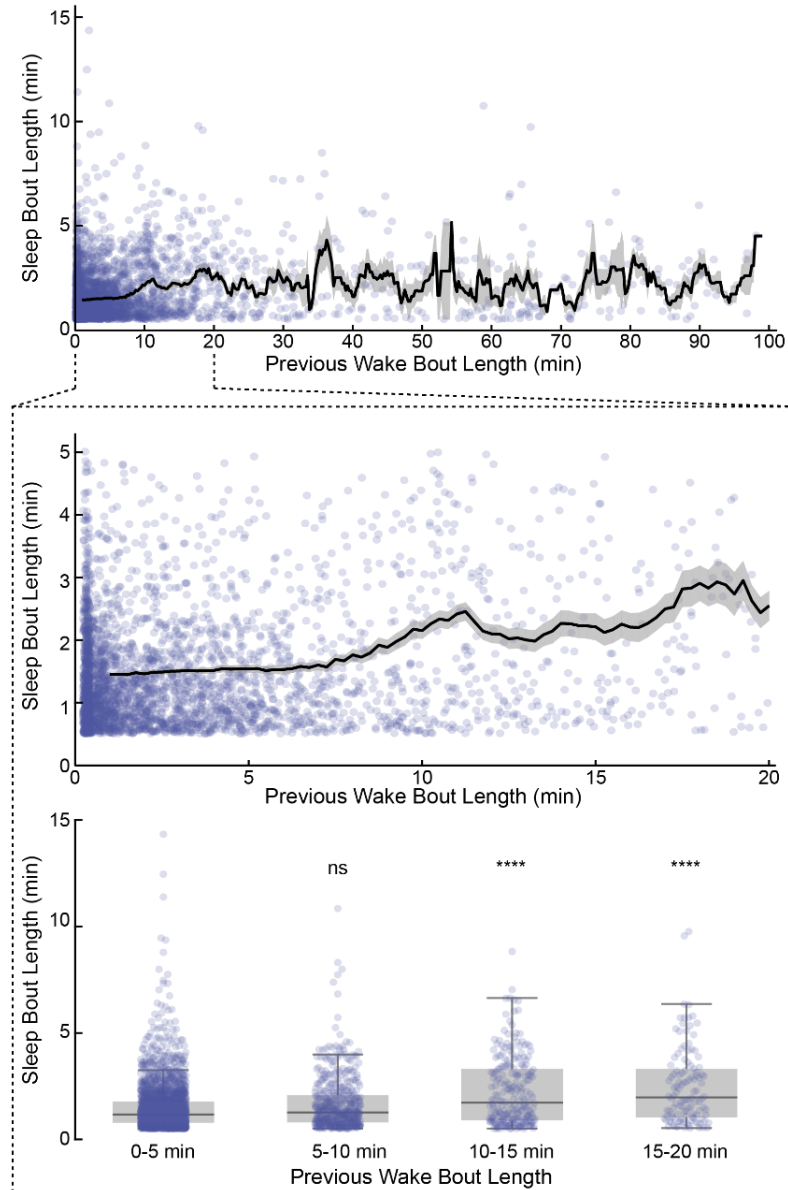


Figure 2.3 – μ Sleep shows micro-homeostatic rebound.

(Top) Sleep bout length vs the previous wake bout length for wake bouts lasting up to 100 min. Data points represent individual sleep and wake bout pairs from data collected from 50

and 500 μm chambers with WT animals (see Figure 2.1, 4 hr-long recordings and Figure 4.1, 2 hr-long recordings, number of animals = 233). Black line is a moving average of all data (\pm sem) calculated with a sliding window 5 min long. (Middle) Zoom of the top plot shows that sleep bouts generally increase in length as the preceding wake bouts increases from 0 to 20 min. (Bottom) Binned data for 5 min windows shows a significant increase in sleep bout length compared to the first 5 min of imaging. (ns = not significant, **** $p < 0.0001$ compared to 0-5 min data set, Kruskal-Wallis with a post-hoc Dunn-Sidak test). (Figure adapted from Gonzales et al., 2019, under review as of April 2019).

2.3. μSleep is dependent on *C. elegans* sleep-promoting neurons

To further validate that μSleep is a sleep state, we interrogated the role of two interneurons, RIS and ALA, known to dominate *C. elegans* developmental and stress-induced sleep, respectively, via at least partially distinct signaling pathways (N. F. Trojanowski et al., 2015; Nicholas F. Trojanowski & Raizen, 2016). To test whether μSleep is also dependent on these neurons, we compared the sleep phenotype of WT animals to *ceh-17(lf)* and *aptf-1(lf)* loss-of-function mutants (Figure 2.4A). *ceh-17(lf)* shows defective axonal growth of the ALA neuron and less SIS (Hill et al., 2014). *aptf-1(lf)* lacks the transcription factor necessary for RIS to signal quiescence via the FLP-11 neuropeptide (Turek et al., 2016, 2013). In our experiments, both *ceh-17(lf)* and *aptf-1(lf)* mutants showed more than 4.5 times less total μSleep than WT animals (Figure 2.4B), further validating that μSleep is a *C. elegans* sleep state controlled by previously-reported neural mechanisms.

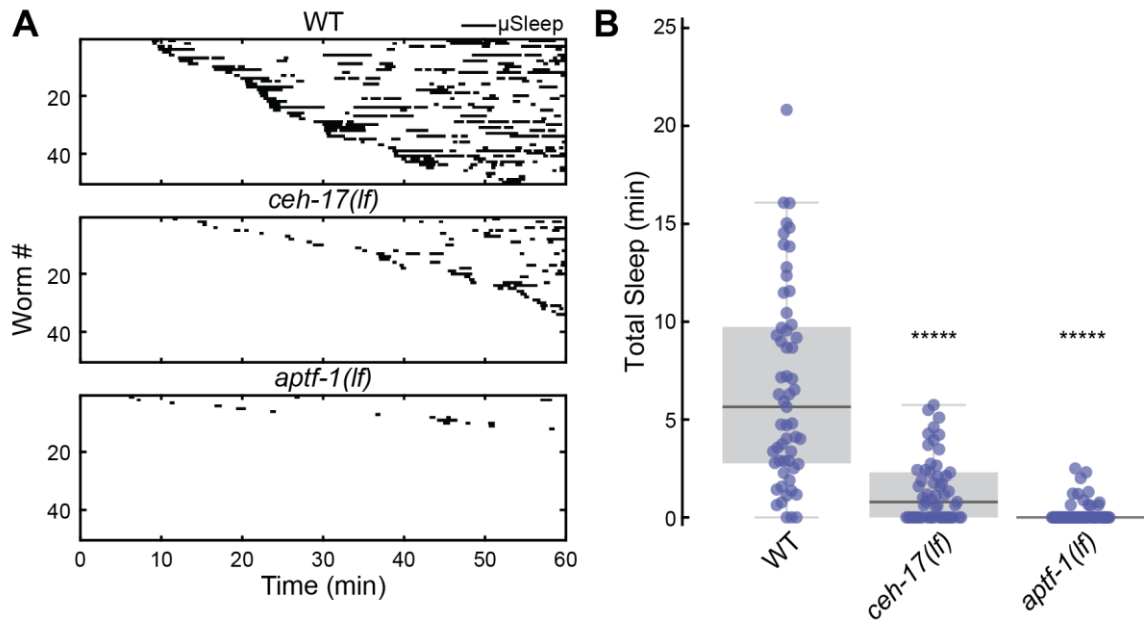


Figure 2.4 – ALA and RIS defective mutants show less sleep compared to WT.

(A) Raster plots of detected sleep bouts from WT, *ceh-17(lf)* and *aptf-1(lf)* animals. Only the top 50 animals showing the most total μSleep are shown. **(B)** Both *ceh-17(lf)* and *aptf-1(lf)* show less total sleep than WT. The data suggest that μSleep is strongly dependent on the ALA and RIS neurons. (WT n = 57, *ceh-17(lf)* n = 57, *aptf-1(lf)* n = 60; *****(p < 0.00001 compared to WT, Kruskal-Wallis with a post-hoc Dunn-Sidak test). (Figure adapted from Gonzales et al., 2019, under review as of April 2019).

A Global Brain-State Transition Underlies μ Sleep Behavior

In the previous chapter, I introduced μ Sleep behavior showed evidence that this is indeed a *C. elegans* sleep state. Having established that μ Sleep meets the criteria for *C. elegans* sleep and is hallmarked by a dramatic behavioral state transition, we also sought to confirm that these spontaneous behavioral transitions were accompanied by an underlying global-brain state transition (Nichols et al., 2017; Skora et al., 2018). We achieved these goals using whole-brain and single-neuron calcium imaging, which were enabled by animal confinement and the microfluidic platform. This chapter is largely adapted from Gonzales, Zhou, & Robinson, 2019, which is currently under review as of April 2019. A non-peer reviewed preprint can be found at <https://doi.org/10.1101/547075>.

3.1. The advantages of μ Sleep for capturing brain-state transitions

Previous work in chemically-paralyzed animals used brain-wide calcium imaging to establish that the *C. elegans* nervous system, with the exception of a few neurons, transitions to a large-scale downregulation of neural activity during sleep (reviewed in Section 1.3.2) (Nichols et al., 2017; Skora et al., 2018). Yet, this global brain activity has only been observed during *C. elegans* developmental sleep (Nichols et al., 2017) and sleep induced by a 16 hr period of starvation (Skora et al., 2018), which are both significantly different conditions compared to μ Sleep. For example, our microfluidic assays use adult animals and we typically observe quiescence within the first hour after removal from food (see Figure 2.1).

Using whole-brain calcium-sensitive imaging we were able to establish that μ Sleep is indeed associated with a global brain state transition (Figure 3.1). For these experiments we found that the μ Sleep behavior has a distinct advantage compared to other whole-brain imaging experimental preparations. Typically, whole-brain calcium imaging in *C. elegans* exists in two paradigms (reviewed in Section 1.3): volumetric imaging of either freely-moving animals (Nguyen et al., 2015, 2017; Venkatachalam et al., 2015) or chemically-paralyzed animals confined in microfluidic chambers (Kato et al., 2015; Nichols et al., 2017; Skora et al., 2018). While imaging freely-moving animals allows for simultaneous quantification of neural activity and behavior, tracking a moving brain during experiments (Nguyen et al., 2015; Venkatachalam et al., 2015) and tracking the location of individual

neurons during post-processing (Nguyen et al., 2017) remains challenging. Alternatively, chemically paralyzing animals simplifies experiments but does not provide a direct behavioral output during imaging (Kato et al., 2015; Nichols et al., 2017; Skora et al., 2018). The major advantage of the μ Sleep behavior for whole-brain imaging is that animals can be confined in microfluidic chambers, which facilitates imaging without the use of paralytics that could disrupt spontaneous sleep-wake transitions (see Figure 2.1).

3.2. μ Sleep is associated with a global-brain state transition

To exploit this advantage, we developed an imaging protocol using a microfluidic chamber geometry similar to previous studies (Kato et al., 2015; Nichols et al., 2017) that partially-immobilizes animals but allows for enough movement to quantify animal behavior and detect μ Sleep during whole-brain calcium imaging (Figure 3.1). By incorporating a period of animal habituation to blue excitation light, we were able to image continuously for 10 minutes using single-plane epifluorescence microscopy and capture spontaneous sleep-wake transitions in approximately 25% of animals (see methods in Chapter 5, Section 5.8). Imaging a single 2D-plane allowed for quantifying both average ganglia activity and the activity of several individual neurons (Figure 3.1B). With this imaging protocol, we observed a distinct correlation between animal behavior and neural activity (Figure 3.1B). During μ Sleep both the average ganglia activity and the

activity of individual neurons dropped significantly ($78 \pm 10\%$ and $55 \pm 10\%$, respectively) (Figure 3.1C).

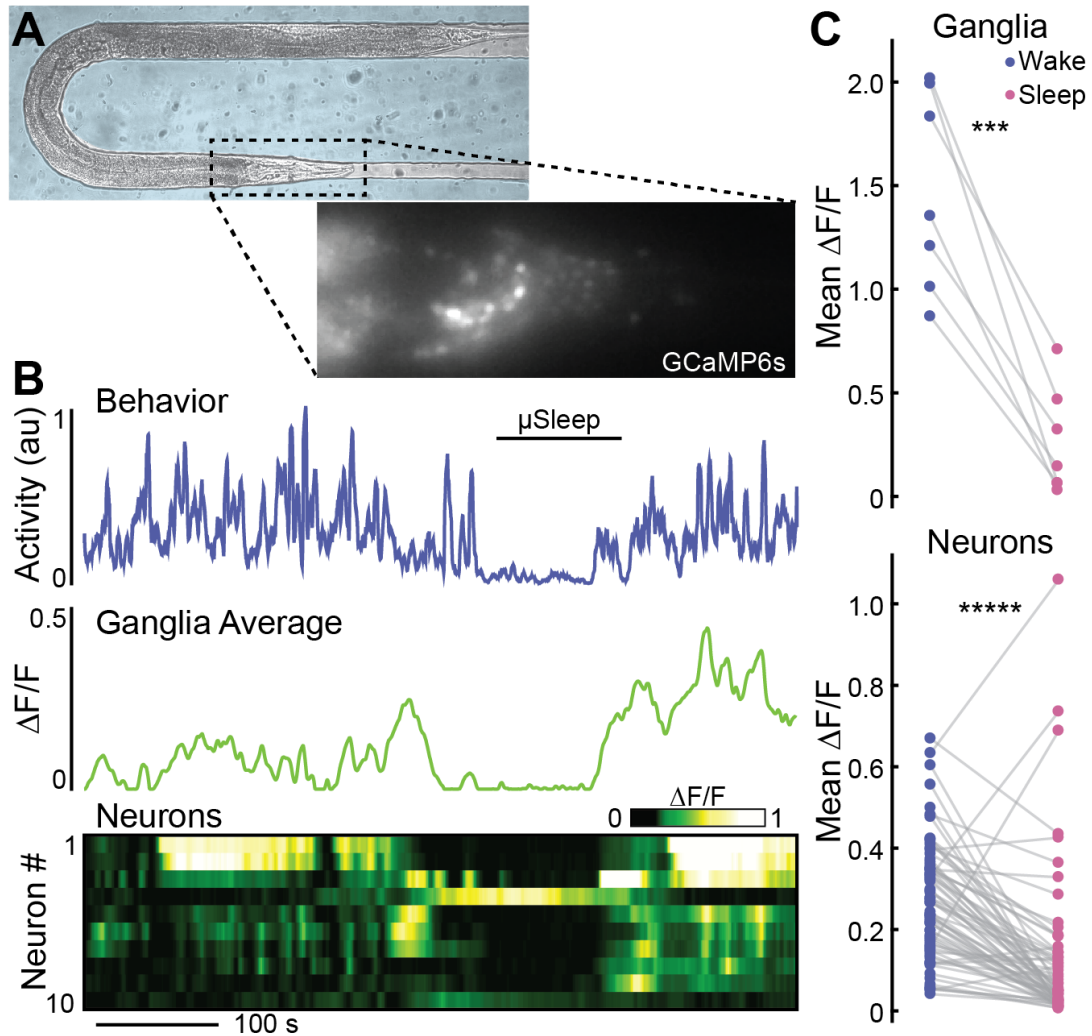


Figure 3.1 - μ Sleep is a global-brain state.

(A) Adult animal immobilized in a microfluidic chamber tailored for whole-brain imaging. (Inset) Single-plane epifluorescence image of an animal with pan-neuronal expression of GCaMP6s. (B) Representative animal shows behavioral quiescence correlates with less neural activity. (Top) Behavioral activity trace quantified by tracking the motion of ten individual neurons. (Middle) Average fluorescence across the whole worm head ganglia. (Bottom) Activity of ten individual neurons show a clear brain-state transition and less neural activity during μ Sleep. (C) Using only behavioral activity, we identified quiescent bouts then quantified neural activity during sleep and wake. During μ Sleep, animals exhibited a large-

scale downregulation of neural activity across both the entire ganglia and most individual neurons. (n = 7 animals; 10 neurons were tracked per animal; ***p < 0.001, *****p < 0.00001, paired t-test). (Figure adapted from Gonzales et al., 2019, under review as of April 2019).

3.3. The RIS neuron is more active during μ Sleep

As expected from previous work (Nichols et al., 2017; Skora et al., 2018; Turek et al., 2016, 2013; Wu et al., 2018), we observed that some neurons actually increased in activity during μ Sleep (Figure 3.1C). These works (reviewed in Section 1.2.1) provide strong evidence that the RIS neuron is a major driver of many types of *C. elegans* sleep behaviors and becomes more active during quiescence (Turek et al., 2016, 2013; Wu et al., 2018). Using single-neuron imaging of the RIS neuron in behaving animals confined in microfluidic channels, we confirmed that RIS becomes more active during μ Sleep (Figure 3.2). This two-color imaging setup included simultaneous imaging of mKate (to get neuron location) and GCaMP3 (to get neuron activity) and showed that RIS negatively-correlates behavioral activity, becoming more active as animal behavior decreased (Figure 3.2). These results confirmed that the RIS neuron is a part of a sleep-promoting neuron for *C. elegans* μ Sleep.

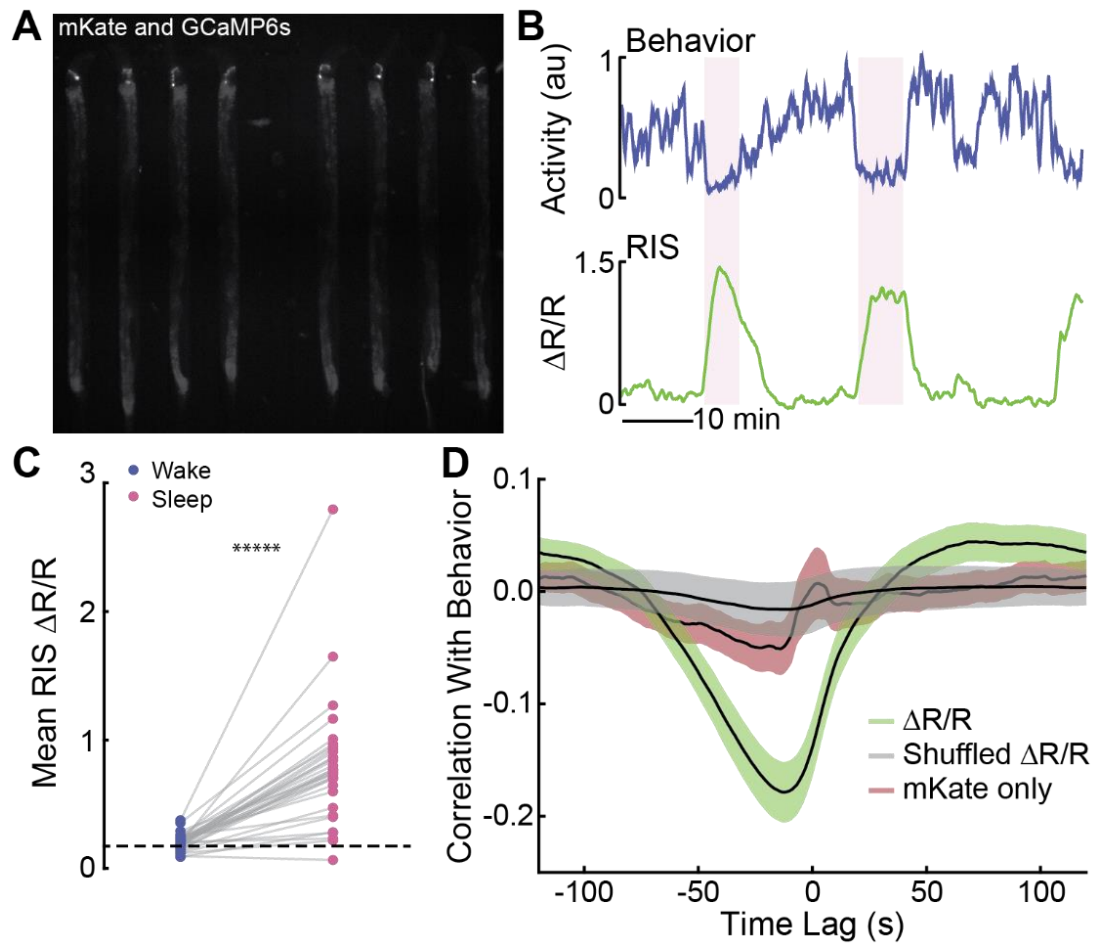


Figure 3.2 – RIS neuron is more active during sleep and low-behavioral activity.

(A) Fluorescent micrograph of the mKate channel, showing HBR1361 animals immobilized in 50 μm -wide chambers and expressing mKate and GCaMP3 in the RIS neurons. (B) Representative traces of animal behavioral activity (top) and RIS calcium activity (bottom). RIS activity dramatically increases during μSleep bouts (shaded regions), opposed to the majority of worm brain activity (see Figure 3.1). (C) RIS is more active during μSleep . We automatically detected sleep bouts across animals, calculated mean RIS activity during wake and μSleep , and quantified mean RIS activity in each behavioral state. Dashed line shows the average RIS activity for animals that did not display a sleep bout. (Data points represent individual animals; $n = 48$ animals total, $n = 31$ animals exhibited at least one sleep bout, $n = 17$ animals did not sleep; ***** $p < 0.00001$, paired t-test). (D) RIS activity negatively correlates with animal behavior. Across all animals, we split behavioral and fluorescence data into 10 min windows and calculated the fluorescence correlation with behavior. $\Delta R/R$ data (green trace) showed a strong negative correlation with behavior, consistent with the hypothesis that RIS becomes more active as behavioral activity falls. Randomly shuffling the $\Delta R/R$ windows as a control removes this strong correlation (gray trace). To test for

movement artifacts that could possibly lead to a correlation between fluorescence and behavior, we performed the same analysis with the mKate channel only (red trace); however, this did not lead to the strong negative correlation with seen in the $\Delta R/R$ data. Thus, RIS activity is strongly correlated with low behavioral activity. (Figure adapted from Gonzales et al., 2019, under review as of April 2019).

These results further support the claim that μ Sleep is a *C. elegans* sleep behavior controlled by sleep-promoting circuits and corroborate previous reports that a unique brain state governs *C. elegans* sleep (Nichols et al., 2017; Skora et al., 2018). Furthermore, these results show that μ Sleep behavior is an advantageous behavioral paradigm that facilitates whole-brain imaging while measuring animal activity without the need for chemically induced paralysis.

μ Sleep is Regulated by Satiety, Thermosensation, and Mechanosensation

The combination of behavioral and calcium-imaging data in previous chapters shows that μ Sleep is hallmarked by a spontaneous brain *and* behavioral state transition (Figure 3.1). We also found that the sleep state is regulated by sleep-promoting neurons like RIS and ALA (Figure 2.4, Figure 3.2). In this chapter, we will describe neural circuits upstream of RIS and ALA that regulate μ Sleep. Recall from Chapter 2 that we measured distinct phenotypes when comparing swimming animals in WorMotel to swimming animals in microfluidic chambers (Figure 2.1). However, the only significant factor distinguishing our microfluidic modules and WorMotel is an \sim 80-fold difference in the size of the chambers that confine animals. Therefore, we hypothesized that *C. elegans* sensory circuits detect features unique to the microfluidic environment and in turn drive sleep behavior. This chapter is largely adapted from Gonzales, Zhou, & Robinson, 2019, which is currently under

review as of April 2019. A non-peer reviewed preprint can be found at <https://doi.org/10.1101/547075>.

4.1. Defining baseline environmental conditions

To elucidate the cues regulating μ Sleep, we used the versatility of microfluidics to perform assays under a variety of conditions (Figure 4.1). Namely, we used the power of microfluidics to control the food availability, environmental temperature, and chamber geometry to observe changes in the μ Sleep phenotype (Figure 4.1). All of these changes were compared to a defined “baseline” behavior. We defined our baseline experimental conditions as: 20 °C cultivation temperature (T_c); animals are transferred directly from seeded nematode growth media (NGM) into the microfluidic device; the microfluidic media (M9 buffer) contains no food source; the temperature during imaging is 22 °C.

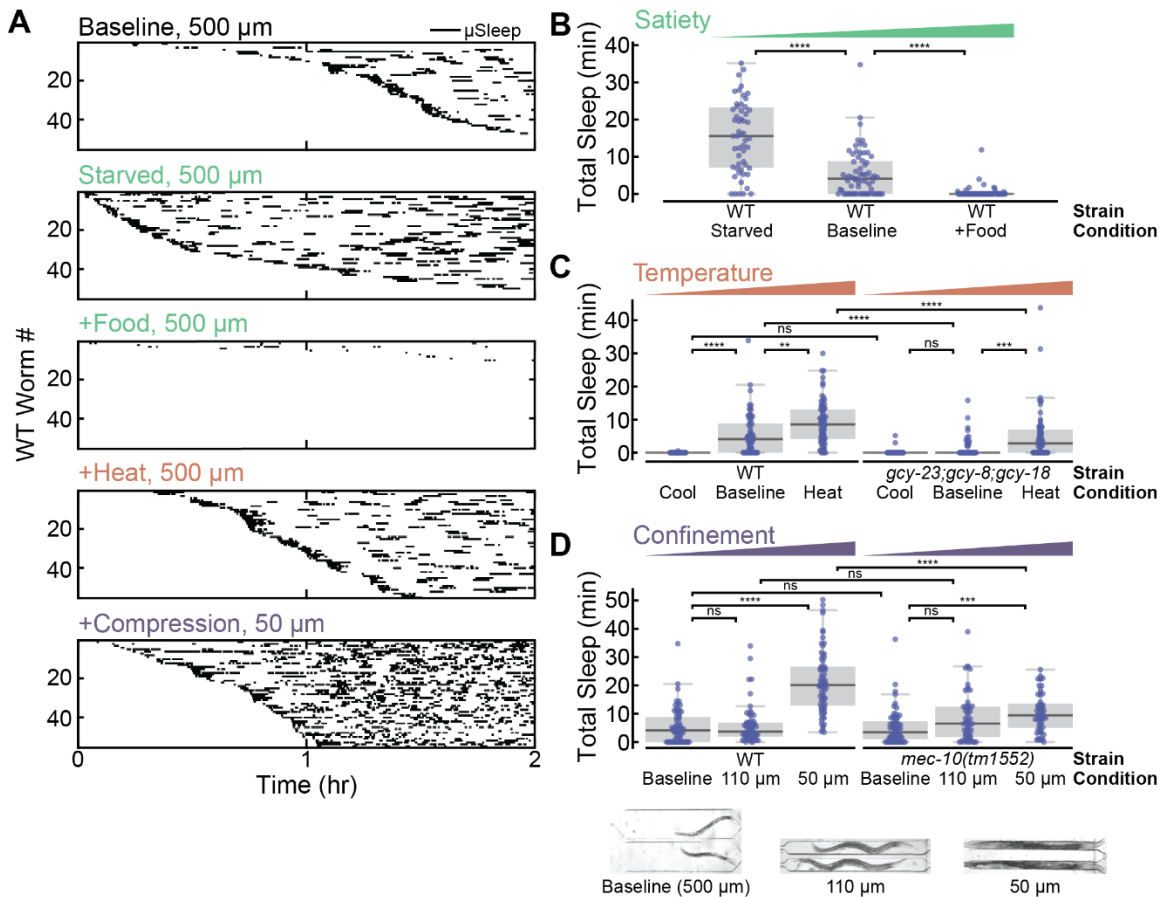


Figure 4.1 – Satiety, thermosensation, and mechanosensation regulate μ Sleep.

(A) Detected sleep bouts for WT animals in several experimental conditions. Raster plots show detected sleep bouts during a 2 hr imaging period. “Baseline” indicates the standard experimental conditions. “Starved” indicates animals that were starved prior to the assay. “+Food” indicates conditions in which *E. coli* OP50 was added into the buffer during recordings. “+Heat” indicates imaging conditions where the temperature was raised to 25 °C. “+Compression” indicates that animals are partially immobilized in 50 μ m-wide chambers. See micrographs under (D) for chamber geometries. In all cases, the sleep phenotype varies dramatically from the baseline. Only the 55 animals that displayed the most sleep are plotted for clarity. Raster plots for all WT and mutant animals are shown in Fig. S4. (B) Total WT sleep under varying satiety conditions. As satiety increases from “Starved” to “+Food,” animals exhibit less μ Sleep (from left to right on the plot the number of animals $n = 55, 68, 67$). (C) Total μ Sleep under varying temperature conditions. “Cool” = 18 °C, “Baseline” = 22 °C, “Heat” = 25 °C. Increasing temperature increases total μ Sleep for WT animals. Thermosensory-defective mutants show the same μ Sleep phenotype as WT at 18 °C, but significantly less sleep as 22 °C and 25 °C, indicating that thermosensory input can act to drive or suppress μ Sleep (from left to right on the plot the number of animals $n = 37, 68, 71, 41, 67, 60$). (D) Total sleep

under different confinement conditions. Micrographs show chamber geometries. When WT animals are confined in smaller chambers, they only show an increase in total μ Sleep when slightly compressed in 50 μm -wide chambers. *mec-10(tm1552)* mutants show an identical phenotype to WT in 500 μm and 110 μm chambers, but dramatically reduced sleep compared to WT when compressed. These results suggest that nociceptive input to mechanosensory neurons regulates μ Sleep (from left to right on the plot the number of animals $n = 68, 64, 69, 66, 64, 57$). (ns = not significant, ** $p < 0.01$, *** $p < 0.001$, **** $p < 0.0001$; Kruskal-Wallis with a post-hoc Dunn-Sidak test). (Figure adapted from Gonzales et al., 2019, under review as of April 2019).

4.2. High satiety abolishes μ Sleep

We first tested how food availability affects the μ Sleep phenotype. The presence of food is known to change the swimming-induced quiescence phenotype (Churgin, McCloskey, et al., 2017; McCloskey et al., 2017), high quality food induces quiescence (You et al., 2008), and extreme starvation also leads to sleep-wake switching (Skora et al., 2018; Wu et al., 2018). Therefore, we hypothesized that the internal satiety state is a significant regulator of μ Sleep. To test this hypothesis, we assayed three satiety states in WT animals: “Starved” animals were starved for 2 hr before being loaded into a chambers with no food; “Baseline” animals were loaded directly from a NGM food source to a microfluidic device with no food; and “+Food” animals were loaded from a NGM food source into a microfluidic device with food dissolved in the buffer. As expected, we observed less total μ Sleep per worm as satiety increased from “Starved” (15 ± 2 min, mean \pm sem) to “Baseline” (5.4 ± 0.9 min) to “+Food” (0.4 ± 0.2 min) (Figure 4.1A-B). These results show that satiety is a

strong regulator for μ Sleep, which may have evolved to optimize the tradeoff between energy conservation and the search for food.

4.3. Bi-directional thermosensory input can increase or decrease total sleep

Other well-known drivers of sleep are noxious environmental stressors, which we also tested in the context of our microfluidic chambers. Heat shock at temperatures greater than 30 °C is a common method to induce cellular stress and *C. elegans* sleep (Hill et al., 2014; Iannacone et al., 2017; Nath et al., 2016; Matthew D. Nelson et al., 2014; Cheryl Van Buskirk & Sternberg, 2007). Although our standard μ Sleep assays were conducted at only 22 °C, we investigated whether these small changes from T_c could be a possible environmental regulator of quiescence. Indeed, we discovered that increasing the assay temperature to 25 °C, which is still well below commonly used temperatures for heat-shock (30-40 °C), increased the total observed sleep 3.5-fold (Figure 4.1A, C). Cooling the device to 18 °C (i.e. below T_c) had the opposite effect and nearly abolished all μ Sleep bouts (Figure 4.1). To show that these changes in phenotype are mediated by *C. elegans* thermosensation, we tested triple-knock-out *gcy-23(nj37);gcy-8(oy44);gcy-18(nj38)* mutants, which show disruption to thermosensation that is specific to the AFD neurons, the primary temperature-sensing neurons in *C. elegans* (Ramot, MacInnis, & Goodman, 2008). In AFD-defective animals we observed no significant change in

total μ Sleep when raising the temperature from 18 °C (“cool”) to 22 °C (“baseline”). Under the same conditions WT animals showed a 540-fold increase in total μ Sleep (Figure 4.1C). Furthermore, thermosensory-defective mutants displayed 80% less μ Sleep at 22 °C (“baseline”) and 45% less μ Sleep at 25 °C (“heat”) when compared to WT animals (Figure 4.1C). These results suggest that AFD neurons transduce changes in environmental temperature and drive downstream sleep-promoting circuits. These results show that temperature changes significantly less than those typically used for heat shock can dramatically change the μ Sleep phenotype. In addition, this is the first indication that thermosensory input can act bidirectionally to either promote or suppress *C. elegans* quiescence.

4.4. Confinement and restraint increase total sleep through mechanosensory circuits

The final environmental factor we investigated was animal confinement. Under baseline conditions, animals swim in large 500 μ m-width chambers (Figure 4.1D, inset). We found that confining animals to a smaller 110 μ m-width chamber, where the primary motion is crawling-like (Figure 4.1D inset) leads to the same amount of total μ Sleep as the baseline chambers (Figure 4.1D). However, when we partially compressed WT animals in small 50 μ m-width chambers, we observed nearly a 4-fold increase in total sleep compared to baseline (Figure 4.1A, D). We hypothesized that this change in phenotype due to immobilization was at least

partially mediated by mechanosensory circuits. For example previous reports showed that touch-defective mutants *mec-10(tm1552)* have a decreased ability to sense spatial patterns in microfluidic arenas (Han et al., 2017). We tested *mec-10(tm1552)* as well and found that when minimal mechanical stress was present (i.e. 500 μm and 110 μm width chambers), total μSleep remained insignificantly unchanged compared to WT (Figure 4.1D, S4). However, when *mec-10(tm1552)* animals were compressed, total animal μSleep decreased by a factor of two compared to WT animals under the same conditions (Figure 4.1D, S4), indicating that mechanosensory pathways are necessary for restraint-induced μSleep . Together, these results show for the first time that *C. elegans* microfluidic immobilization induces sleep behavior through mechanosensory pathways.

4.5. μSleep phenotypes partially correlate with animal stress

Given the dependence of μSleep on satiety, temperature, and mechanical stress (Figure 4.1), we hypothesized that each of these factors could act as stressors that contribute to a slow-onset form of stress-induced sleep. To test this hypothesis, we assayed DAF-16::GFP animals in the identical environmental conditions shown in Figure 4.1. While normally diffuse in the cytoplasm, under unfavorable environmental conditions (e.g. heat shock), DAF-16::GFP localizes to the nucleus (Henderson & Johnson, 2001), serving as a quantifiable proxy for *C. elegans* stress. We quantified puncta formation in different environmental conditions and observed that DAF-16::GFP localization correlated with μSleep phenotypes in only some cases

(Figure 4.2). For example, we found that compared to Baseline animals, +Heat animals showed greater than a 250% increase in the number of cumulative puncta (Figure 4.2). Conversely, +Compression animals showed no significant difference in the number of DAF-16 puncta compared to Baseline (Figure 4.2), despite displaying dramatically more total μ Sleep (Figure 4.1). These results suggest that animal stress may not completely explain the changes in μ Sleep we observe during environmental manipulations. Therefore, μ Sleep is likely a result of many factors, including stress, starvation, and the metabolic state.

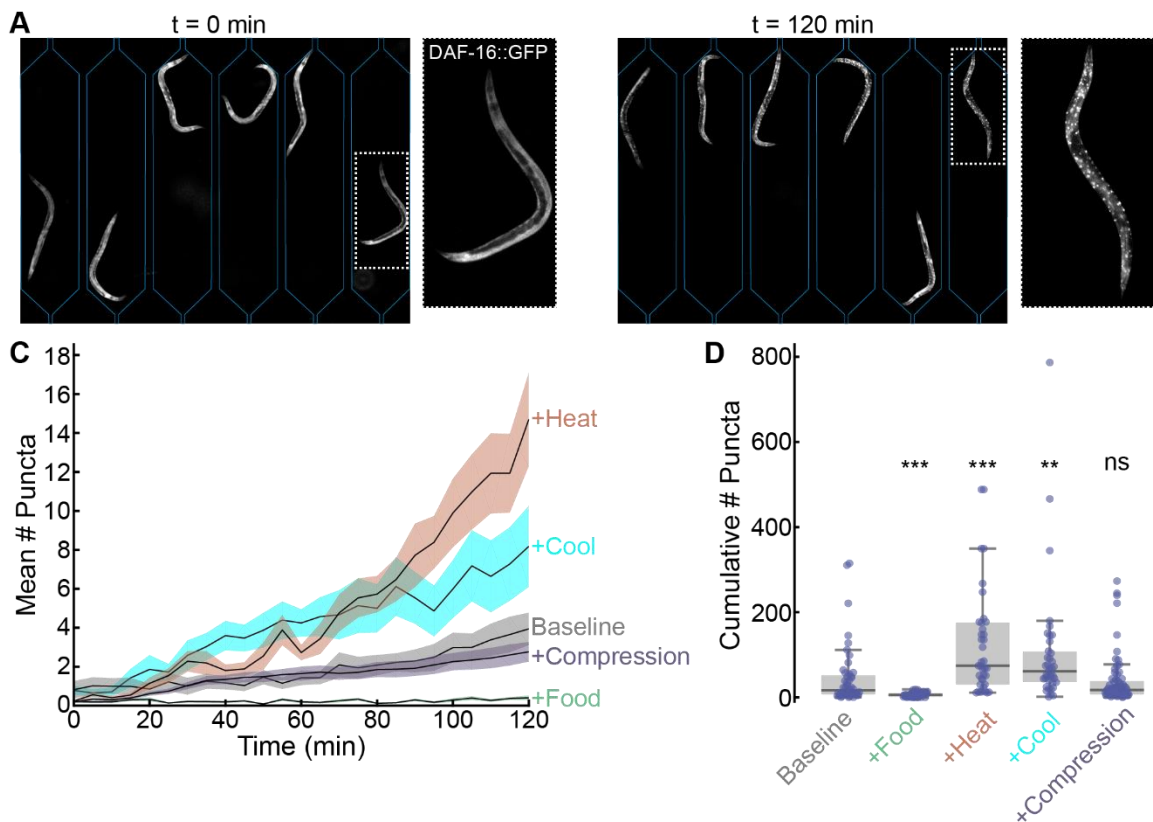


Figure 4.2 – DAF-16::GFP imaging shows that μ Sleep partially correlates with *C. elegans* stress.

(A) Fluorescent micrographs (with background subtracted) of DAF16::GFP animals confined to 500 μm -wide chambers during the +Heat condition. Microfluidic chambers are outlined. Left image ($t = 0$ min) shows diffuse DAF-16::GFP. Over the course of 2 hr, DAF-16 localizes to the nucleus (right image). (B) Puncta formation with respect to time for Baseline, +Food, +Heat, +Cool, and +Compression conditions (see Methods, Figure 4.1). (C) Cumulative number of puncta during imaging. Individual data points represent individual animals. (Baseline $n = 48$, +Food $n = 46$, +Heat $n = 38$, +Cool $n = 39$, +Compression $n = 71$; ** $p < 0.01$, *** $p < 0.001$, ns = not significant, Kruskal-Wallis with a post-hoc Dunn-Sidak test). (Figure adapted from Gonzales et al., 2019, under review as of April 2019).

4.6. Constantly replenishing fluidic buffer does not reduce μSleep

In addition to environmental elements like mechanical compression and temperature that change sleep, we ruled out the possibility that O_2 depletion, CO_2 buildup, or the buildup of other unknown substances dramatically affect μSleep by constantly replenishing the chamber buffer using a gentle flow (Figure 4.3). This flow should stabilize gas concentrations as well as remove and animal byproducts. Surprisingly, we observed that the gentle flow led to more sleep (Figure 4.3). Therefore, a lack of O_2 or a buildup of CO_2 are not major drivers of μSleep .

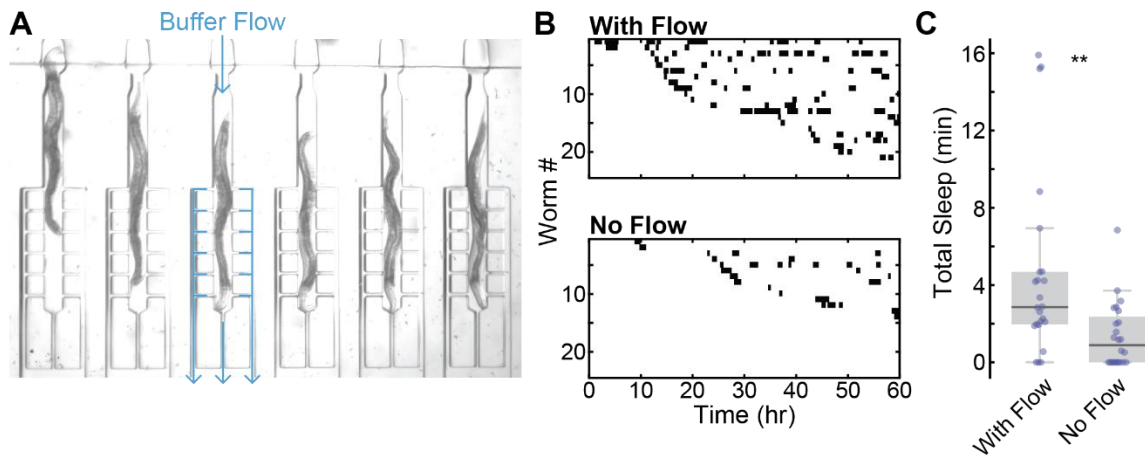


Figure 4.3 – Constantly replenishing fluidic buffer does not reduce sleep.

(A) Image of animals confined in microfluidic chambers designed for constantly flowing buffer to stabilize O_2 concentrations and remove the buildup of CO_2 and other byproducts. Blue paths indicate the direction of flow for a single chamber. Flow rate was ~ 1 mL/hr. (B) Raster plots of detected μ Sleep with and without flow using the geometry in (A). (C) We surprisingly observed more sleep with the buffer flow, indicating μ Sleep is likely not driven by changing gas concentration levels biological byproducts ($n = 24$ for each cohort, $**p < 0.01$, unpaired t-test). (Figure adapted from Gonzales et al., 2019, under review as of April 2019).

4.7. Summary of factors that regulate μ Sleep

Overall, our environmental manipulations conclusively show that the animal satiety state, the mechanical environment, and the local temperature strongly regulate the μ Sleep phenotype. Starvation, increased temperature and increased confinement all increase the amount of measured μ Sleep. Thus, μ Sleep is a multisensory-regulated sleep behavior that is also strongly modulated by internal physiological factors.

Environmental changes, particularly to the chamber geometry also led to phenotypic changes not captured by quantifying total μ Sleep (Figure 4.4). For

transparency, all detected sleep bouts are shown in Figure 4.4. For example, WT animals in 110 μm chambers showed an accelerated onset of sleep bouts (Figure 4.4). Future work will continue to interrogate how sensory mechanisms regulate sleep and arousal.

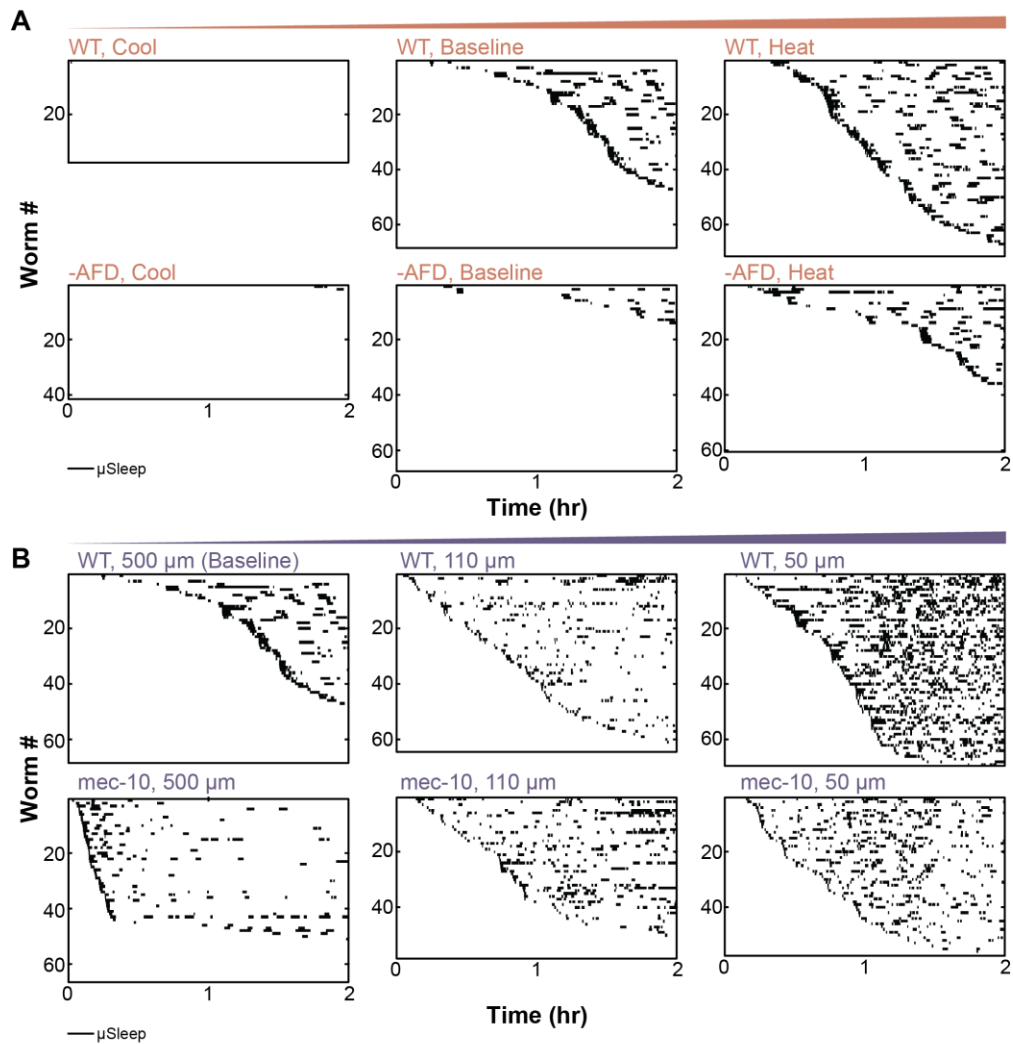


Figure 4.4 – Raster plots of detected sleep for all animals during temperature and mechanical regulation.

These data are quantified in Figure 4.1. (A) Changing environmental temperature. “Cool” = 18 °C, “Baseline” = 22 °C, “Heat” = 25 °C. “-AFD” = *gcy-23(nj37);gcy-8(oy44);gcy-18(nj38)*

mutants. (B) Changing animal confinement in 500 μm , 110 μm and 50 μm -width chambers. “mec-10” refers to *mec-10(tm1552)* mutants. Raster plots show interesting phenotypes not captured when quantifying total μSleep (Figure 4.1). For example, WT animals in 110 μm chambers show accelerated sleep onset but shortened sleep bout lengths, leading to no overall change in total μSleep (Figure 4.1). Likewise, in 500 μm chambers *mec-10* animals also show different temporal dynamics compared to WT. Further work will continue to interrogate these phenotypic changes. (Figure adapted from Gonzales et al., 2019, under review as of April 2019).

Experimental Methods and Data Analysis

This chapter details the specific methods and analyses used to perform experiments and animals behavioral and calcium-imaging data. As with Chapter 2, This chapter is largely adapted from Gonzales, Zhou, & Robinson, 2019, which is currently under review as of April 2019. A non-peer reviewed preprint can be found at <https://doi.org/10.1101/547075>.

5.1. *C. elegans* strains and maintenance

Animals were raised in a temperature-controlled environment at 20 °C on standard NGM seeded with *E. coli* OP50. All experiments were performed with day-1 adult animals. The strains used for each experiment are as follows:

- Figure 2.1: N2
- Figure 2.2: N2

- Figure 2.3: N2
- Figure 2.4: N2, IB16 *ceh-17(np1)* I; HBR227 *aptf-1(gk794)* II.
- Figure 3.1: AML32 (*wtfls5* [*prab-3::NLS::GCaMP6s*; *prab-3::NLS::tagRFP*])
- Figure 3.2: HRB1361 (*goIs304[pflp-11::SL1-GCaMP3.35-SL2::mKate2-unc-54-3'UTR, unc-119(+)]*)
- Figure 4.1: N2, IK597 *gcy-23(nj37);gcy-8(oy44);gcy-18(nj38)* IV, ZB2551 *mec-10(tm1552)*
- Figure 4.4: N2, IK597 *gcy-23(nj37);gcy-8(oy44);gcy-18(nj38)* IV, ZB2551 *mec-10(tm1552)*
- Figure 4.2: TJ356 (*zIs356 [daf-16p::daf-16a/b::GFP + rol-6(su1006)]*)
- Figure 4.3: N2
- Figure 6.2: AML32 (*wtfls5* [*prab-3::NLS::GCaMP6s*; *prab-3::NLS::tagRFP*])
- Figure 6.3: AML32 (*wtfls5* [*prab-3::NLS::GCaMP6s*; *prab-3::NLS::tagRFP*])
- Figure 6.4: N2

5.2. Microfluidic device fabrication

Standard photo- and soft-lithography techniques were used to fabricate microfluidic devices (San-Miguel & Lu, 2013). Microfluidic geometries were custom

designed in CAD software. Most photomasks were transparencies (CAD/Art Services Inc.), but glass photomasks (Front Range Photomask) were used for higher-resolution devices. All master molds were fabricated using SU-8 2075 (MicroChem). The SU-8 height for worm behavioral channels was 75 μm (spin: 20 s – 500 rpm, 30 s – 3000 rpm), but we used a height of 50 μm (spin: 20 s – 500 rpm, 30 s – 4000 rpm) for whole-brain imaging devices to further constrict animal movement. We used polydimethylsiloxane (PDMS) Sylgard for all microfluidic chips. All behavioral chips were double-layer devices to incorporate push-down valves for sealing the chamber entrances or delivering mechanical stimuli. The bottom worm layer (20:1 ratio, spin: 930 rpm for 30s) was bonded to the upper valve layer (10:1 ratio) using a 30 s exposure to oxygen plasma (200 W, 330 mTorr), then baked together for at least 12 hr. The PDMS devices were permanently bonded to either a standard glass slide for behavior, or a 300 μm -thick quartz wafer (NOVA Electronics Materials) for whole-brain imaging.

5.3. Behavioral quantification and sleep detection

To quantify *C. elegans* activity, we used frame-by-frame subtraction. This method subtracts consecutive frames from one another, then counts the number of pixels that substantially change value. Worm movement leads to a large number of pixels that change from frame-to-frame. Quiescent animals, which move very little, lead to few pixels that change values from frame-to-frame. We performed frame-by-frame subtraction, drew regions-of-interest around each animal, then counted the

number of pixels in the ROI that changed by a value greater than 30 (a number well above the noise level of the CMOS sensor). This yields a raw activity trace for each animal. We also used standardized methods to normalize activity traces (Churgin, McCloskey, et al., 2017; McCloskey et al., 2017), which accounts for changes in brightness across the field-of-view (FOV), and allowed us to set a consistent sleep detection threshold across populations. In most cases, we smoothed activity traces across 20 s, then normalized to the top 95th percentile, yielding a normalized activity trace for each animal with values approximately between 0 and 1. For analysis that required finer timescales on the order of less than 20 s (Figure 2.2), we did not smooth activity traces.

Once we normalized the activity trace, we thresholded the data to detect sleep. The threshold depended on the microfluidic geometry. For example, in large microfluidic chambers, movement could still be detected during μ Sleep as animals drifted across the chamber. In smaller microfluidic geometries, worm activity was already significantly constrained, so a stricter threshold was needed to detect sleep. We determined thresholds by manually scoring 20 sleep bouts, calculating the mean activity during those bouts, then doubling the mean activity. The thresholds used for each geometry were: WorMotel – 0.15; 500 μ m microfluidic chambers – 0.15; 110 μ m microfluidic chambers – 0.08; 50 μ m chambers – 0.06. A minimum sleep bout time of 30 s was used to reduce false detections. In addition, during a sleep state brief animal twitching lasting less than 15 s was not counted as a wake period.

5.4. Standard microfluidic behavioral assays

Unless otherwise stated, behavioral assays took place on an enclosed AmScope SM-2T-LED stereo microscope. Red transparency was used to filter out LED wavelengths that potentially affect animal behavior. Imaging was performed at 3 fps with either a Point Grey Grasshopper (GS3-U3-23S6M-C) or Basler Ace (acA1920-40um) CMOS cameras, which have nearly identical sensor specifications. While the experiments were typically carried out in a room held at 20 °C, the heat from the LED raised the microfluidic device temperature to 21-22 °C (the “Baseline” temperature in Figure 4.1).

M9 buffer was used for all experiments, with no food added unless otherwise stated. During standard experimental conditions, we used a hair pick to transfer day-1 adults directly from seeded NGM into the buffer of an open syringe cap. We then suctioned animals into Tygon tubing that led to the microfluidic chambers. The process of loading 6-12 animals into the chambers (depending on the geometry used) typically took less than 5 min. A push-down valve closed off the entrance of all worm chambers to prevent animals from escaping during imaging. After use each day, devices were flushed with ~6 mL of DI water, sonicated for 10 min, flushed again with DI water, boiled for 15 min, and flushed a final time before storage at ~80 °C overnight.

5.5. WorMotel assays

A 48-well WorMotel molded from PDMS was provided by the Fang-Yen Lab (Churgin, Jung, et al., 2017). Only 12 wells were used simultaneously. Prior to use, the PDMS was exposed to oxygen plasma for 30 s to make the surface hydrophilic. Each well was then filled with 8 μ L of M9 buffer. Using a hair pick, we removed individual animals from seeded NGM, washed them in an M9 droplet, then transferred them into the WorMotel wells. For imaging, the PDMS was inverted and reversibly sealed on a glass slide during imaging (see Churgin *et al.* 2017). The glass slide was treated with Rain-X to prevent condensation. The device was illuminated obliquely with three AmScope Goose-neck LEDs that were filtered with red transparency. As with microfluidic devices, the temperature during imaging was 21-22 C. We imaged from below at 3 fps with a Point Grey Grasshopper (GS3-U3-23S6M-C).

5.6. Heat-shock

Device setup and animal loading was performed as previously stated (see Section 5.4). However, the device was preheated to 30 °C with two Peltier heaters placed on each side of the glass slide. Heat was applied for the initial 30 min of imaging, after which the current through the Peltier heaters was reversed such that the device was rapidly brought to the standard 22 °C. This heat-shock protocol was adapted from that used for agar plates in Hill *et al.* 2014.

5.7. Reversibility and decreased response to stimuli

Reversibility assays were conducted on an inverted Nikon microscope and performed with 50 μm -wide microfluidic chambers. Animals were loaded into the chambers and left for 30 min. Between 30 and 60 min, upon visual confirmation of sleep, we initiated a protocol of 60 s of imaging at 10 fps. At 30 s, a strong light stimulus (460 nm light at 5 mW/mm^2) was presented for 5 s to awaken animals. Only animals that were asleep for the full 30 s prior to the light stimulus were kept for analysis.

To test for a decreased response to stimuli, we fabricated 110 x 1100 μm microfluidic chambers to confine animals. In addition to the push-down valve used to keep animals in each chamber, we incorporated two push-down valves used for mechanical stimulation. The two valves ensured that animals were almost always in contact with at least one valve during pressurization. For strong and weak stimulation we used a valve pressure of 30 and 15 psi, respectively. 7 groups of animals were used for weak stimulation and 4 for strong stimulation; each group consisted of 8-12 animals. During the hour-long assay, animals received a 0.5 s valve pulse every 3 min. During post-processing, we analyzed animal activity around each stimulation timepoint. For the 10 s prior to each stimulation timepoint, we classified animals as quiescent, slow-moving, or fast-moving. Two categories for wake behavior (i.e. slow-moving and fast-moving) were necessary because a behavioral response could not be detected in animals that were already moving with a high

activity. That is, an animal that was clearly awake and moving with high activity in the microfluidic chamber did not display increased activity after receiving mechanical stimuli. However, a detectable behavioral response was apparent in wake, but low-activity animals. We used an activity threshold of < 0.08 for quiescent animals, $0.08-0.35$ for low-activity animals, and > 0.35 for high-activity animals (the average animal activity across all traces was 0.36). This classification was performed for each stimulation (20 stimulations for each animal). After classifying animals into each group, we also calculated the mean activity for 10 s post-stimulation, excluding a 2 s period where the microfluidic valves caused movement artifacts. The pre- and post-stimulation activities for quiescent and low-activity comprise the data shown in Figure 2.2.

5.8. Whole-brain imaging

Microfluidic devices were fabricated as previously described (see Section 5.2), and geometries were modeled off of previous methods for whole-brain imaging (Kato et al., 2015; Nichols et al., 2017; Skora et al., 2018); however, animals were not chemically paralyzed. We used transgenic animals with pan-neuronal expression of GCaMP6s in the nuclei of all neurons (Nguyen et al., 2015, 2017). Experiments were performed on an inverted Nikon microscope with a 40X water-immersion objective (NA = 1.15). An Andor Zyla 4.2 USB 3.0 sCMOS captured the images at 5 fps (50 ms exposures, 2x2 binning). Because blue light can wake *C. elegans*, when animals were immobilized in the chambers, we first initialized a

“habituation” protocol. Here, we flashed the 460 nm excitation light for 0.15 s at 1 Hz for 30 min. This habituated animals without photobleaching the calcium indicator. After the habituation period, we imaged continuously for 15 min, but only analyzed the first 10 min of data due to photobleaching. With this protocol, we captured a sleep-wake transition in ~25% of animals.

To analyze data, we chose 10 neurons at random to track by hand in ImageJ. An 8x8 pixel ROI was then used for each neuron in each frame. A neuron near the center of the ganglia was used to draw an ROI around the head ganglia to calculate average brain fluorescence in each frame. We calculated animal activity in two ways: by frame-by-frame subtraction (sampling the frames at 3 Hz), and by calculating the average displacement of the tracked neurons. Both methods were prone to fluctuating baselines that were not present during behavioral-only recordings, making it difficult to set a standard threshold across animals. However, clear quiescent periods were subjectively apparent. Therefore, for each animal we plotted only the animal behavioral activity and selected sleep bouts manually. As before, only bouts longer than 30 s were counted. We then calculated the mean ganglia and neuron fluorescence during sleep and wake for each worm.

Behavioral activity was smoothed over 3 s and normalized as previously described (see Section 5.3). Raw ganglia and neuron activity was smoothed over 3 s before calculating $\Delta F/F$. We denote $\Delta F/F$ as $[F(t) - F_0(t)]/F_0(t)$ where $F_0(t)$ is the minimum fluorescence value up to time t .

5.9. RIS imaging

7-10 animals per trial (6 trials total) were confined and imaged simultaneously under 10X magnification in the 50 μm -wide chamber geometry. HRB1361 animals expressed both GCaMP3 and mKate in RIS neurons under the FLP-11 promoter. Experiments took place on an inverted Nikon microscope, with dual excitation and emission for simultaneous two-color imaging (FF01-468/553-25 and F01-512/630-25 BrightLine dual-band bandpass filters for excitation and emission, respectively). An X-Cite XLED1 light source provided both 460 nm and 565 nm excitation light and a Tucam image splitter (Andor) split the mKate and GCaMP channels onto two Andor Zyla 4.2 CMOS cameras. We imaged animals for 2 hr and used a data-acquisition box (National Instruments) controlled with custom Matlab scripts to simultaneously trigger 10 ms camera exposures and 30 ms XLED flashes at 0.5 Hz (3x3 binning). Following experiments, we flushed animals from the device and recorded the background for each color channel.

For post-processing, we used the mKate channel to quantify behavior and track the location of RIS neurons. After subtracting background, we calculated animal activity by drawing an ROI around each animal and performing the same frame-by-frame subtraction method as previously described (see “Behavioral Quantification and Sleep Detection” subsection), but here we used a pixel change threshold of 400 because of the high dynamic range of the Zyla sensor. After normalizing behavioral activity, a threshold of 0.2 was used to detect sleep bouts,

with a minimum sleep time of 60 s. To detect the RIS location in each frame, we again subtracted the image background. We then isolated and binarized each animal ROI, leaving only the RIS neuron and, occasionally, pieces of its processes. The largest object in the ROI was the RIS soma, which we used to attain the soma centroid. To get the average RIS fluorescence in the frame, we drew a 25x25 pixel ROI around the centroid in each channel (a region larger enough to ensure the neuron is within the ROI) and averaged the 20 largest pixel values (presumably, the 20 brightest pixels within the neuron ROI make up the neuron soma). We normalized this raw fluorescence in each channel by calculating $\Delta F/F = [F(t) - F_0(t)]/F_0(t)$, where $F_0(t)$ is the minimum fluorescence value up to time t . Following this normalization, we calculated the ratio of each color channel $R = (\Delta F/F)_{\text{GCaMP}}/(\Delta F/F)_{\text{mKate}}$. Finally, the reported ratio values are $\Delta R/R = [R(t) - R_0]/R_0$, where R_0 is the lower 20th percentile value.

5.10. Environmental control

The microfluidic setup during environmental manipulation was identical the previously stated (see Section 5.4); however, for each condition we manipulated individual aspects of the environment.

The baseline phenotype in 500 μm -wide chambers was chosen because animals could move freely in a manner similar to swimming, thereby reducing the overall effect of the microfluidic confinement.

Most assays involved transferring animals directly from seeded NGM into the microfluidic device. However, under “Starved” conditions we used a hair pick to remove animals from seeded NGM, washed them in a droplet of M9 buffer, then placed them onto a fresh, unseeded NGM plate. After 2 hr, animals were loaded into the microfluidic device with no food in the buffer. Therefore, animals were deprived of a food source for 2 hr when imaging began and did not have access to food during the experiment.

Most assays were also performed with no food in the M9 buffer. However, under “+Food” conditions, we dissolved 4.56 mg/mL of freeze-dried OP50 (LabTie) into the M9 buffer, providing a food source for animals throughout the imaging time.

In “+Compression” conditions, animals were confined to 50 x 1100 μm -wide microfluidic chambers.

As previously stated, the standard imaging temperature due to LED lighting was 21-22 °C (see Section 5.4). We controlled temperature in the same manner as heat-shock experiments, using Peltier devices to heat or cool the microfluidic chips to 24-25 °C or 17-18 °C, respectively.

5.11. DAF-16::GFP imaging

Experiments took place over the course of 2 hr on Nikon inverted scope with an Andor Zyla 4.2 USB 3.0 sCMOS and 4X magnification for multi-worm imaging.

Environmental control took place as described in Section 5.10 subsection. Every 5 min, we captured 7 frames (20 ms exposures) at 1 Hz with 1x1 binning. Otherwise, animals were in darkness. Following imaging, we flushed animals from the chamber and recorded background frames.

Puncta quantification took place similar to previous methods (Kopito & Levine, 2014). We subtracted the background from each frame and smoothed the image with a median filter. We thresholded this image to detect animal bodies and drew a ROI around each. The smoothed image was further processed with a 3x3 high frequency filter, which enhanced the contrast of puncta and allowed us to binarize the image to detect most DAF-16 aggregations in the frame. For each animal ROI, we then found puncta by counting all objects with a size between 2 and 30 pixels. To mitigate the effects of animal movement, which caused some animals to appear blurred and reduced puncta count, of the 7 frames that were captured every 5 min, we averaged the 3 largest puncta counts for each ROI. This average makes up the final puncta count for each animal at the given timepoint. The puncta count reported (Figure 4.2) are likely lower than the true count that would be attained with high-magnification imaging. Low-magnification not only increases the number of animals imaged per trial but was also necessary to capture the full length of the large microfluidic chambers. Because we applied the same algorithm to all environmental conditions, we expect the reported trends to remain true in high-magnification conditions.

Summary of μ Sleep, Future Directions, and Outlook on *C. elegans* Sleep

6.1. Summary of results

In this thesis, I described a spontaneous *C. elegans* brain and behavioral state transition that is unique to microfluidic chambers, which facilitates whole-brain imaging and precise regulation of the environment (summarized in Figure 6.1). μ Sleep regulation appears to be at least partially linked to a slow-onset form of stress-induced sleep (Figure 4.2), and may also be related to swimming-induced quiescence (R. Ghosh & Emmons, 2008; McCloskey et al., 2017). Despite these potential similarities, the behavioral phenotype we measured is quantitatively distinct from these previously reported worm quiescent behaviors (Figure 2.1). We showed that μ Sleep is reversible (Figure 2.2A), that animals exhibit a decreased response to sensory stimuli while quiescent (Figure 2.2B-C), and that quiescence is dependent on known *C. elegans* sleep-promoting neurons, ALA and RIS (Figure 2.4). Thus, μ Sleep meets the precedent set for worm sleep behavior (Hill et al., 2014;

Nicholas F. Trojanowski & Raizen, 2016). In addition, we found that thermosensory input via the AFD neuron acts as a bidirectional controller of sleep; cooler temperatures promote wake, while warmer temperatures promote sleep (Figure 4.1). Furthermore, we showed for the first time that animal restraint can act through mechanosensory pathways to drive sleep behavior (Figure 4.1). Finally, a dramatic brain-state transitions and global downregulation of neural activity, with the exception of a few neurons, underlies μ Sleep behavioral transitions (Figure 3.1).

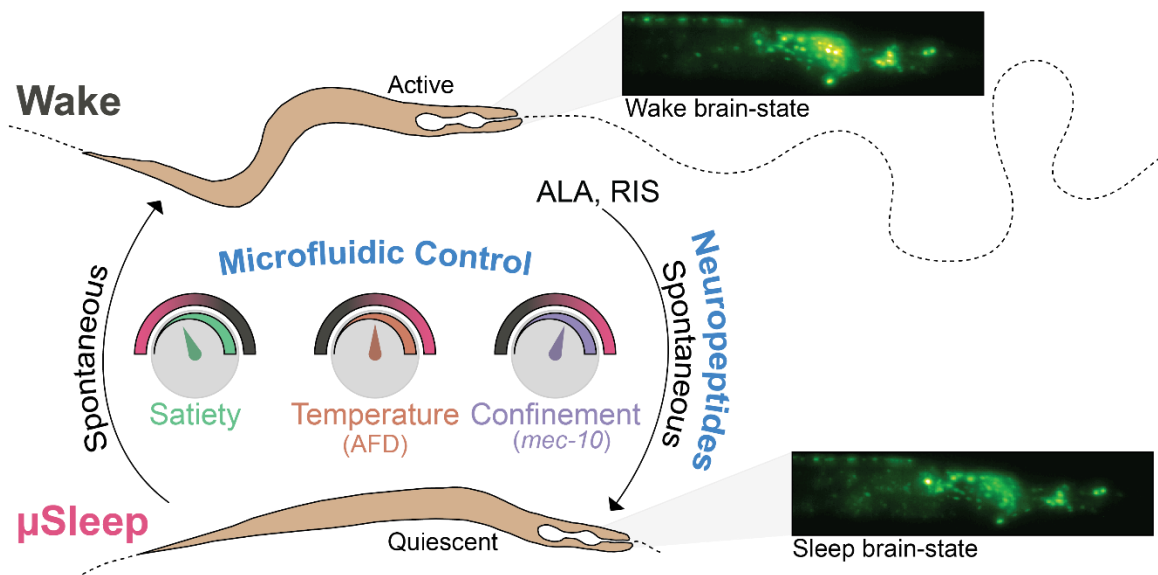


Figure 6.1 – Summary of μ Sleep results.

Graphical summary of results depicting spontaneous transitions between wake and μ Sleep behavioral states driven by microfluidic-controlled satiety, temperature, and confinement. Fluorescent micrographs show the high and low-activity brain states that correspond to wake and sleep, respectively.

6.2. Future directions with μ Sleep behavior

The μ Sleep platform has the advantages of microfluidic environmental control, whole-brain imaging, and potential for high-throughput experimentation. Here, I list several immediate goals and show preliminary data that would make this platform even more valuable for studying sleep, brain-state transitions, and *C. elegans* behavior.

6.2.1. Capturing the activity of more neurons during sleep-wake transitions

The whole-brain imaging data reported for μ Sleep conclusively showed that the sleep behavior was governed by a global downregulation of neural activity (see Figure 3.1). However, this single-plane imaging data is likely not suitable for uncovering the circuits and patterns of neural activity that drive brain-state transitions. Future work is necessary to capture the activity of more neurons (50-100) during state transitions to understand how the rapid and spontaneous brain-state transitions emerge.

One potential method to achieve this goal is to paralyze animals to facilitate high-resolution volumetric imaging (reviewed in Section 1.3.2) (Kato et al., 2015; Nichols et al., 2017; Prevedel et al., 2014; Schrödel et al., 2013; Skora et al., 2018). When applied to our microfluidic platform, indeed, this method yielded high-quality data and the stereotypically coordinated activity across much of the worm brain

(Figure 6.2A). In these data, clear state transitions occurred synonymous to what we observed during whole-brain imaging in behaving animals—a large-scale downregulation of activity—but a handful of neurons that dramatically increase in activity (Figure 6.2A). Furthermore, using PCA, we can replicate the cyclical and fixed-point attractor dynamics on the low-dimensional manifold during wake and sleep, respectively (Figure 6.2B, see Figure 1.15 for comparison) (Nichols et al., 2017). However, this method has severe drawbacks. The μ Sleep state must be assumed from neural activity and cannot be confirmed with behavior. In addition, while we captured μ Sleep during whole-brain imaging in $\sim 25\%$ of behaving animals (see Section 3.2), this percentage falls by an order of magnitude for paralyzed animals, suggesting that animals must be actively behaving to reliably exhibit spontaneous μ Sleep.

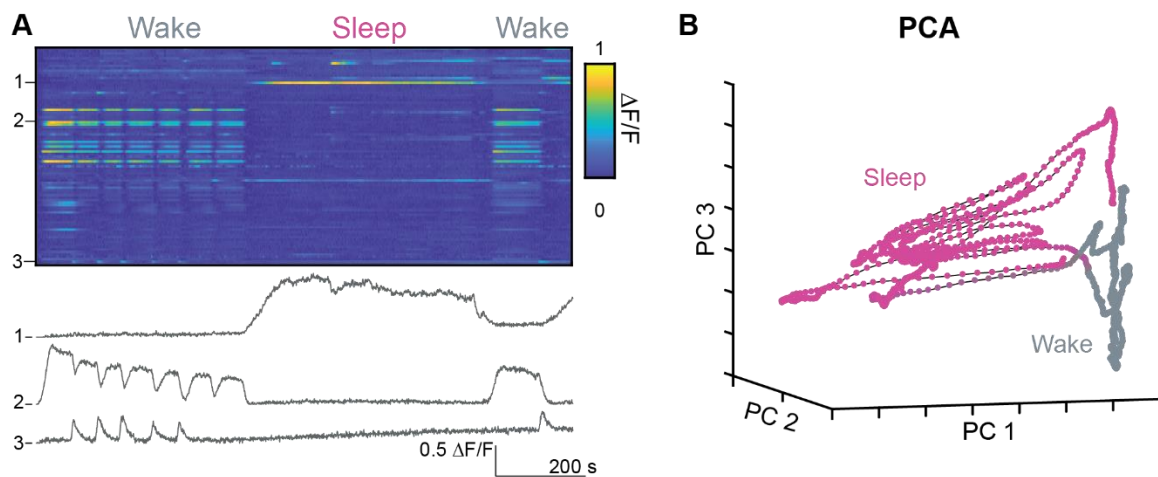


Figure 6.2 -Whole-brain imaging during μ Sleep in paralyzed animals.

(A) Heatmap of whole-brain imaging data from a paralyzed animal. Traces from select individual neurons are shown below the heatmap. We captured the activity of ~ 85 neurons and detected a dramatic brain-state transition assumed to be μ Sleep. (B) Performing PCA

replicates the results previously shown for *C. elegans* brain dynamics during sleep (Nichols et al., 2017).

In order to perform volumetric imaging in non-paralyzed animals, we developed a system for two-color whole-brain imaging, similar to the systems previously reviewed (see Section 1.3.1); however, because animals are restrained there is no need to track animal movement in real-time during imaging (Figure 6.3). The setup is essentially identical to the two-color imaging used to record single-neuron RIS data (Figure 3.2, see Section 5.9 for Methods); however a high-magnification objective is mounted onto a piezo scanner for volumetric imaging. This setup allows for using the RFP channel to track neuron location and the GCaMP channel to record neuron activity. Yet, as previously discussed (see Section 1.3.3), this and the necessary image processing comes with many challenges. Though animals are partially immobilized, the relatively slow scanning rate (~ 4 vol/s) leads to large amounts of neuron movement between volumes, making neuron tracking difficult to automate. In addition, computational methods to understand brain-wide transitions in neural dynamics are in their infancy. Thus, the necessary improvements described in Section 1.3.3 to improve whole-brain imaging experimentation in *C. elegans* should be applied to the μ Sleep platform as well. A faster imaging rate (20-30 vol/s), higher signal-to-noise ratios, accessible automated neuron tracking, and powerful computational methods for analyzing high-dimensional data sets are all future goals that should be incorporated into the

μ Sleep imaging pipeline. These advances will enable studies that uncover the ensemble neural dynamics driving spontaneous brain state transitions.

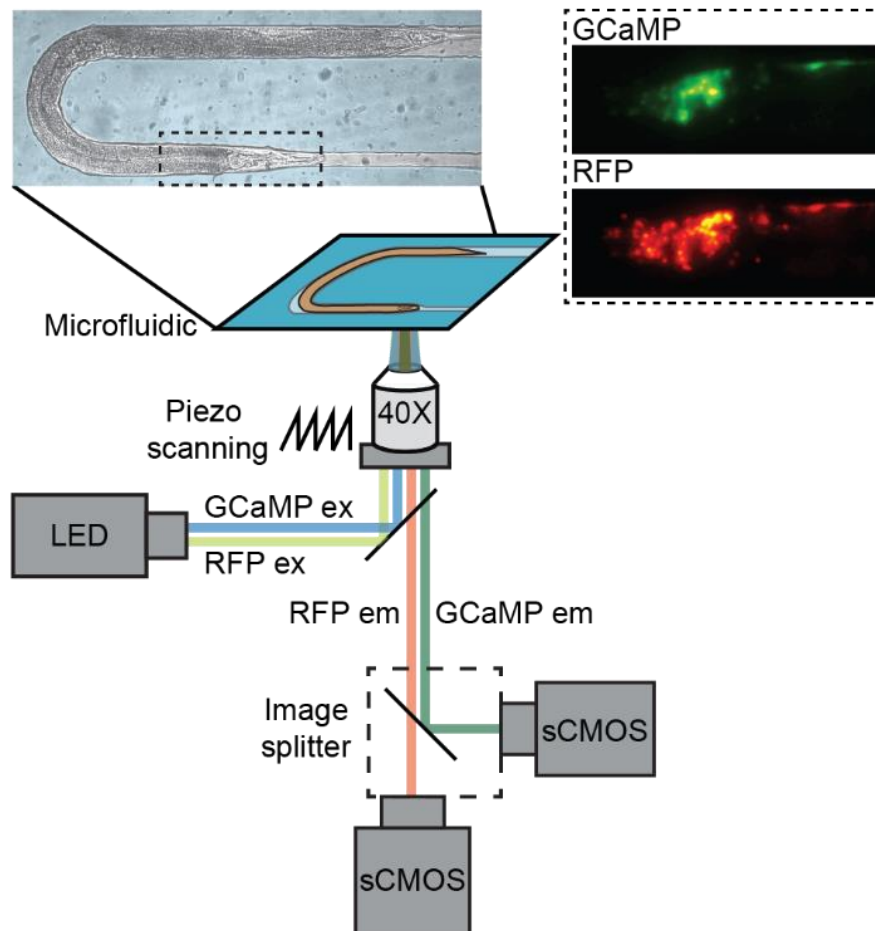


Figure 6.3 – Setup for two-color whole-brain volumetric imaging.

Schematic of the light paths for both excitation and emission wavelengths to image RFP and GCaMP simultaneously. An image splitter projects the emission wavelengths onto two sCMOS sensors. Inset shows a representative max-projections for each color channel during whole-brain imaging. See Section 5.9 for specific details.

6.2.2. High-throughput behavior

Fully understanding the mechanisms of *C. elegans* μ Sleep requires assaying many genetic mutants, changing culture conditions, and dynamically controlling the environment. Future work will likely include dozens of mutant strains to reveal the dependence of μ Sleep on sensory circuits, specific neurons, neuropeptides, and metabolic signaling. In anticipating of the need for a high-throughput behavioral platform, we are developing microdevices that can accommodate up to 30 animals simultaneously (Figure 6.4), more than tripling the current experimental throughput and leading to recordings from > 100 animals/day.

With these devices, we can isolate and image individual animals over the course of several hours, allowing for rapid behavioral phenotyping of several strains in a single day (Figure 6.4). Furthermore, we specifically designed this device so that the magnification and camera resolution is high enough to analyze animal posture during post-processing. For analysis only requiring quantification of worm movement (with frame-by-frame subtraction only, i.e. no posture analysis), the magnification can be further reduced, and the device can be scaled up to image from nearly 100 animals simultaneously.

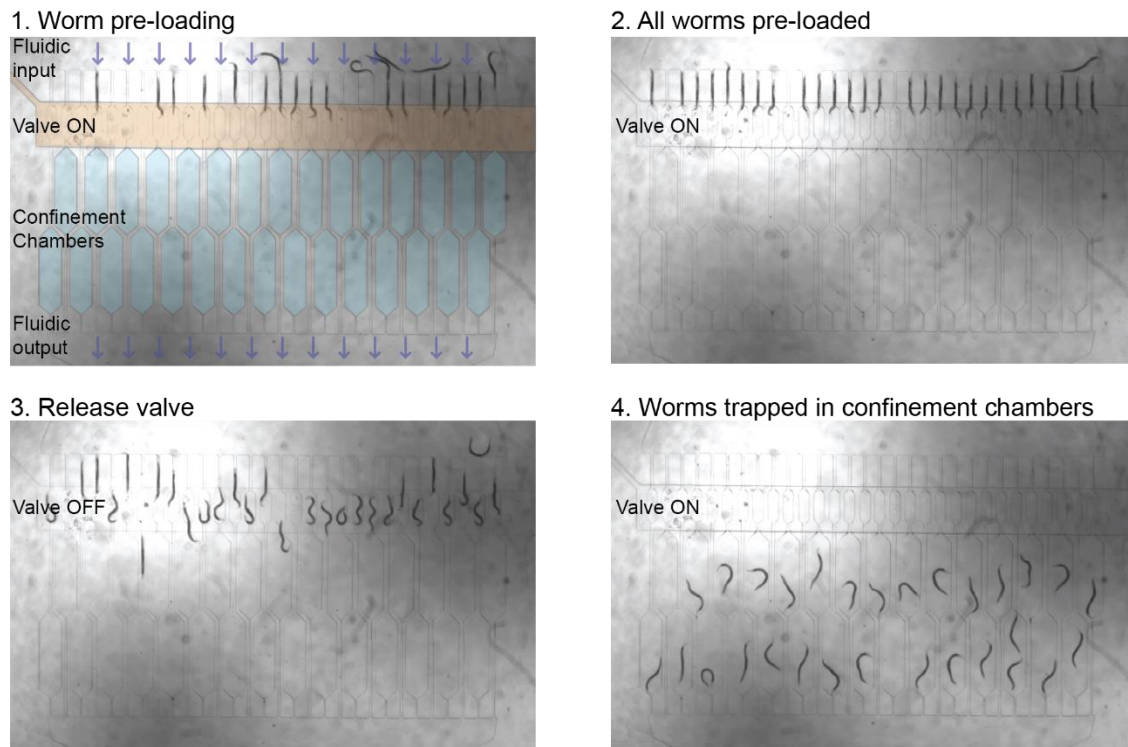


Figure 6.4 – High-throughput behavioral measurements in microfluidics.

Device for simultaneously imaging up to 30 animals simultaneously. 1. The device layout with false-coloring to indicate fluidic flow, microfluidic valve, and confinement chambers. When “on,” the microfluidic valve pinches off the worm channels, preventing animals from escaping into the confinement chambers. 2. Animals continue to be suctioned into the pre-loading chambers. These chambers are tailored to fit single day-1 adults and serves the purpose of isolating individual animals. 3. The valve is turned off, allowed animals to move into the confinement chambers. 4. Nearly all chambers are full and contain single animals. Behavioral monitoring can be performed over many hours.

With this device, we will continue to test the mechanisms regulating μ Sleep and the underlying multisensory integration driving this behavior. For example, increased environmental temperature increased the amount of total sleep (Section 4.3), but we also showed that the addition of food in baseline temperature conditions nearly abolished μ Sleep (Section 4.2). By combining these stimuli and

running experiments at multiple temperatures with multiple food concentrations, we can test the internal hierarchy *C. elegans* use to balance these two sensory stimuli. We likely expect food availability to trump small changes in environmental temperatures, leading to overall less μ Sleep in many instances. However, at more extreme temperature (25-30 °C), one can imagine that the need for sleep as a protective mechanism might overcome the need for an energy source, leading to an increased amount of μ Sleep. Notably, such intriguing behavioral findings may also be mapped within the nervous system and measured with calcium imaging in sensory circuits. This behavior-to-brain pipeline using μ Sleep is a potentially powerful behavior to study fundamental properties of multisensory integration at the circuit level.

6.2.3. Longitudinal imaging for understanding the need for invertebrate sleep

Combining our high-throughput platform with behavioral measurements over the lifetime of animals will also help to test the role of μ Sleep and other sleep states as a survival strategy. Recent reports make the controversial claim that normal invertebrate sleep (developmental sleep in *C. elegans* and circadian sleep in *Drosophila*) is not an essential function for survival or a normal lifespan (H. L. Bennett et al., 2018; Geissmann et al., 2019; Wu et al., 2018). However strong evidence indeed suggests that *C. elegans* sleep during stressful conditions, such as heat shock and starvation, is vital for survival (Hill et al., 2014; Wu et al., 2018). How

can both of these results be correct? Is *C. elegans* sleep vital for survival, or not? **I propose that binary measurements of survival are not adequate to determine whether invertebrate sleep is essential for a normal lifespan.**

No reports have analyzed *C. elegans* **healthspan** in sleepless mutants (Bansal, Zhu, Yen, & Tissenbaum, 2015; Keith, Amrit, Ratnappan, & Ghazi, 2014). While sleepless *C. elegans* mutants may show the same lifespan as WT animals, we would anticipate a lack of sleep to have a wide-range of detrimental effects in behavior (feeding, locomotion, taxis) and neural activity (response to external stimuli, coordinated neural dynamics, etc.). Uncovering these phenotypes requires longitudinal measurements across an entire lifetime (Churgin, Jung, et al., 2017). For example, mutants such as *ceh-17* and *aptf-1* that showed reduced μ Sleep (Figure 2.4) might potentially show reduced lifespans compared to WT animals. However, these sleepless mutant animals may exhibit accelerated age-related decline such as a lower behavioral activity, less feeding, and a reduced response to external stimuli. With our high-throughput behavioral platform, we can assay lifespan, measure changes in behavior, and deliver precise stimuli over the lifetimes of many individual animals. Such a platform will help uncover how invertebrate sleep serves as a basic function for healthspan.

6.3. Metabolic tradeoffs as a potential unifying mechanism for *C. elegans* sleep

Though we observe μ Sleep in the context of microfluidic confinement, it is not hard to imagine that *C. elegans* may use this behavior and downregulation of neural activity in its natural environment. One unifying hypothesis for *C. elegans* μ Sleep regulation could be rooted in energy conservation. Factors that decreased μ Sleep, such as food and cooler temperatures, may indicate favorable conditions for active roaming behavior. Conversely, factors that increased μ Sleep, such as elevated temperatures and animal restraint, may indicate more harmful environments in which roaming and expending energy is not an optimal survival strategy. Furthermore, the changes we made to the environment may change the animal's metabolic state. *C. elegans* metabolism is known to increase with increasing temperature (Van Voorhies & Ward, 1999). Additionally, one can imagine that the microfluidic restraint we used drives an escape response, leading to increased muscle activation and high energy expenditure. Therefore, it is possible that all changes in μ Sleep phenotypes we observed were rooted in optimizing energy use by balancing the tradeoff between expending energy to move and the expected value of finding food.

Recall that there were significant links between the metabolic state, energy consumption, and food availability in previously discussed *C. elegans* quiescent states (reviewed in Section 1.2):

- Developmental sleep occurs during molting periods, which is an energy-intensive process (Corsi et al., 2015; Raizen et al., 2008)
- Stress-induced sleep occurs during recovery from cellular stress, when a large amount of physiological resources are likely allocated towards cellular repair and regaining protein homeostasis (Hill et al., 2014)
- Animals in the absence of food will begin to spontaneously transition between roaming and quiescence (R. Ghosh & Emmons, 2008; McCloskey et al., 2017; Wu et al., 2018)
- High satiety and high-quality food drive quiescence, and digesting these large amounts of food is energy intensive (T. Gallagher et al., 2013; You et al., 2008).

Thus, in all observations of *C. elegans* quiescence and sleep, a case can be made that metabolic regulation is the global underlying factor. This hypothesis is not surprising considering essentially all *C. elegans* behaviors can be considered as a method to optimize the search for food. **I propose that energy conservation and metabolic regulation are the primary reasons that *C. elegans* exhibit sleep behaviors.**

Future work is needed to continue to elucidate these mechanisms and prove this hypothesis for μ Sleep. Genetic mutants, different culture conditions, low- and high-quality food resources, combining sensory stimuli with food availability, and direct measurements of animal energy output are potential methods to uncover

these cues. These methods can also be applied to other *C. elegans* sleep behaviors; however, our microfluidic-based platform allows for easily controlling food availability, temperature, and mechanosensory feedback. Indeed, the discovery of μ Sleep behavior provides a valuable platform to study how sleep behavior may serve as an evolutionary advantage and successful survival strategy.

References

- Ahrens, M. B., Li, J. M., Orger, M. B., Robson, D. N., Schier, A. F., Engert, F., & Portugues, R. (2012). Brain-wide neuronal dynamics during motor adaptation in zebrafish. *Nature*. <http://doi.org/10.1038/nature11057>
- Ahrens, M. B., Orger, M. B., Robson, D. N., Li, J. M., & Keller, P. J. (2013). Whole-brain functional imaging at cellular resolution using light-sheet microscopy. *Nat Methods*, *10*(5), 413–420. <http://doi.org/10.1038/nmeth.2434>
- Aimon, S., Katsuki, T., Jia, T., Grosenick, L., Broxton, M., Deisseroth, K., ... Greenspan, R. J. (2018). Fast near-whole brain imaging in adult *Drosophila* during responses to stimuli and behavior. *BioRxiv*. <http://doi.org/10.1101/033803>
- Albrecht, D. R., & Bargmann, C. I. (2011). High-content behavioral analysis of *Caenorhabditis elegans* in precise spatiotemporal chemical environments. *Nature Methods*, *8*(7), 599–605. <http://doi.org/10.1038/nmeth.1630>
- Allen, W. E., Kauvar, I. V., Chen, M. Z., Richman, E. B., Yang, S. J., Chan, K., ... Deisseroth, K. (2017). Global Representations of Goal-Directed Behavior in Distinct Cell Types of Mouse Neocortex. *Neuron*. <http://doi.org/10.1016/j.neuron.2017.04.017>
- Anderson, D. J. (2016). Circuit modules linking internal states and social behaviour in flies and mice. *Nature Reviews Neuroscience*.

<http://doi.org/10.1038/nrn.2016.125>

Apfeld, J., & Kenyon, C. (1999). Regulation of lifespan by sensory perception in *Caenorhabditis elegans*. *Nature*. <http://doi.org/10.1038/45544>

Avery, L. (2010). *Caenorhabditis elegans* behavioral genetics: Where are the knobs? *BMC Biology*. <http://doi.org/10.1186/1741-7007-8-69>

Avery, L., & You, Y.-J. (2012). *C. elegans* feeding. *WormBook*, Ed. *The C. Elegans Research Community, WormBook*. <http://doi.org/10.1895/wormbook.1.150.1>

Badhiwala, K. N., Gonzales, D. L., Vercosa, D. G., Avants, B. W., & Robinson, J. T. (2018). Microfluidics for electrophysiology, imaging, and behavioral analysis of *Hydra*. *Lab on a Chip*, *18*, 2523–2539. <http://doi.org/10.1039/C8LC00475G>

Bansal, A., Zhu, L. J., Yen, K., & Tissenbaum, H. a. (2015). Uncoupling lifespan and healthspan in *Caenorhabditis elegans* longevity mutants. *Proceedings of the National Academy of Sciences*, *112*(3), E277–E286. <http://doi.org/10.1073/pnas.1412192112>

Bargmann, C. (2006). Chemosensation in *C. elegans*. *WormBook*. <http://doi.org/10.1895/wormbook.1.123.1>

Bargmann, C. I., & Marder, E. (2013). From the connectome to brain function. *Nature Methods*. <http://doi.org/10.1038/nmeth.2451>

Ben Arous, J., Laffont, S., & Chatenay, D. (2009). Molecular and sensory basis of a

food related two-state behavior in *C. elegans*. *PLoS ONE*.

<http://doi.org/10.1371/journal.pone.0007584>

Bennett, C., Arroyo, S., & Hestrin, S. (2013). Subthreshold mechanisms underlying state-dependent modulation of visual responses. *Neuron*.

<http://doi.org/10.1016/j.neuron.2013.08.007>

Bennett, H. L., Khoruzhik, Y., Hayden, D., Huang, H., Sanders, J., Walsh, M. B., ... Hart, A. C. (2018). Normal sleep bouts are not essential for *C. elegans* survival and FoxO is important for compensatory changes in sleep. *BMC Neuroscience*.

<http://doi.org/10.1186/s12868-018-0408-1>

Berger, S., Lattmann, E., Aegerter-Wilmsen, T., Hengartner, M., Hajnal, A., Demello, A., & Casadevall I Solvas, X. (2018). Long-term: *C. elegans* immobilization enables high resolution developmental studies in vivo. *Lab on a Chip*.

<http://doi.org/10.1039/c7lc01185g>

Björn Rasch and Jan Born. (2013). ABOUT SLEEP'S ROLE IN MEMORY. *Physiol Rev*.

<http://doi.org/10.1152/physrev.00032.2012>

Bouchard, M. B., Voleti, V., Mendes, C. S., Lacefield, C., Grueber, W. B., Mann, R. S., ... Hillman, E. M. C. (2015). Swept confocally-aligned planar excitation (SCAPE) microscopy for high speed volumetric imaging of behaving organisms. *Nature Photonics*, 9(2), 113–119. <http://doi.org/10.1038/nphoton.2014.323>

Bretscher, A. J., Kodama-Namba, E., Busch, K. E., Murphy, R. J., Soltesz, Z., Laurent, P.,

- & de Bono, M. (2011). Temperature, oxygen, and salt-sensing neurons in *C. elegans* are carbon dioxide sensors that control avoidance behavior. *Neuron*.
<http://doi.org/10.1016/j.neuron.2011.02.023>
- Broussard, G. J., Liang, R., & Tian, L. (2014a). Monitoring activity in neural circuits with genetically encoded indicators. *Frontiers in Molecular Neuroscience*, 7(December), 97. <http://doi.org/10.3389/fnmol.2014.00097>
- Broussard, G. J., Liang, R., & Tian, L. (2014b). Monitoring activity in neural circuits with genetically encoded indicators. *Frontiers in Molecular Neuroscience*, 7(December), 97. <http://doi.org/10.3389/fnmol.2014.00097>
- Brown, R. E., Basheer, R., McKenna, J. T., Strecker, R. E., & McCarley, R. W. (2012). Control of Sleep and Wakefulness. *Physiological Reviews*.
<http://doi.org/10.1152/physrev.00032.2011>
- Busch, K. E., Laurent, P., Soltesz, Z., Murphy, R. J., Faivre, O., Hedwig, B., ... De Bono, M. (2012). Tonic signaling from O₂ sensors sets neural circuit activity and behavioral state. *Nature Neuroscience*. <http://doi.org/10.1038/nn.3061>
- Calhoun, A. J., & Murthy, M. (2017). Quantifying behavior to solve sensorimotor transformations: advances from worms and flies. *Current Opinion in Neurobiology*. <http://doi.org/10.1016/j.conb.2017.08.006>
- Campbell, S. S., & Tobler, I. (1984). Animal sleep: A review of sleep duration across phylogeny. *Neuroscience and Biobehavioral Reviews*.

[http://doi.org/10.1016/0149-7634\(84\)90054-X](http://doi.org/10.1016/0149-7634(84)90054-X)

Cassada, R. C., & Russell, R. L. (1975). The dauerlarva, a post-embryonic developmental variant of the nematode *Caenorhabditis elegans*. *Developmental Biology*. [http://doi.org/10.1016/0012-1606\(75\)90109-8](http://doi.org/10.1016/0012-1606(75)90109-8)

Chalasani, S. H., Chronis, N., Tsunozaki, M., Gray, J. M., Ramot, D., Goodman, M. B., & Bargmann, C. I. (2007). Dissecting a circuit for olfactory behaviour in *Caenorhabditis elegans*. *Nature*, *450*(7166), 63–70.
<http://doi.org/10.1038/nature06540>

Chalfie, M. (2014). Assaying mechanosensation. *WormBook*.
<http://doi.org/10.1895/wormbook.1.172.1>

Chen, D., Taylor, K. P., Hall, Q., & Kaplan, J. M. (2016). The neuropeptides FLP-2 and PDF-1 act in concert to arouse *Caenorhabditis elegans* locomotion. *Genetics*.
<http://doi.org/10.1534/genetics.116.192898>

Chen, T.-W., Wardill, T. J., Sun, Y., Pulver, S. R., Renninger, S. L., Baohan, A., ... Kim, D. S. (2013). Ultrasensitive fluorescent proteins for imaging neuronal activity. *Nature*, *499*(7458), 295–300. <http://doi.org/10.1038/nature12354>

Chen, X., Mu, Y., Hu, Y., Kuan, A. T., Nikitchenko, M., Randlett, O., ... Ahrens, M. B. (2018). Brain-wide Organization of Neuronal Activity and Convergent Sensorimotor Transformations in Larval Zebrafish. *Neuron*.
<http://doi.org/10.1016/j.neuron.2018.09.042>

Chhetri, R. K., Amat, F., Wan, Y., Höckendorf, B., Lemon, W. C., & Keller, P. J. (2015).

Whole-animal functional and developmental imaging with isotropic spatial resolution. *Nature Methods*. <http://doi.org/10.1038/nmeth.3632>

Cho, C. E., Brueggemann, C., L'Etoile, N. D., & Bargmann, C. I. (2016). Parallel

encoding of sensory history and behavioral preference during *Caenorhabditis elegans* olfactory learning. *ELife*. <http://doi.org/10.7554/eLife.14000>

Cho, J. Y., & Sternberg, P. W. (2014). Multilevel modulation of a sensory motor circuit

during *C. elegans* sleep and arousal. *Cell*, *156*(1-2), 249–260.

<http://doi.org/10.1016/j.cell.2013.11.036>

Cho, Y., Oakland, D. N., Lee, S. A., Schafer, W. R., & Lu, H. (2018). On-chip functional

neuroimaging with mechanical stimulation in: *Caenorhabditis elegans* larvae for studying development and neural circuits. *Lab on a Chip*.

<http://doi.org/10.1039/c7lc01201b>

Cho, Y., Porto, D. A., Hwang, H., Grundy, L. J., Schafer, W. R., & Lu, H. (2017).

Automated and controlled mechanical stimulation and functional imaging in vivo in *C. elegans*. *Lab Chip*, *17*(15), 2609–2618.

<http://doi.org/10.1039/C7LC00465F>

Choi, S., Chatzigeorgiou, M., Taylor, K. P., Schafer, W. R., & Kaplan, J. M. (2013).

Analysis of NPR-1 reveals a circuit mechanism for behavioral quiescence in *C.elegans*. *Neuron*, *78*(5), 869–880.

<http://doi.org/10.1016/j.neuron.2013.04.002>

Chokshi, T. V., Bazopoulou, D., & Chronis, N. (2010). An automated microfluidic platform for calcium imaging of chemosensory neurons in *Caenorhabditis elegans*. *Lab on a Chip*, *10*(20), 2758–63. <http://doi.org/10.1039/c004658b>

Chronis, N., Zimmer, M., & Bargmann, C. I. (2007). Microfluidics for in vivo imaging of neuronal and behavioral activity in *Caenorhabditis elegans*. *Nature Methods*, *4*(9), 727–731. <http://doi.org/10.1038/nmeth1075>

Chung, K., Crane, M. M., & Lu, H. (2008). Automated on-chip rapid microscopy, phenotyping and sorting of *C. elegans*. *Nature Methods*, *5*(7), 637–643. <http://doi.org/10.1038/nmeth.1227>

Chung, K., Zhan, M., Srinivasan, J., Sternberg, P. W., Gong, E., Schroeder, F. C., & Lu, H. (2011). Microfluidic chamber arrays for whole-organism behavior-based chemical screening. *Lab on a Chip*. <http://doi.org/10.1039/c1lc20400a>

Churgin, M. A., Jung, S. K., Yu, C. C., Chen, X., Raizen, D. M., & Fang-Yen, C. (2017). Longitudinal imaging of *caenorhabditis elegans* in a microfabricated device reveals variation in behavioral decline during aging. *ELife*. <http://doi.org/10.7554/eLife.26652>

Churgin, M. A., McCloskey, R. J., Peters, E., & Fang-Yen, C. (2017). Antagonistic serotonergic and octopaminergic neural circuits mediate food-dependent locomotory behavior in *Caenorhabditis elegans*. *The Journal of Neuroscience*,

39(33), 7811–7823. <http://doi.org/10.1523/JNEUROSCI.2636-16.2017>

Clark, D. A., Freifeld, L., & Clandinin, T. R. (2013). Mapping and Cracking Sensorimotor Circuits in Genetic Model Organisms. *Neuron*.
<http://doi.org/10.1016/j.neuron.2013.05.006>

Cohen, D., Volovich, M., Zeevi, Y., Elbaum, L., Louie, K., Levy, D. J., & Rechavi, O. (2018). Bounded Rationality in *C. elegans*. *BioRxiv*, 257535.
<http://doi.org/10.1101/257535>

Cong, L., Wang, Z., Chai, Y., Hang, W., Shang, C., Yang, W., ... Wen, Q. (2017). Rapid whole brain imaging of neural activity in freely behaving larval zebrafish (*Danio rerio*). *ELife*. <http://doi.org/10.7554/eLife.28158>

Cornaglia, M., Krishnamani, G., Mouchiroud, L., Sorrentino, V., Lehnert, T., Auwerx, J., & Gijs, M. A. M. (2016). Automated longitudinal monitoring of in vivo protein aggregation in neurodegenerative disease *C. elegans* models. *Molecular Neurodegeneration*, 11(1), 17. <http://doi.org/10.1186/s13024-016-0083-6>

Cornaglia, M., Lehnert, T., & Gijs, M. A. M. (2017). Microfluidic systems for high-throughput and high-content screening using the nematode: *Caenorhabditis elegans*. *Lab on a Chip*. <http://doi.org/10.1039/c7lc00509a>

Corsi, A. K., Wightman, B., & Chalfie, M. (2015). A transparent window into biology: A primer on *Caenorhabditis elegans*. *Genetics*.
<http://doi.org/10.1534/genetics.115.176099>

- Crane, M. M., Stirman, J. N., Ou, C.-Y., Kurshan, P. T., Rehg, J. M., Shen, K., & Lu, H. (2012). Autonomous screening of *C. elegans* identifies genes implicated in synaptogenesis. *Nature Methods*, 9(10), 977–980.
<http://doi.org/10.1038/nmeth.2141>
- Cunningham, J. P., & Yu, B. M. (2014). Dimensionality reduction for large-scale neural recordings. *Nature Neuroscience*. <http://doi.org/10.1038/nn.3776>
- Dana, H., Mohar, B., Sun, Y., Narayan, S., Gordus, A., Hasseman, J. P., ... Kim, D. S. (2016). Sensitive red protein calcium indicators for imaging neural activity. *ELife*, 5(MARCH2016), 1–24. <http://doi.org/10.7554/eLife.12727>
- Davis, K. C., Choi, Y. I., Kim, J., & You, Y. J. (2018). Satiety behavior is regulated by ASI/ASH reciprocal antagonism. *Scientific Reports*.
<http://doi.org/10.1038/s41598-018-24943-6>
- DeBardleben, H. K., Lopes, L. E., Nessel, M. P., & Raizen, D. M. (2017). Stress-induced sleep after exposure to ultraviolet light is promoted by p53 in *Caenorhabditis elegans*. *Genetics*. <http://doi.org/10.1534/genetics.117.300070>
- Driver, R. J., Lamb, A. L., Wyner, A. J., & Raizen, D. M. (2013). DAF-16/FOXO regulates homeostasis of essential sleep-like behavior during larval transitions in *C. elegans*. *Current Biology*. <http://doi.org/10.1016/j.cub.2013.02.009>
- Dunn, T. W., Mu, Y., Narayan, S., Randlett, O., Naumann, E. A., Yang, C. T., ... Ahrens, M. B. (2016). Brain-wide mapping of neural activity controlling zebrafish

exploratory locomotion. *ELife*. <http://doi.org/10.7554/eLife.12741>

Dupre, C., & Yuste, R. (2017). Non-overlapping Neural Networks in *Hydra vulgaris*.

Current Biology. <http://doi.org/10.1016/j.cub.2017.02.049>

Edwards, S. L., Charlie, N. K., Milfort, M. C., Brown, B. S., Gravlin, C. N., Knecht, J. E., &

Miller, K. G. (2008). A novel molecular solution for ultraviolet light detection in *Caenorhabditis elegans*. *PLoS Biology*, 6(8), 1715–1729.

<http://doi.org/10.1371/journal.pbio.0060198>

Faumont, S., Lindsay, T. H., & Lockery, S. R. (2012). Neuronal microcircuits for

decision making in *C. elegans*. *Current Opinion in Neurobiology*, 22(4), 580–591.

<http://doi.org/10.1016/j.conb.2012.05.005>

Feierstein, C. E., Portugues, R., & Orger, M. B. (2015). Seeing the whole picture: A

comprehensive imaging approach to functional mapping of circuits in behaving zebrafish. *Neuroscience*. <http://doi.org/10.1016/j.neuroscience.2014.11.046>

Fenk, L. A., & de Bono, M. (2015). Environmental CO₂ inhibits *Caenorhabditis*

elegans egg-laying by modulating olfactory neurons and evokes widespread changes in neural activity. *Proceedings of the National Academy of Sciences*.

<http://doi.org/10.1037/cou0000088>

Ferry, M. S., Razinkov, I. A., & Hasty, J. (2011). *Microfluidics for Synthetic Biology*.

Synthetic Biology, Part A (1st ed., Vol. 497). Elsevier Inc.

<http://doi.org/10.1016/B978-0-12-385075-1.00014-7>

- Fetsch, C. R., Deangelis, G. C., & Angelaki, D. E. (2013). Bridging the gap between theories of sensory cue integration and the physiology of multisensory neurons. *Nature Reviews Neuroscience*. <http://doi.org/10.1038/nrn3503>
- Flavell, S. W., Pokala, N., Macosko, E. Z., Albrecht, D. R., Larsch, J., & Bargmann, C. I. (2013). Serotonin and the neuropeptide PDF initiate and extend opposing behavioral states in *C. Elegans*. *Cell*. <http://doi.org/10.1016/j.cell.2013.08.001>
- Flytzanis, N. C., Bedbrook, C. N., Chiu, H., Engqvist, M. K. M., Xiao, C., Chan, K. Y., ... Gradinaru, V. (2014). Archaelhodopsin variants with enhanced voltage-sensitive fluorescence in mammalian and *Caenorhabditis elegans* neurons. *Nature Communications*, 5, 4894. <http://doi.org/10.1038/ncomms5894>
- Foltényi, K., Greenspan, R. J., & Newport, J. W. (2007). Activation of EGFR and ERK by rhomboid signaling regulates the consolidation and maintenance of sleep in *Drosophila*. *Nature Neuroscience*. <http://doi.org/10.1038/nn1957>
- Gallagher, T., Bjorness, T., Greene, R., You, Y. J., & Avery, L. (2013). The Geometry of Locomotive Behavioral States in *C. elegans*. *PLoS ONE*. <http://doi.org/10.1371/journal.pone.0059865>
- Gallagher, T., Kim, J., Oldenbroek, M., Kerr, R., & You, Y.-J. (2013). ASI Regulates Satiety Quiescence in *C. elegans*. *Journal of Neuroscience*. <http://doi.org/10.1523/JNEUROSCI.4493-12.2013>
- Gallagher, T., & You, Y.-J. (2014). Falling asleep after a big meal. *Worm*.

<http://doi.org/10.4161/worm.27938>

Gallego, J. A., Perich, M. G., Miller, L. E., & Solla, S. A. (2017). Neural Manifolds for the Control of Movement. *Neuron*, 94(5), 978–984.

<http://doi.org/10.1016/j.neuron.2017.05.025>

Geissmann, Q., Beckwith, E. J., & Gilestro, G. F. (2019). Most sleep does not serve a vital function: Evidence from *Drosophila melanogaster*. *Science Advances*, 5(2), eaau9253. <http://doi.org/10.1126/sciadv.aau9253>

Ghanbari, L., Carter, R. E., Rynes, M. L., Dominguez, J., Chen, G., Naik, A., ...

Kodandaramaiah, S. B. (2018). Cortex-wide neural interfacing via transparent polymer skulls. *BioRxiv*, 387142. <http://doi.org/10.1101/387142>

Ghosh, D. D., Nitabach, M. N., Zhang, Y., & Harris, G. (2017). Multisensory integration in *C. elegans*. *Current Opinion in Neurobiology*.

<http://doi.org/10.1016/j.conb.2017.01.005>

Ghosh, K. K., Burns, L. D., Cocker, E. D., Nimmerjahn, A., Ziv, Y., Gamal, A. El, &

Schnitzer, M. J. (2011). Miniaturized integration of a fluorescence microscope. *Nature Methods*. <http://doi.org/10.1038/nmeth.1694>

Ghosh, R., & Emmons, S. W. (2008). Episodic swimming behavior in the nematode *C. elegans*. *The Journal of Experimental Biology*, 211(Pt 23), 3703–3711.

<http://doi.org/10.1242/jeb.023606>

Ghosh, R., & Emmons, S. W. (2010). Calcineurin and Protein kinase G regulate *C.*

Elegans behavioral quiescence during locomotion in liquid. *BMC Genetics*.

<http://doi.org/10.1186/1471-2156-11-7>

Gong, J., Yuan, Y., Ward, A., Kang, L., Zhang, B., Wu, Z., ... Xu, X. Z. S. (2016). The

C. elegans Taste Receptor Homolog LITE-1 Is a Photoreceptor. *Cell*, *167*(5),

1252–1263.e10. <http://doi.org/10.1016/j.cell.2016.10.053>

Gonzales, D. L., Badhiwala, K. N., Vercosa, D. G., Avants, B. W., Liu, Z., Zhong, W., &

Robinson, J. T. (2017). Scalable electrophysiology in intact small animals with

nanoscale suspended electrode arrays. *Nature Nanotechnology*, *12*, 694–691.

<http://doi.org/10.1038/nnano.2017.55>

Gonzales, D. L., Zhou, J., & Robinson, J. (2019). Satiety, Thermosensation and

Mechanosensation Regulate a Spontaneous *C. elegans* Sleep State. *BioRxiv*,

547075. <http://doi.org/10.1101/547075>

Goodman, M. B., Hall, D. H., Avery, L., & Lockery, S. R. (1998). Active Current

Regulate Sensitivity and Dynamic Range in *C. elegans* Neurons. *Neuron*, *20*,

763–772.

Goodman, M. B., Lindsay, T. H., Lockery, S. R., & Richmond, J. E. (2012).

Electrophysiological methods for Caenorhabditis elegans neurobiology. Methods

in cell biology (Second Edi, Vol. 107). Elsevier Inc.

<http://doi.org/10.1016/B978-0-12-394620-1.00014-X>

- Gordus, A., Pokala, N., Levy, S., Flavell, S. W., & Bargmann, C. I. (2015). Feedback from network states generates variability in a probabilistic olfactory circuit. *Cell*, 161(2), 215–227. <http://doi.org/10.1016/j.cell.2015.02.018>
- Goya, M. E., Romanowski, A., Caldart, C. S., Bénard, C. Y., & Golombek, D. A. (2016). Circadian rhythms identified in *Caenorhabditis elegans* by in vivo long-term monitoring of a bioluminescent reporter. *Proceedings of the National Academy of Sciences*, 201605769. <http://doi.org/10.1073/pnas.1605769113>
- Gray, J. M., Hill, J. J., & Bargmann, C. I. (2005). A circuit for navigation in *Caenorhabditis elegans*. *Proceedings of the National Academy of Sciences of the United States of America*, 102(9), 3184–3191. <http://doi.org/10.1073/pnas.0409009101>
- Gray, J. M., Karow, D. S., Lu, H., Chang, A. J., Chang, J. S., Ellis, R. E., ... Bargmann, C. I. (2004). Oxygen sensation and social feeding mediated by a *C. elegans* guanylate cyclase homologue. *Nature*, 430(6997), 317–322. <http://doi.org/10.1038/nature02714>
- Gupta, B., & Rezai, P. (2016). Microfluidic Approaches for Manipulating, Imaging, and Screening *C. elegans*. *Micromachines*, 7(7), 123. <http://doi.org/10.3390/mi7070123>
- Haesemeyer, M., Robson, D. N., Li, J. M., Schier, A. F., & Engert, F. (2018). A Brain-wide Circuit Model of Heat-Evoked Swimming Behavior in Larval Zebrafish.

Neuron. <http://doi.org/10.1016/j.neuron.2018.04.013>

Han, B., Dong, Y., Zhang, L., Liu, Y., Rabinowitch, I., & Bai, J. (2017). Dopamine signaling tunes spatial pattern selectivity in *C. elegans*. *ELife*, 6, 1–14.
<http://doi.org/10.7554/eLife.22896>

Hardin, P. E., Hall, J. C., & Rosbash, M. (1990). Feedback of the *Drosophila* period gene product on circadian cycling of its messenger RNA levels. *Nature*.
<http://doi.org/10.1038/343536a0>

Henderson, S. T., & Johnson, T. E. (2001). *daf-16* integrates developmental and environmental inputs to mediate aging in the nematode *Caenorhabditis elegans*. *Current Biology*. [http://doi.org/10.1016/S0960-9822\(01\)00594-2](http://doi.org/10.1016/S0960-9822(01)00594-2)

Hendricks, J. C., Finn, S. M., Panckeri, K. A., Chavkin, J., Williams, J. A., Sehgal, A., & Pack, A. I. (2000). Rest in *Drosophila* is a sleep-like state. *Neuron*.
[http://doi.org/10.1016/S0896-6273\(00\)80877-6](http://doi.org/10.1016/S0896-6273(00)80877-6)

Hendricks, M., Ha, H., Maffey, N., & Zhang, Y. (2012). Compartmentalized calcium dynamics in a *C. elegans* interneuron encode head movement. *Nature*, 487(7405), 99–103. <http://doi.org/10.1038/nature11081>

Herndon, L. A., Schmeissner, P. J., Dudaronek, J. M., Brown, P. A., Listner, K. M., Sakano, Y., ... Driscoll, M. (2002). Stochastic and genetic factors influence tissue-specific decline in ageing *C. elegans*. *Nature*, 419(6909), 808–814.
<http://doi.org/10.1038/nature01135>

- Hill, A. J., Mansfield, R., Lopez, J. M. N. G., Raizen, D. M., & Buskirk, C. Van. (2014). Cellular Stress Induces a Protective Sleep-like State in *C. elegans*. *Current Biology*, 1–7. <http://doi.org/10.1016/j.cub.2014.08.040>
- Hsu, A.-L., Murphy, C. T., & Kenyon, C. (2003). Regulation of aging and age-related disease by DAF-16 and heat-shock factor. *Science (New York, N.Y.)*, 300(5622), 1142–1145. <http://doi.org/10.1126/science.1083701>
- Hu, C., Dillon, J., Kearn, J., Murray, C., O'Connor, V., Holden-Dye, L., & Morgan, H. (2013). NeuroChip: a microfluidic electrophysiological device for genetic and chemical biology screening of *Caenorhabditis elegans* adult and larvae. *PLoS One*, 8(5), e64297. <http://doi.org/10.1371/journal.pone.0064297>
- Huang, C., Xiong, C., & Kornfeld, K. (2004). Measurements of age-related changes of physiological processes that predict lifespan of *Caenorhabditis elegans*. *Proceedings of the National Academy of Sciences*. <http://doi.org/10.1073/pnas.0400848101>
- Huang, H., Hayden, D. J., Zhu, C.-T., Bennett, H. L., Venkatachalam, V., Skuja, L. L., & Hart, A. C. (2018). Gap Junctions and NCA Cation Channels Are Critical for Developmentally-Timed Sleep and Arousal in *Caenorhabditis elegans*. *Genetics*, 210(4), 1369–1381. <http://doi.org/10.1534/genetics.118.301551>
- Huang, H., Singh, K., & Hart, A. (2017). Measuring *Caenorhabditis elegans* Sleep during the Transition to Adulthood Using a Microfluidics-based System. *BIO-*

PROTOCOL. <http://doi.org/10.21769/BioProtoc.2174>

Hulme, S. E., Shevkoplyas, S. S., Apfeld, J., Fontana, W., & Whitesides, G. M. (2007). A microfabricated array of clamps for immobilizing and imaging *C. elegans*. *Lab on a Chip*, 7(11), 1515–1523. <http://doi.org/10.1039/b707861g>

Hulme, S. E., Shevkoplyas, S. S., McGuigan, A. P., Apfeld, J., Fontana, W., & Whitesides, G. M. (2010). Lifespan-on-a-chip: Microfluidic chambers for performing lifelong observation of *C. elegans*. *Lab on a Chip*. <http://doi.org/10.1039/b919265d>

Iannacone, M. J., Beets, I., Lopes, L. E., Churgin, M. A., Fang-Yen, C., Nelson, M. D., ... Raizen, D. M. (2017). The RFamide receptor DMSR-1 regulates stress-induced sleep in *C. elegans*. *ELife*. <http://doi.org/10.7554/eLife.19837>

Iwanir, S., Tramm, N., Nagy, S., Wright, C., Ish, D., & Biron, D. (2013). The microarchitecture of *C. elegans* behavior during lethargus: homeostatic bout dynamics, a typical body posture, and regulation by a central neuron. *Sleep*. <http://doi.org/10.5665/sleep.2456>

Jones, D., & Candido, E. P. M. (1999). Feeding is inhibited by sublethal concentrations of toxicants and by heat stress in the nematode *Caenorhabditis elegans*: Relationship to the cellular stress response. *Journal of Experimental Zoology*. [http://doi.org/10.1002/\(SICI\)1097-010X\(19990701\)284:2<147::AID-JEZ4>3.0.CO;2-Z](http://doi.org/10.1002/(SICI)1097-010X(19990701)284:2<147::AID-JEZ4>3.0.CO;2-Z)

Juozaityte, V., Pladevall-Morera, D., Podolska, A., Nørgaard, S., Neumann, B., &

- Pocock, R. (2017). The ETS-5 transcription factor regulates activity states in *Caenorhabditis elegans* by controlling satiety. *Proceedings of the National Academy of Sciences*. <http://doi.org/10.1073/pnas.1610673114>
- Kaplan, H. S., Nichols, A. L. A., & Zimmer, M. (2018). Sensorimotor integration in *Caenorhabditis elegans*: A reappraisal towards dynamic and distributed computations. *Philosophical Transactions of the Royal Society B: Biological Sciences*. <http://doi.org/10.1098/rstb.2017.0371>
- Kato, S., Kaplan, H. S., Schrödel, T., Skora, S., Lindsay, T. H., Yemini, E., ... Zimmer, M. (2015). Global Brain Dynamics Embed the Motor Command Sequence of *Caenorhabditis elegans*. *Cell*, *163*(3), 656–669. <http://doi.org/10.1016/j.cell.2015.09.034>
- Kato, S., Xu, Y., Cho, C. E., Abbott, L. F., & Bargmann, C. I. (2014). Temporal Responses of *C.elegans* Chemosensory Neurons Are Preserved in Behavioral Dynamics. *Neuron*, *81*(3), 616–628. <http://doi.org/10.1016/j.neuron.2013.11.020>
- Kayser, M. S., & Biron, D. (2016). Sleep and development in genetically tractable model organisms. *Genetics*. <http://doi.org/10.1534/genetics.116.189589>
- Keith, S. A., Amrit, F. R. G., Ratnappan, R., & Ghazi, A. (2014). The *C. elegans* healthspan and stress-resistance assay toolkit. *Methods*. <http://doi.org/10.1016/j.ymeth.2014.04.003>
- Keller, P. J., Ahrens, M. B., & Freeman, J. (2014). Light-sheet imaging for systems

neuroscience. *Nature Methods*. <http://doi.org/10.1038/nmeth.3214>

Kenyon, C., Chang, J., Gensch, E., Rudner, A., & Tabtiang, R. (1993). A *C. elegans* mutant that lives twice as long as wild type. *Nature*.
<http://doi.org/10.1038/366461a0>

Kerr, R. a. (2006). Imaging the activity of neurons and muscles. *WormBook : The Online Review of C. Elegans Biology*, 1–13.
<http://doi.org/10.1895/wormbook.1.113.1>

Kim, D. H., Kim, J., Marques, J. C., Grama, A., Hildebrand, D. G. C., Gu, W., ... Robson, D. N. (2017). Pan-neuronal calcium imaging with cellular resolution in freely swimming zebrafish. *Nature Methods*. <http://doi.org/10.1038/nmeth.4429>

Kim, T. H., Zhang, Y., Lecoq, J., Jung, J. C., Li, J., Zeng, H., ... Schnitzer, M. J. (2016). Long-Term Optical Access to an Estimated One Million Neurons in the Live Mouse Cortex. *Cell Reports*. <http://doi.org/10.1016/j.celrep.2016.12.004>

Kopito, R. B., & Levine, E. (2014). Durable spatiotemporal surveillance of *Caenorhabditis elegans* response to environmental cues. *Lab on a Chip*.
<http://doi.org/10.1039/c3lc51061a>

Krajniak, J., & Lu, H. (2010). Long-term high-resolution imaging and culture of *C. elegans* in chip-gel hybrid microfluidic device for developmental studies. *Lab on a Chip*. <http://doi.org/10.1039/c001986k>

- Kramer, A., Yang, F. C., Snodgrass, P., Li, X., Scammell, T. E., Davis, F. C., & Weitz, C. J. (2001). Regulation of daily locomotor activity and sleep by hypothalamic EGF receptor signaling. *Science*. <http://doi.org/10.1126/science.1067716>
- Krieg, M., Dunn, A. R., & Goodman, M. B. (2015). Mechanical systems biology of *C. elegans* touch sensation. *BioEssays*. <http://doi.org/10.1002/bies.201400154>
- Kunitomo, H., Sato, H., Iwata, R., Satoh, Y., Ohno, H., Yamada, K., & Iino, Y. (2013). Concentration memory-dependent synaptic plasticity of a taste circuit regulates salt concentration chemotaxis in *Caenorhabditis elegans*. *Nature Communications*. <http://doi.org/10.1038/ncomms3210>
- Kutz, J. N. (2019). Neurosensory network functionality and data-driven control. *Current Opinion in Systems Biology*. <http://doi.org/10.1016/j.coisb.2018.08.013>
- Larsch, J., Flavell, S. W., Liu, Q., Gordus, A., Albrecht, D. R., & Bargmann, C. I. (2015). A Circuit for Gradient Climbing in *C. elegans* Chemotaxis. *Cell Reports*, 12(11), 1748–1760. <http://doi.org/10.1016/j.celrep.2015.08.032>
- Larsch, J., Ventimiglia, D., Bargmann, C. I., & Albrecht, D. R. (2013). High-throughput imaging of neuronal activity in *Caenorhabditis elegans*. *Proceedings of the National Academy of Sciences of the United States of America*, 110(45), E4266–E4273. <http://doi.org/10.1073/pnas.1318325110>
- Laurent, P., Soltesz, Z., Nelson, G., Chen, C., Arellano-Carbajal, F., Levy, E., & de Bono, M. (2015). Decoding a neural circuit controlling global animal state in *C.*

Elegans. *ELife*. <http://doi.org/10.7554/eLife.04241>

Lee, H., Kim, S. A., Coakley, S., Mugno, P., Hammarlund, M., Hilliard, M. A., & Lu, H. (2014). A multi-channel device for high-density target-selective stimulation and long-term monitoring of cells and subcellular features in *C. elegans*. *Lab on a Chip*. <http://doi.org/10.1039/c4lc00789a>

Lee, S. S., Kennedy, S., Tolonen, A. C., & Ruvkun, G. (2003). DAF-16 target genes that control *C. elegans* Life-span and metabolism. *Science*. <http://doi.org/10.1126/science.1083614>

Leinwand, S. G., & Chalasani, S. H. (2013). Neuropeptide signaling remodels chemosensory circuit composition in *Caenorhabditis elegans*. *Nature Neuroscience*. <http://doi.org/10.1038/nn.3511>

Lemon, W. C., Pulver, S. R., Höckendorf, B., McDole, K., Branson, K., Freeman, J., & Keller, P. J. (2015). Whole-central nervous system functional imaging in larval *Drosophila*. *Nature Communications*, 6(May), 7924. <http://doi.org/10.1038/ncomms8924>

Lim, R. S., Eyjólfsson, E., Shin, E., Perona, P., & Anderson, D. J. (2014). How food controls aggression in *Drosophila*. *PLoS ONE*. <http://doi.org/10.1371/journal.pone.0105626>

Lockery, S. R., Hulme, S. E., Roberts, W. M., Robinson, K. J., Laromaine, A., Lindsay, T. H., ... Weeks, J. C. (2012). A microfluidic device for whole-animal drug screening

using electrophysiological measures in the nematode *C. elegans*. *Lab on a Chip*, 12(12), 2211–2220. <http://doi.org/10.1039/c2lc00001f>

Lockery, S. R., Lawton, K. J., Doll, J. C., Faumont, S., Coulthard, S. M., Thiele, T. R., ... Pruitt, B. L. (2008). Artificial dirt: microfluidic substrates for nematode neurobiology and behavior. *Journal of Neurophysiology*, 99(6), 3136–43. <http://doi.org/10.1152/jn.91327.2007>

Luo, L., Clark, D. a, Biron, D., Mahadevan, L., & Samuel, A. D. T. (2006). Sensorimotor control during isothermal tracking in *Caenorhabditis elegans*. *The Journal of Experimental Biology*, 209(3), 4652–4662. <http://doi.org/10.1242/jeb.02590>

Luo, L., Wen, Q., Ren, J., Hendricks, M., Gershow, M., Qin, Y., ... Zhang, Y. (2014). Dynamic encoding of perception, memory, and movement in a *C. elegans* chemotaxis circuit. *Neuron*. <http://doi.org/10.1016/j.neuron.2014.05.010>

MacOsko, E. Z., Pokala, N., Feinberg, E. H., Chalasani, S. H., Butcher, R. A., Clardy, J., & Bargmann, C. I. (2009). A hub-and-spoke circuit drives pheromone attraction and social behaviour in *C. elegans*. *Nature*. <http://doi.org/10.1038/nature07886>

Marder, E. (2012). Neuromodulation of Neuronal Circuits: Back to the Future. *Neuron*. <http://doi.org/10.1016/j.neuron.2012.09.010>

McClanahan, P. D., Xu, J. H., & Fang-Yen, C. (2017). Comparing: *Caenorhabditis elegans* gentle and harsh touch response behavior using a multiplexed

hydraulic microfluidic device. *Integrative Biology (United Kingdom)*.

<http://doi.org/10.1039/c7ib00120g>

McCloskey, R. J., Fouad, A. D., Churgin, M. A., & Fang-Yen, C. (2017). Food

Responsiveness Regulates Episodic Behavioral States in *Caenorhabditis elegans*.

Journal of Neurophysiology, jn.00555.2016.

<http://doi.org/10.1152/jn.00555.2016>

McCormick, K. E., Gaertner, B. E., Sottile, M., Phillips, P. C., & Lockery, S. R. (2011).

Microfluidic devices for analysis of spatial orientation behaviors in semi-restrained *Caenorhabditis elegans*. *PLoS ONE*, 6(10).

<http://doi.org/10.1371/journal.pone.0025710>

McGinley, M. J., Vinck, M., Reimer, J., Batista-Brito, R., Zaghera, E., Cadwell, C. R., ...

McCormick, D. A. (2015). Waking State: Rapid Variations Modulate Neural and Behavioral Responses. *Neuron*. <http://doi.org/10.1016/j.neuron.2015.09.012>

McGrath, P. T., Rockman, M. V., Zimmer, M., Jang, H., Macosko, E. Z., Kruglyak, L., &

Bargmann, C. I. (2009). Quantitative Mapping of a Digenic Behavioral Trait Implicates Globin Variation in *C. elegans* Sensory Behaviors. *Neuron*.

<http://doi.org/10.1016/j.neuron.2009.02.012>

Miyazaki, S., Liu, C. Y., & Hayashi, Y. (2017). Sleep in vertebrate and invertebrate

animals, and insights into the function and evolution of sleep. *Neuroscience*

Research. <http://doi.org/10.1016/j.neures.2017.04.017>

Molleman, A. (2002). Patch Clamping. *Wiley*, 167.

<http://doi.org/10.1002/0470856521>

Mondal, S., Hegarty, E., Martin, C., Gökçe, S. K., Ghorashian, N., & Ben-Yakar, A.

(2016). Large-scale microfluidics providing high-resolution and high-throughput screening of *Caenorhabditis elegans* poly-glutamine aggregation model. *Nature Communications*, 7, 13023.

<http://doi.org/10.1038/ncomms13023>

Monsalve, G. C., Van Buskirk, C., & Frand, A. R. (2011). LIN-42/PERIOD controls

cyclical and developmental progression of *C. elegans* molts. *Current Biology*.

<http://doi.org/10.1016/j.cub.2011.10.054>

Murphy, C. T., McCarroll, S. A., Bargmann, C. I., Fraser, A., Kamath, R. S., Ahringer, J., ...

Kenyon, C. (2003). Genes that act downstream of DAF-16 to influence the lifespan of *Caenorhabditis elegans*. *Nature*.

<http://doi.org/10.1038/nature01789>

Muto, A., Ohkura, M., Kotani, T., Higashijima, S., Nakai, J., & Kawakami, K. (2011).

Genetic visualization with an improved GCaMP calcium indicator reveals spatiotemporal activation of the spinal motor neurons in zebrafish. *Proceedings of the National Academy of Sciences of the United States of America*, 108(13),

5425–5430. <http://doi.org/10.1073/pnas.1000887108>

Nagy, S., Raizen, D. M., & Biron, D. (2014). Measurements of behavioral quiescence in

Caenorhabditis elegans. *Methods*, 68(3), 500–507.

<http://doi.org/10.1016/j.ymeth.2014.03.009>

Nagy, S., Tramm, N., Sanders, J., Iwanir, S., Shirley, I. A., Levine, E., & Biron, D. (2014).

Homeostasis in *C. elegans* sleep is characterized by two behaviorally and genetically distinct mechanisms. *ELife*. <http://doi.org/10.7554/eLife.04380>

Nath, R. D., Bedbrook, C. N., Abrams, M. J., Basinger, T., Bois, J. S., Prober, D. A., ...

Goentoro, L. (2017). The Jellyfish *Cassiopea* Exhibits a Sleep-like State. *Current Biology*. <http://doi.org/10.1016/j.cub.2017.08.014>

Nath, R. D., Chow, E. S., Wang, H., Schwarz, E. M., & Sternberg, P. W. (2016).

C. elegans Stress-Induced Sleep Emerges from the Collective Action of Multiple Neuropeptides. *Current Biology*. <http://doi.org/10.1016/j.cub.2016.07.048>

Nekimken, A. L., Fehlauer, H., Kim, A. A., Manosalvas-Kjono, S. N., Ladpli, P., Memon,

F., ... Krieg, M. (2017). Pneumatic stimulation of *C. elegans* mechanoreceptor neurons in a microfluidic trap. *Lab Chip*, 17(6), 1116–1127.

<http://doi.org/10.1039/C6LC01165A>

Nekimken, A. L., Mazzochette, E. A., Goodman, M. B., & Pruitt, B. L. (2017). Forces

applied during classical touch assays for *Caenorhabditis elegans*. *PLoS ONE*.

<http://doi.org/10.1371/journal.pone.0178080>

Nelson, M. D., Janssen, T., York, N., Lee, K. H., Schoofs, L., & Raizen, D. M. (2015).

FRPR-4 is a G-protein coupled neuropeptide receptor that regulates behavioral

quiescence and posture in *Caenorhabditis elegans*. *PLoS ONE*.

<http://doi.org/10.1371/journal.pone.0142938>

Nelson, M. D., Lee, K. H., Churgin, M. A., Hill, A. J., Van Buskirk, C., Fang-Yen, C., &

Raizen, D. M. (2014). FMRamide-like FLP-13 Neuropeptides Promote

Quiescence following Heat Stress in *Caenorhabditis elegans*. *Current Biology*.

<http://doi.org/10.1016/j.cub.2014.08.037>

Nelson, M. D., Trojanowski, N. F., George-Raizen, J. B., Smith, C. J., Yu, C. C., Fang-Yen,

C., & Raizen, D. M. (2013). The neuropeptide NLP-22 regulates a sleep-like state in *Caenorhabditis elegans*. *Nature Communications*.

<http://doi.org/10.1038/ncomms3846>

Nguyen, J. P., Linder, A. N., Plummer, G. S., Shaevitz, J. W., & Leifer, A. M. (2017).

Automatically tracking neurons in a moving and deforming brain. *PLoS*

Computational Biology, 13(5), e1005517.

<http://doi.org/10.1371/journal.pcbi.1005517>

Nguyen, J. P., Shipley, F. B., Linder, A. N., Plummer, G. S., Liu, M., Setru, S. U., ... Leifer,

A. M. (2015). Whole-brain calcium imaging with cellular resolution in freely behaving *Caenorhabditis elegans*. *Proceedings of the National Academy of*

Sciences of the United States of America, 33.

<http://doi.org/10.1073/pnas.1507110112>

Nichols, A. L. A., Eichler, T., Latham, R., & Zimmer, M. (2017). A global brain state

underlies *C. elegans* sleep behavior. *Science*, 356(1247), eaam6851:1-9.

<http://doi.org/10.1126/science.aam6851>

Nitz, D. A., Van Swinderen, B., Tononi, G., & Greenspan, R. J. (2002).

Electrophysiological correlates of rest and activity in *Drosophila melanogaster*.

Current Biology. [http://doi.org/10.1016/S0960-9822\(02\)01300-3](http://doi.org/10.1016/S0960-9822(02)01300-3)

Oda, S., Tomioka, M., & Iino, Y. (2011). Neuronal plasticity regulated by the insulin-

like signaling pathway underlies salt chemotaxis learning in *Caenorhabditis*

elegans. *Journal of Neurophysiology*. <http://doi.org/10.1152/jn.01029.2010>

Ohno, H., Sakai, N., Adachi, T., & Iino, Y. (2017). Dynamics of Presynaptic

Diacylglycerol in a Sensory Neuron Encode Differences between Past and

Current Stimulus Intensity. *Cell Reports*.

<http://doi.org/10.1016/j.celrep.2017.08.038>

Ouellette, M.-H., Desrochers, M. J., Gheta, I., Ramos, R., & Hendricks, M. (2018). A

Gate-and-Switch Model for Head Orientation Behaviors in *Caenorhabditis*

elegans. *Eneuro*, 5(6), ENEURO.0121-18.2018.

<http://doi.org/10.1523/ENEURO.0121-18.2018>

Pandarínath, C., O'Shea, D. J., Collins, J., Jozefowicz, R., Stavisky, S. D., Kao, J. C., ...

Sussillo, D. (2018). Inferring single-trial neural population dynamics using

sequential auto-encoders. *Nature Methods*. [http://doi.org/10.1038/s41592-](http://doi.org/10.1038/s41592-018-0109-9)

[018-0109-9](http://doi.org/10.1038/s41592-018-0109-9)

Persson, A., Gross, E., Laurent, P., Busch, K. E., Bretes, H., & De Bono, M. (2009).

Natural variation in a neural globin tunes oxygen sensing in wild

Caenorhabditis elegans. *Nature*. <http://doi.org/10.1038/nature07820>

Piggott, B. J., Liu, J., Feng, Z., Wescott, S. a, & Xu, X. Z. S. (2011). The neural circuits

and synaptic mechanisms underlying motor initiation in *C. elegans*. *Cell*, *147*(4),

922–33. <http://doi.org/10.1016/j.cell.2011.08.053>

Portugues, R., Feierstein, C. E., Engert, F., & Orger, M. B. (2014). Whole-brain activity

maps reveal stereotyped, distributed networks for visuomotor behavior.

Neuron. <http://doi.org/10.1016/j.neuron.2014.01.019>

Prahlad, V., Cornelius, T., & Morimoto, R. I. (2008). Regulation of the cellular heat

shock response in *Caenorhabditis elegans* by thermosensory neurons. *Science*.

<http://doi.org/10.1126/science.1156093>

Prevedel, R., Yoon, Y.-G., Hoffmann, M., Pak, N., Wetzstein, G., Kato, S., ... Vaziri, A.

(2014). Simultaneous whole-animal 3D imaging of neuronal activity using light-field microscopy. *Nature Methods*, *11*(7), 727–30.

<http://doi.org/10.1038/nmeth.2964>

Pujol, N., Torregrossa, P., Ewbank, J. J., & Brunet, J. F. (2000). The homeodomain

protein CePHOX2/CEH-17 controls antero-posterior axonal growth in *C.*

elegans. *Development (Cambridge, England)*.

Raizen, D. M., & Avery, L. (1994). Electrical Activity and Behavior in the Pharynx of

Caenorhabditis elegans. *Neuron*, 12, 483–495.

Raizen, D. M., Zimmerman, J. E., Maycock, M. H., Ta, U. D., You, Y., Sundaram, M. V., & Pack, A. I. (2008). Lethargus is a *Caenorhabditis elegans* sleep-like state. *Nature*, 451(January), 569–72. <http://doi.org/10.1038/nature06535>

Ramot, D., MacInnis, B. L., & Goodman, M. B. (2008). Bidirectional temperature-sensing by a single thermosensory neuron in *C. elegans*. *Nature Neuroscience*, 11(8), 908–915. <http://doi.org/10.1038/nn.2157>

Richmond, J. E., & Jorgensen, E. M. (1999). One GABA and two acetylcholine receptors function at the *C. elegans* neuromuscular junction. *Nature Neuroscience*, 2(9), 791–797.

Rohde, C. B., Zeng, F., Gonzalez-Rubio, R., Angel, M., & Yanik, M. F. (2007). Microfluidic system for on-chip high-throughput whole-animal sorting and screening at subcellular resolution. *Proceedings of the National Academy of Sciences*, 104(35), 13891–13895.

Sadtler, P. T., Quick, K. M., Golub, M. D., Chase, S. M., Ryu, S. I., Tyler-Kabara, E. C., ... Batista, A. P. (2014). Neural constraints on learning. *Nature*. <http://doi.org/10.1038/nature13665>

Saigusa, T., Ishizaki, S., Watabiki, S., Ishii, N., Tanakadate, A., Tamai, Y., & Hasegawa, K. (2002). Circadian behavioural rhythm in *Caenorhabditis elegans* [1]. *Current Biology*. [http://doi.org/10.1016/S0960-9822\(01\)00669-8](http://doi.org/10.1016/S0960-9822(01)00669-8)

- San-Miguel, A., & Lu, H. (2013). Microfluidics as a tool for *C. elegans* research. In *Wormbook* (The *C. elegans*, pp. 1–19). <http://doi.org/10.1895/wormbook.1.162.1>
- Saper, C. B., Fuller, P. M., Pedersen, N. P., Lu, J., & Scammell, T. E. (2010). Sleep State Switching. *Neuron*, *68*(6), 1023–1042.
<http://doi.org/10.1016/j.neuron.2010.11.032>
- Sawin, E. R., Ranganathan, R., & Horvitz, H. R. (2000). *C. elegans* locomotory rate is modulated by the environment through a dopaminergic pathway and by experience through a serotonergic pathway. *Neuron*.
[http://doi.org/10.1016/S0896-6273\(00\)81199-X](http://doi.org/10.1016/S0896-6273(00)81199-X)
- Scholz, M., Linder, A. N., Randi, F., Sharma, A. K., Yu, X., Shaevitz, J. W., & Leifer, A. (2018). Predicting natural behavior from whole-brain neural dynamics. *BioRxiv*.
<http://doi.org/10.1101/445643>
- Schrödel, T., Prevedel, R., Aumayr, K., Zimmer, M., & Vaziri, A. (2013). Brain-wide 3D imaging of neuronal activity in *Caenorhabditis elegans* with sculpted light. *Nature Methods*, *10*(10), 1013–20. <http://doi.org/10.1038/nmeth.2637>
- Schwarz, J., Lewandrowski, I., & Bringmann, H. (2011). Reduced activity of a sensory neuron during a sleep-like state in *Caenorhabditis elegans*. *Current Biology*, *21*(24), R983–R984. <http://doi.org/10.1016/j.cub.2011.10.046>
- Schwarz, J., Spies, J.-P., & Bringmann, H. (2012). Reduced muscle contraction and a relaxed posture during sleep-like Lethargus. *Worm*.

<http://doi.org/10.4161/worm.19499>

Severi, K. E., Portugues, R., Marques, J. C., O'Malley, D. M., Orger, M. B., & Engert, F. (2014). Neural Control and Modulation of Swimming Speed in the Larval Zebrafish. *Neuron*. <http://doi.org/10.1016/j.neuron.2014.06.032>

Simonetta, S. H., Migliori, M. L., Romanowski, A., & Golombek, D. A. (2009). Timing of locomotor activity circadian rhythms in *Caenorhabditis elegans*. *PLoS ONE*. <http://doi.org/10.1371/journal.pone.0007571>

Singh, K., Chao, M. Y., Somers, G. A., Komatsu, H., Corkins, M. E., Larkins-Ford, J., ... Hart, A. C. (2011). *C. elegans* notch signaling regulates adult chemosensory response and larval molting quiescence. *Current Biology*. <http://doi.org/10.1016/j.cub.2011.04.010>

Singh, K., Ju, J. Y., Walsh, M. B., Dilorio, M. A., & Hart, A. C. (2014). Deep conservation of genes required for both *Drosophila melanogaster* and *Caenorhabditis elegans* sleep includes a role for dopaminergic signaling. *Sleep*. <http://doi.org/10.5665/sleep.3990>

Skora, S., Mende, F., & Zimmer, M. (2018). Energy Scarcity Promotes a Brain-wide Sleep State Modulated by Insulin Signaling in *C. elegans*. *Cell Reports*, 22(4), 953–966. <http://doi.org/10.1016/j.celrep.2017.12.091>

Spies, J., & Bringmann, H. (2018). Automated detection and manipulation of sleep in *C. Elegans* reveals depolarization of a sleep-active neuron during mechanical

stimulation-induced sleep deprivation. *Scientific Reports*.

<http://doi.org/10.1038/s41598-018-28095-5>

Steriade, M., McCormick, D. A., & Sejnowski, T. J. (1993). Thalamocortical oscillations in the sleeping and aroused brain. *Science*.

<http://doi.org/10.1126/science.8235588>

Stickgold, R., & Walker, M. P. (2005). Sleep and memory: The ongoing debate. *Sleep*.

<http://doi.org/10.1093/sleep/28.10.1225>

Storace, D., Rad, M. S., Kang, B., Cohen, L. B., Hughes, T., & Baker, B. J. (2016). Toward better genetically encoded sensors of membrane potential. *Trends in*

Neurosciences, 39(5), 1–29. <http://doi.org/10.1016/j.tins.2016.02.005>

Talsma, D., Senkowski, D., Soto-Faraco, S., & Woldorff, M. G. (2010). The multifaceted interplay between attention and multisensory integration. *Trends in Cognitive*

Sciences. <http://doi.org/10.1016/j.tics.2010.06.008>

Tang, S., & Whitesides, G. (2010). Basic microfluidic and soft lithographic

techniques. *Optofluidics: Fundamentals, Devices, and Applications*, 7–32.

Retrieved from <http://www2.egr.uh.edu/~nvaradar/private/Refs/Litho.pdf>

Tian, L., Hires, S. A., Mao, T., Huber, D., Chiappe, M. E., Chalasani, S. H., ... Looger, L. L. (2009). Imaging neural activity in worms, flies and mice with improved GCaMP

calcium indicators. *Nature Methods*, 6(12), 875–881.

<http://doi.org/10.1038/nmeth.1398>

- Tomida, T., Oda, S., Takekawa, M., Iino, Y., & Saito, H. (2012). The temporal pattern of stimulation determines the extent and duration of MAPK activation in a *Caenorhabditis elegans* sensory neuron. *Science Signaling*.
<http://doi.org/10.1126/scisignal.2002983>
- Tramm, N., Oppenheimer, N., Nagy, S., Efrati, E., & Biron, D. (2014). Why do sleeping nematodes adopt a hockey-stick-like posture? *PLoS ONE*.
<http://doi.org/10.1371/journal.pone.0101162>
- Trojanowski, N. F., Nelson, M. D., Flavell, S. W., Fang-Yen, C., & Raizen, D. M. (2015). Distinct Mechanisms Underlie Quiescence during Two *Caenorhabditis elegans* Sleep-Like States. *Journal of Neuroscience*, *35*(43), 14571–14584.
<http://doi.org/10.1523/JNEUROSCI.1369-15.2015>
- Trojanowski, N. F., & Raizen, D. M. (2016). Call it Worm Sleep. *Trends in Neurosciences*, *39*(2), 54–62. <http://doi.org/10.1016/j.tins.2015.12.005>
- Turek, M., Besseling, J., Spies, J. P., König, S., & Bringmann, H. (2016). Sleep-active neuron specification and sleep induction require FLP-11 neuropeptides to systemically induce sleep. *eLife*. <http://doi.org/10.7554/eLife.12499>
- Turek, M., Lewandrowski, I., & Bringmann, H. (2013). An AP2 transcription factor is required for a sleep-active neuron to induce sleep-like quiescence in *C. elegans*. *Current Biology*, *23*(22), 2215–2223. <http://doi.org/10.1016/j.cub.2013.09.028>
- Tye, K. M. (2018). Neural Circuit Motifs in Valence Processing. *Neuron*, *100*(2), 436–

452. <http://doi.org/10.1016/j.neuron.2018.10.001>

Unger, M. A. (2000). Monolithic Microfabricated Valves and Pumps by Multilayer Soft Lithography. *Science*, 288(5463), 113–116.

<http://doi.org/10.1126/science.288.5463.113>

Uno, M., & Nishida, E. (2016). Lifespan-regulating genes in *C. elegans*. *Npj Aging and Mechanisms of Disease*. <http://doi.org/10.1038/npjamd.2016.10>

Van Atteveldt, N., Murray, M. M., Thut, G., & Schroeder, C. E. (2014). Multisensory integration: Flexible use of general operations. *Neuron*.

<http://doi.org/10.1016/j.neuron.2014.02.044>

Van Buskirk, C., & Sternberg, P. W. (2007). Epidermal growth factor signaling induces behavioral quiescence in *Caenorhabditis elegans*. *Nature Neuroscience*, 10(10), 1300–1307. <http://doi.org/10.1038/nn1981>

Van Buskirk, C., & Sternberg, P. W. (2010). Paired and LIM class homeodomain proteins coordinate differentiation of the *C. elegans* ALA neuron. *Development*.

<http://doi.org/10.1242/dev.040881>

Van Voorhies, W. A., & Ward, S. (1999). Genetic and environmental conditions that increase longevity in *Caenorhabditis elegans* decrease metabolic rate.

Proceedings of the National Academy of Sciences.

<http://doi.org/10.1073/pnas.96.20.11399>

- Venkatachalam, V., Ji, N., Wang, X., Clark, C., Mitchell, J. K., Klein, M., ... Samuel, A. D. T. (2015). Pan-neuronal imaging in roaming *Caenorhabditis elegans*. *Proceedings of the National Academy of Sciences of the United States of America*, 201507109. <http://doi.org/10.1073/pnas.1507109113>
- Vladimirov, N., Wang, C., Höckendorf, B., Pujala, A., Tanimoto, M., Mu, Y., ... Ahrens, M. B. (2018). Brain-wide circuit interrogation at the cellular level guided by online analysis of neuronal function. *Nature Methods*, 15(12), 1117–1125. <http://doi.org/10.1038/s41592-018-0221-x>
- Vorster, A. P. A., Krishnan, H. C., Cirelli, C., & Lyons, L. C. (2014). Characterization of Sleep in *Aplysia californica*. *SLEEP*. <http://doi.org/10.5665/sleep.3992>
- Waggoner, L. E., Zhou, G. T., Schafer, R. W., & Schafer, W. R. (1998). Control of alternative behavioral states by serotonin in *Caenorhabditis elegans*. *Neuron*. [http://doi.org/10.1016/S0896-6273\(00\)80527-9](http://doi.org/10.1016/S0896-6273(00)80527-9)
- Ward, A., Liu, J., Feng, Z., & Xu, X. Z. S. (2008). Light-sensitive neurons and channels mediate phototaxis in *C. elegans*. *Nature Neuroscience*, 11(8), 916–922. <http://doi.org/10.1038/nn.2155>
- Watanabe, K., Chiu, H., Pfeiffer, B. D., Wong, A. M., Hoopfer, E. D., Rubin, G. M., & Anderson, D. J. (2017). A Circuit Node that Integrates Convergent Input from Neuromodulatory and Social Behavior-Promoting Neurons to Control Aggression in *Drosophila*. *Neuron*.

<http://doi.org/10.1016/j.neuron.2017.08.017>

Weeks, J. C., Roberts, W. M., Robinson, K. J., Keaney, M., Vermeire, J. J., Urban, J. F., ... Hawdon, J. M. (2016). Microfluidic platform for electrophysiological recordings from host-stage hookworm and *Ascaris suum* larvae: A new tool for anthelmintic research. *International Journal for Parasitology: Drugs and Drug Resistance*. <http://doi.org/10.1016/j.ijpddr.2016.08.001>

Wolf, S., Supatto, W., Debrégeas, G., Mahou, P., Kruglik, S. G., Sintès, J.-M., ... Candelier, R. (2015). Whole-brain functional imaging with two-photon light-sheet microscopy. *Nature Methods*. <http://doi.org/10.1038/nmeth.3371>

Wu, Y., Masurat, F., Preis, J., & Bringmann, H. (2018). Sleep Counteracts Aging Phenotypes to Survive Starvation-Induced Developmental Arrest in *C. elegans*. *Current Biology*, 28, 1–14. <http://doi.org/10.1001/archinte.168.13.1371>

Xian, B., Shen, J., Chen, W., Sun, N., Qiao, N., Jiang, D., ... Han, J. D. J. (2013). WormFarm: A quantitative control and measurement device toward automated *Caenorhabditis elegans* aging analysis. *Aging Cell*. <http://doi.org/10.1111/acel.12063>

Xie, L., Kang, H., Xu, Q., Chen, M. J., Liao, Y., Thiyagarajan, M., ... Nedergaard, M. (2013). Sleep drives metabolite clearance from the adult brain. *Science*. <http://doi.org/10.1126/science.1241224>

Yanik, M. F., Rohde, C. B., & Pardo-Martin, C. (2011). Technologies for

micromanipulating, imaging, and phenotyping small invertebrates and vertebrates. *Annual Review of Biomedical Engineering*, 13, 185–217.

<http://doi.org/10.1146/annurev-bioeng-071910-124703>

Yoshida, K., Hirotsu, T., Tagawa, T., Oda, S., Wakabayashi, T., Iino, Y., & Ishihara, T. (2012). Odour concentration-dependent olfactory preference change in *C. elegans*. *Nature Communications*. <http://doi.org/10.1038/ncomms1750>

You, Y. jai, Kim, J., Raizen, D. M., & Avery, L. (2008). Insulin, cGMP, and TGF- β Signals Regulate Food Intake and Quiescence in *C. elegans*: A Model for Satiety. *Cell Metabolism*. <http://doi.org/10.1016/j.cmet.2008.01.005>

Zaslaver, A., Liani, I., Shtangel, O., Ginzburg, S., Yee, L., & Sternberg, P. W. (2015). Hierarchical sparse coding in the sensory system of *Caenorhabditis elegans*. *Proceedings of the National Academy of Sciences*. <http://doi.org/10.1073/pnas.1423656112>

Zhdanova, I. V., Wang, S. Y., Leclair, O. U., & Danilova, N. P. (2001). Melatonin promotes sleep-like state in zebrafish. *Brain Research*. [http://doi.org/10.1016/S0006-8993\(01\)02444-1](http://doi.org/10.1016/S0006-8993(01)02444-1)

Zhen, M., & Samuel, A. D. (2015). *C. elegans* locomotion: small circuits, complex functions. *Current Opinion in Neurobiology*, 33, 117–126. <http://doi.org/10.1016/j.conb.2015.03.009>

Zhuo, W., Lu, H., & McGrath, P. T. (2017). Microfluidic platform with

spatiotemporally controlled micro-environment for studying long-term: *C. elegans* developmental arrests. *Lab on a Chip*.

<http://doi.org/10.1039/c6lc01573e>

Zimmer, M., Gray, J. M., Pokala, N., Chang, A. J., Karow, D. S., Marletta, M. A., ...

Bargmann, C. I. (2009). Neurons Detect Increases and Decreases in Oxygen Levels Using Distinct Guanylate Cyclases. *Neuron*, *61*(6), 865–879.

<http://doi.org/10.1016/j.neuron.2009.02.013>

Zimmerman, J. E., Naidoo, N., Raizen, D. M., & Pack, A. I. (2008). Conservation of

sleep: insights from non-mammalian model systems. *Trends in Neurosciences*.

<http://doi.org/10.1016/j.tins.2008.05.001>